Polymer-Based Systems for Drug Delivery Studies

Dissertation

zur Erlangung des Grades

"Doktor der Naturwissenschaften"

im Promotionsfach Chemie

am Fachbereich Chemie, Pharmazie und Geowissenschaften

der Johannes Gutenberg-Universität in Mainz

vorgelegt von

Jennifer Schultze

geboren in Schwerin

Mainz, Mai 2018

Die vorliegende Arbeit wurde im Zeitraum von Januar 2015 bis Mai 2018 am Max-Planck-Institut für Polymerforschung in Mainz unter der Anleitung von [redacted] und [redacted] angefertigt.

Erster Gutachter: [redacted]

Zweiter Gutachter: [redacted]

Tag der müdlichen Prüfung: 21.06.2018

“Life isn’t about waiting for the storm to pass…

It’s about learning to dance in the rain”

Vivian Greene

Zusammenfassung

Nanopartikel-basierte Wirkstofftransportsysteme sind sehr vielversprechend für die Behandlung verschiedenster Krankheiten. Mithilfe von Nanopartikeln können Wirkstoffe eingeschlossen, transportiert und freigesetzt werden. Trotz vieler vorhandener Systeme, ist ein tieferes Verständis der Prozesse notwendig. Das Ziel dieser Dissertation war es, einen tieferen Einblick in zwei hierfür relevante Themen zu erhalten: (i) eine Herstellungsmethode für nanopartikuläre Wirkstofftransportsysteme und (ii) ein neues Zellmembranmodell für Untersuchungen auf zellulärer Ebene.

Für ein besseres Verständnis der Wirkstoffaufnahme in Zellen und der Passage der Membran werden Zellmodelle verwendet. Ein beliebtes Modell sind die gigantischen unilamellaren Vesikel (GUV). Diese Arbeit stellt eine neue Methode vor, mit der GUV mithilfe eines oberflächenstrukturierten Polymerhydrogels größenspezifisch hergestellt werden können. Die Herstellung hunderter verankerter GUV in drei verschiedenen Größen und der Nutzen dieser Herstellungsmethode wird anhand von zwei Anwendungsbeispielen in dieser Dissertation veranschaulicht.

Im zweiten Projekt liegt der Fokus auf einer Herstellungsmethode für Polystyrol (PS)-Nanopartikel als Wirkstoffträgersysteme. Der Verlauf der Partikelbildung aus Nanotropfen wurde untersucht. Die Veränderung dieser Tropfen und deren PS-Anteil konnte mithilfe von fluoreszierenden Rotormolekülen, deren Fluoreszenzlebenszeit sich abhängig von der Viskosität ändert, beobachtet und analysiert werden.

In beiden Projekten dieser Arbeit wird die Fluoreszenzspektroskopie zur Analyse genutzt.

In Kooperationsprojekten innerhalb des Sonderforschungsbereichs 1066 wurde die Fluoreszenzkorrelationsspektroskopie zur Analyse von verschiedenen Polymersystems für Wirkstofftransportanwendungen eingesetzt. Die Projekte sind am Ende dieser Dissertation zusammengefasst.

Abstract

Nanocarrier-based drug delivery is a promising approach for treating various diseases. Nanocarriers can encapsulate and deliver drug molecules and a lot of work has been done in developing new systems. But still, a deeper understanding of the processes is needed. The aim of this thesis is to look deeper into two relevant processes for drug delivery studies: (i) on the extracellular level - studying the formation of polymer nanoparticles as nanocarriers and (ii) on the cellular level – developing a new cell membrane model.

In this regard, a new cell-model formation method is introduced in the first part of the thesis. Giant unilamellar vesicles (GUVs) serve as cell membrane models. Based on a functionalized polymer hydrogel, anchored GUVs of a defined size were produced using a very fast procedure. Three different sizes of GUVs were prepared on the pre-structured polymer hydrogel surface. Two application examples show the advantages of the array of hundreds of uniform anchored vesicles.

Polymer nanoparticles for drug carrier systems can be prepared in a diversity of methods. In the second part of this thesis, the physico-chemical underpinnings of the preparation and development of polystyrene (PS) nanoparticles by solvent evaporation from emulsion droplets (SEED) were studied to understand the process. The formation of the nanodroplets and the fraction of PS inside the droplets was monitored via fluorescence spectroscopy measurements of a fluorescent molecular rotor in the system.

Both projects profit from the usage of fluorescence molecules and their analysis via fluorescence spectroscopy.

As joint work with the collaborative research center 1066, fluorescence correlation spectroscopy (FCS) was used in many cooperative projects to analyze different polymer-based systems for drug delivery applications. The projects are summarized at the end of the thesis.

Contents

1 Introduction

Polymer science is present in various research areas, ranging from medical applications to electronics. Polymers are not only plastic bottles made from polyethylene terephthalate (PET) or polystyrene (PS) in the form of Styrofoam. Polymers also play a significant role in biology and medicine. Natural polymers are for example DNA molecules or proteins, which are essential for every living species. Both types, natural and synthetic polymers, are highly interesting for researchers of different fields and studies on polymers are growing year after year.

One research area, in which polymers gain more and more importance, is the field of biomedical systems. The natural polymers, such as the DNA or the variety of proteins, are mainly investigated in the biological sciences. But in terms of polymer research it is not possible to define the main natural sciences' discipline, in which polymers are studied. Polymers bring many disciplines together and lead to interdisciplinary work.

A very popular interdisciplinary topic is the research of polymeric drug delivery systems.[1] New innovative drug molecules show high potential to treat specific diseases, but researchers often face the problem of bringing the drug molecules to the body area of interest. In this regard, polymers are often selected to work as nanocarrier systems.[2–7] In some cases the cargo or drug is attached to the polymer nanoparticle, in other cases the drug is encapsulated by a polymer shell, that can be opened in the appropriate area in the body by external stimuli.[8] The diversity of nanocarrier systems is huge: copolymer micelles, polymer nanoparticles, nanohydrogel particles, polymer capsules, liposomes or dendritic polymers.[9] In every case, the carrier together with the cargo needs to be brought to a certain place in the body. This uptake ensures the best treatment.[1,5–7,10]

Regarding the research on nanocarrier-based drug delivery, two main research areas exist. One area deals with the studies in aqueous solutions, including all studies performed outside the body or the cells. Here, the researchers look at the particle formation, the encapsulation of the drug molecules and the biocompatibility of the carrier systems. Also important in this field is the analysis of the carrier's properties, such as size, stability or drug loading efficiency.[9,11–13] The other research area looks at the cellular level of the nanocarrier-based drug delivery. Here, questions about targeted delivery, cellular uptake and drug release play an important role.[14] The systems must ensure, that the cargo is attached to the (nano-)carrier, and that the whole carrier systems reaches the place where the cargo should be released. Furthermore, it is important that the cargo can be released and that the carrier, the uptake and the whole process does not harm the healthy cells or the body in any way. In this challenging field, many research groups focus on the synthesis of the carriers, on drug loading, release and cellular uptake.

This thesis deals with two topics that play an important role in the field of polymer systems for drug delivery. The first topic is related to research on cellular level, whereas the second topic belongs to the category of ex-vivo studies of nanoparticles and their characterization.

The first part of the thesis describes a newly developed method for the preparation of a cell membrane model. This method is based on a polymer system, more precisely a (poly(N-isopropylacrylamide) (PNIPAAm) terpolymer hydrogel. PNPAAm was polymerized with functional comonomers and cross-linked to a covalently bound swellable network. Via photo-lithography this polymer network can be patterned, in order to form a template for the preparation of size-defined cell membrane models on its surface. The type of cell model is called giant unilamellar vesicle (GUV) and was formed from phospholipids. These size-defined GUVs can be used as cell models for an easier understanding of the cell membrane. Furthermore, model systems are useful for gaining insight into drug delivery research.

In the second topic the focus is on the research of the nanoparticle systems and the understanding of their formation processes. A lot of work has been done regarding the synthesis or preparation of nanoparticles as well as their applications, especially in drug delivery studies. This project focuses on the physico-chemical understanding of the process of polymer nanoparticle formation via so-called “solvent evaporation from emulsion droplets (SEED)”. Polystyrene nanoparticles were prepared with this kind of formation method and the process of solvent evaporation from the nanodroplets was monitored with the help of a fluorescent molecular rotor. This type of molecule changes its fluorescence lifetime depending on the microenvironment. The lifetime was measured via time-correlated single photon counting (TCSPC) experiments. Furthermore, the size and concentration of the nanodroplets during the evaporation process was monitored via fluorescence correlation spectroscopy. Both studies were obtained simultaneously in a single experiment. Polymer nanoparticles for drug delivery can be prepared by the SEED process. Therefore, it is important to understand the process and the particle formation, in order to control the method to obtain ideal drug delivery systems.

The analysis of polymer-based systems for drug delivery studies via fluorescence correlation spectroscopy (FCS) was a third part of this work. FCS was used in many cooperative projects to determine the diffusion coefficients, hydrodynamic radii and aggregation behavior or to confirm successful chemical reactions. In the last chapter, the joint projects are presented.

2 Physico-Chemical Concepts and Methods

For the characterization and the physico-chemical understanding of molecules, it is necessary to understand the underlying physical and physico-chemical concepts. Furthermore, various characterization methods, which are used in chemical, biomedical or material sciences, are based on physical phenomena. In this work, the main physical concept was the fluorescence of molecules. The first part of the thesis used confocal laser scanning microscopy (CLSM) as main method for imaging. This required samples, which were labeled with fluorescent dyes. Additionally, fluorescence correlation spectroscopy (FCS) was used to demonstrate the application of the developed method. In the second part of this work, the fluorescence was even more important, because a fluorescent molecular rotor was used, which changed the fluorescence lifetime depending on the microenvironment. The formation of polystyrene nanoparticles and concentration changes in the nanodroplets were monitored with the help of this rotor molecule by fluorescence spectroscopy via time-correlated single photon counting and fluorescence correlation spectroscopy.

This chapter briefly explains the physico-chemical concept of fluorescence and the fluorescence based methods that were used in this work.

2.1 Fluorescence

Fluorescence is a widely used phenomenon, not only in nature, but also in research. The fluorescence of molecules gains a lot of interest in many disciplines and fluorescence spectroscopy methods are research tools in chemistry, physics, biotechnology or medical diagnostics.[15]

Fluorescence is a phenomenon of luminescence, which is the emission of light from electronically excited states. Depending on the nature of this excited state, the emission is either called fluorescence or phosphorescence.[15] The emission and absorption of light is only possible in discrete increments of energy and can be explained using photons, if light is considered as discrete particles.[16] Molecules, that are able to absorb and emit photons, are called fluorophores. The absorption and emission processes are illustrated in the Jablonski diagram (Figure 1). This diagram schematically explains the electronic states as well as absorption and emission processes of a molecule. In Figure 1 the singlet electronic states (S_0, S_1, S_2) and their numerous vibrational levels (0,1,2,...) as well as the triplet state (T_1) are shown. When a fluorophore absorbs light, different processes occur. Usually, the molecule is excited to some higher vibrational levels of the S_1 or S_2 state. When the fluorophore relaxes to the lowest vibrational level of S_1, the process is called internal conversion. Another process can occur when a molecule in the S_1 state undergoes a spin conversion, called intersystem crossing, to the T_1 state. In general, the emission from this state is shifted to longer wavelengths and is described as phosphorescence. The emission of a fluorophore from the lowest energy vibrational level of S_1 to S_0 state is described as fluorescence. In case of fluorescence, the electron in the excited orbital of the excited singlet state is paired to the electron in the ground state orbital. Hence, the return of the excited electron to the ground state is very fast and leads to the emission of a photon. The general fluorescence emission rates are around 10^8 s^{-1}. Typically, the absorption energy is higher than the emission energy, and

fluorescence appears at lower energies and longer wavelengths, respectively.[15]

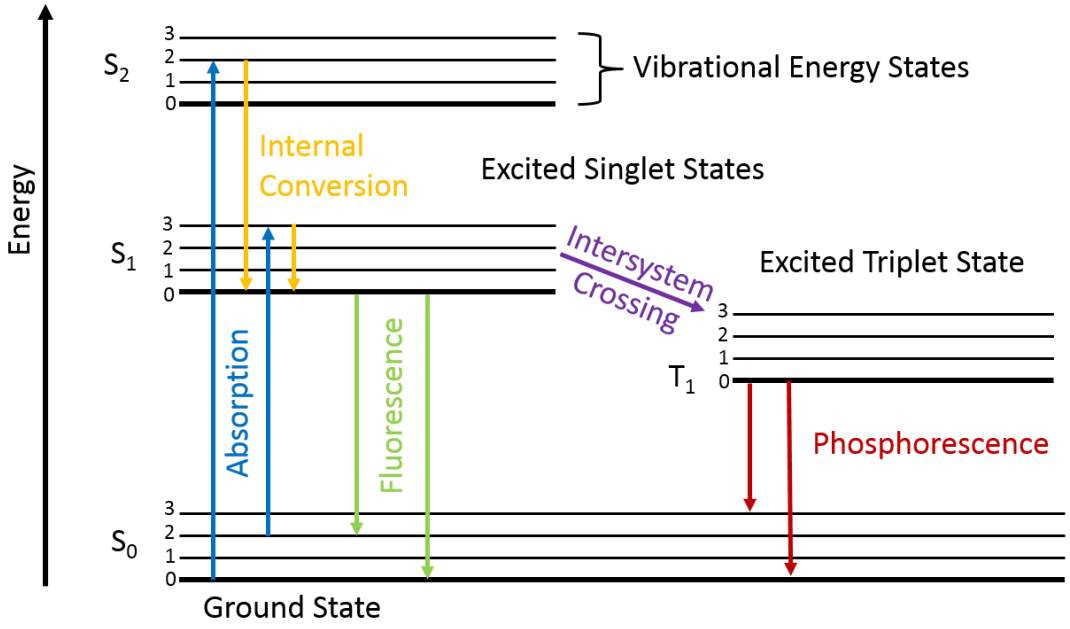

Figure 1: Jablonski diagram, showing the absorption and emission characteristics of fluorescence and phosphorescence processes. The singlet electronic states (S_0, S_1, S_2) and their numerous vibrational levels (0,1,2,…) as well as the triplet state (T_1) are shown. When a fluorophore absorbs light, it is excited to some higher vibrational levels of the S_1 or S_2 state. Relaxation to the lowest vibrational level of S_1 is called internal conversion. When a molecule in the S_1 state undergoes a spin conversion to the T_1 state it is called intersystem crossing. Emission from this state is shifted to longer wavelengths and is called phosphorescence. The emission of a fluorophore from the lowest energy vibrational level of S_1 to S_0 state is called fluorescence.

The fluorescence lifetime τ of a fluorophore is the average time that the molecule is in the excited state before returning to the ground state. Typically, fluorescence lifetimes are around 10 ns.[15]

Fluorescence is the basic concept of various analytical methods, such as fluorescence spectroscopy or microscopy. It is also the underlying concept for other phenomena, such as Förster resonance energy transfer (FRET).

The fluorescence of a molecule can be different, depending on the environment, such as the solvent, if the molecule is in a solution. Additional substances in the solution can also influence the fluorescence behavior. They are often reacting as quencher molecules.[15]

Typical commercially available fluorescent dyes for fluorescence spectroscopy or microscopy are sold under the brand names Alexa Fluor and Atto. Usually these dye molecules have conjugated double bond systems, often in form of aromatic ring system. Small changes in the functionalities of the molecules lead to different excitation and emission spectra of these dyes. In case of Alexa Fluor dyes, a variety of different structure exist, which can be excited at wavelengths from 350 nm up to 790 nm.[17]

Besides the commercial fluorescent dyes used for spectroscopy and microscopy, many other fluorescent molecules are of interest. One special example will be discussed in the next section.

2.2 Fluorescent Molecular Rotors

Commercially available fluorescent dyes are very useful for various applications and studies in the fields of microscopy and spectroscopy. Especially in biomedical sciences fluorescent molecules are of high interest. This chapter introduces a special type of fluorescent dyes: fluorescent molecular rotors.

Fluorescence molecular rotors are fluorophores which undergo twisted intramolecular charge transfer (TICT).[18,19] These molecules consist of an electron-donating unit and an electron-accepting unit. Typically a π-conjugated moiety allows electron transfer in the planar conformation.[18,19] Upon irradiation, electrostatic forces occur and result in the formation of a twisted state around the σ-bond between both parts of the molecule. This twisted conformation has a lower excited-state energy and can either show a red-shifted fluorescence emission or can show a non-radiative process.[18–21] The TICT of the rotor molecule strongly depends on the environment.[18,21,22] Inside a high viscosity environment, the intramolecular rotation is hindered and the non-radiative pathway is prevented. This results in the relaxation of the molecule via the radiative pathway, restoring the fluorescence.[18–21] A scheme of the excitation pathway is shown in Figure 2.[23]

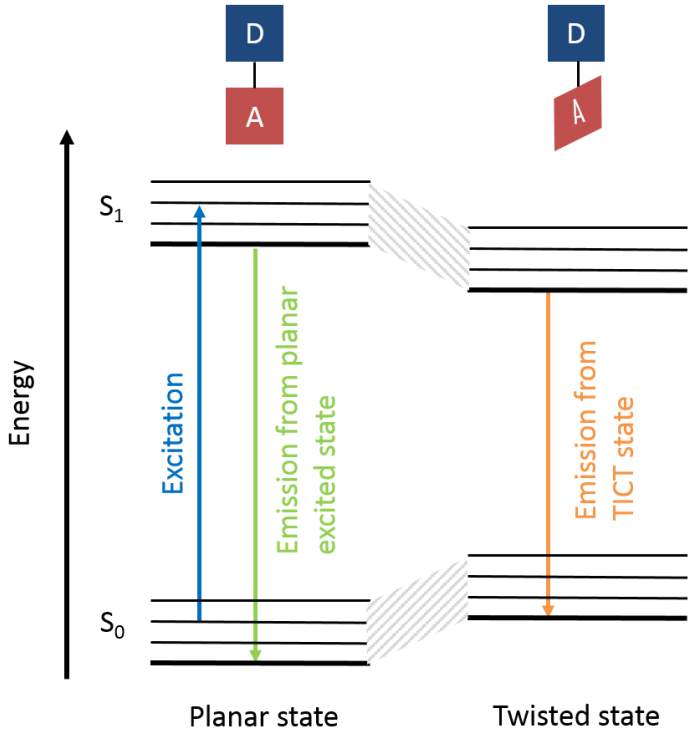

Figure 2: Scheme of the electronic states and possible relaxation process for a fluorescent molecular rotor. If the electron donor part (D) of the molecular rotor and the acceptor (A) are in the planar state, the excitation and emission process is the same as for conventional fluorophores. This is the case for a high viscosity environment, resulting in longer fluorescence lifetimes. For the twisted state of molecular rotors (in low viscosity environment), the Jablonski diagram needs to be extended. The excited-state energy for a twisting molecule is lower in the TICT state, whereas the ground-state energy is higher. The energy gab between these states is lower and the fluorescence lifetime is shorter. Adapted from [19].

The spectroscopic properties of the molecular rotor are dependent on several aspects. Besides the viscosity and the polarity of the solvent, the formation of hydrogen bonds and the excimer formation should be taken into account. Polar solvents, for example, stabilize the TICT state of the molecule and increase the relaxation time from this state. The polarity is linked to the ability to build hydrogen bonds. And the formation of these bonds between the molecule and the solvent increases the TICT formation rate. Nevertheless, the viscosity, predominantly the viscosity of the microenvironment of the molecule, is often the dominating factor.[19]

Molecular rotors can be found in several chemical classes. Examples of molecular rotors are benzylidene malononitriles, stilbenes or benzonitrile-based fluorophores.[24–26] The molecule that was used in this project is called

LBX37 and pictured in Figure 3. It is composed of a naphthalene unit, the electron-acceptor and a dibenzoazepine unit, the electron-donor.[27]

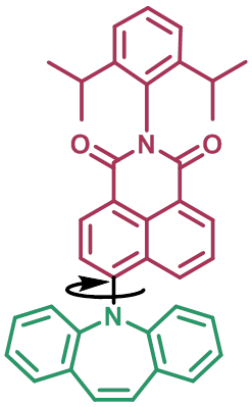

Figure 3: Chemical structure of the molecular rotor LBX37 used in this work. The molecule rotates around the axis of the C-N-bond between the naphthalene unit, which is the electron-acceptor (red, upper part) and the dibenzoazepine unit, which is the electron-donor (green, lower part).

Fluorescence molecular rotors are often applied for real-time monitoring of polymerization reactions or aggregation phenomena. Furthermore, the usage for reporting protein conformation changes was reported.[28] In biological research fields, molecular rotors have the advantage to result in a quantitative fluorescence response, compared to qualitative data for other fluorescent probes.[19]

In this work, the fluorescence molecular rotor was used to monitor the formation of nanoparticles via a solvent evaporation (SEED) process. The fast response of its fluorescence lifetime to changes in the microenvironment enabled determination of the concentration in the nanodroplets during SEED.

2.3 Fluorescence Spectroscopy via Time-Correlated Single Photon Counting

Fluorescence spectroscopy methods are of high interest in all natural science disciplines. Especially time-resolved fluorescence spectroscopy is a powerful tool in the analysis of molecules. In this regard, time-correlated single photon counting (TCSPC) enables temporal resolution to obtain fluorescence lifetimes as well as the decay shape, in order to resolve not only mono-exponential, but multi-exponential decays.[29] The arrival time of every individual photon is measured by TCSPC.[16] The method works as following: A fluorescent sample is excited repetitively by short laser pulses and the time between excitation and emission is measured.[29] The principle of TCSPC (Figure 4) can be described with a stop-watch. The laser pulse resembles the start of the clock, whereas the clock stops when the first photon arrives at the detector. This process is repeated many times to count the number of photons arriving at a certain time or time rage (bin). According to their arrival time, the photons are sorted into a histogram.

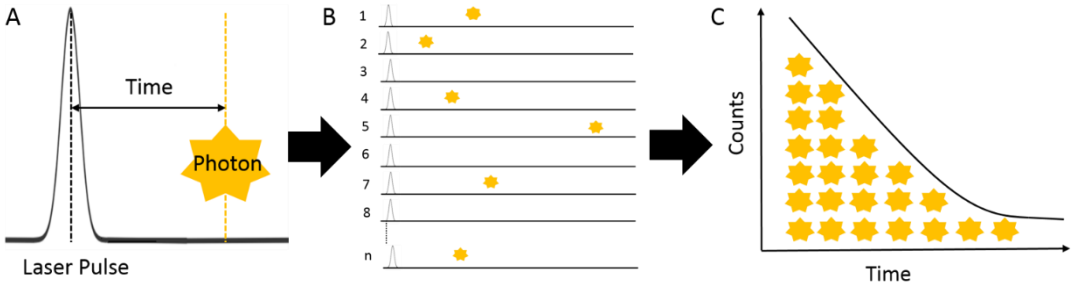

Figure 4: Principle of time-correlated single photon counting (TCSPC). (A) A fluorescent sample is excited repetitively by short laser pulses and the time between excitation and emission is measured. The laser pulse is the start and the photon arrival time at the detector is the stop. The time in between is measured. (B) This process is repeated many times to count the number of photons arriving at a certain time or time rage. (C) According to their arrival time, the photons are sorted into a histogram. Adapted from [15,16,29].

The counts or the intensity I is plotted against the photon arrival time t and the fluorescence lifetime τ can be determined from the slope of the exponential decay fit function (equation 1).[30]

$$I_t = I_0 \cdot e^{-\frac{t}{\tau}} \quad (1)$$

In case the measured sample shows two different fluorescence lifetimes (τ_1, τ_2), the decay curve is the sum of two intensity decay curves and can be expressed as following (equation 2) to obtain both fluorescence lifetimes:

$$I_t = I_{1,t=0} \cdot e^{-\frac{t}{\tau_1}} + I_{2,t=0} \cdot e^{-\frac{t}{\tau_2}} \quad (2)$$

The general term (equation 3) for samples with more than one lifetime is described with the amplitude A as:

$$I_t = \sum_{i=1}^{n} A_i \cdot e^{-\frac{t}{\tau_i}} \quad (3)$$

The resolution of TCSPC experiments is given by its instrument response function (IRF), that contains the pulse shape of the laser, the temporal dispersion in the optical system, the detector as well as the electronic characteristics.[16] Ideally, the IRF is infinitely narrow, due to an infinitely sharp excitation pulse and infinitely accurate detectors and electronics.

To define an average fluorescence lifetime value for each measurement or each decay curve, the weighted average fluorescence lifetime τ_{wa} can be used. This lifetime takes the different single lifetimes τ_i as well as their amplitudes A_i into account as described in equation 4.

$$\tau_{wa} = \frac{\sum_{i=1}^{n} A_i \cdot \tau_i}{\sum_{i=1}^{n} A_i} \quad (4)$$

In this work, TCSPC was used to determine the fluorescence lifetime of the fluorescent molecular rotor LBX37, in order to monitor the formation process of nanoparticles via a solvent evaporation process.

2.4 Confocal Laser Scanning Microscopy

Confocal laser scanning microscopy (CLSM) is a versatile tool to image fluorescently labeled probes.[31] The confocal scanning microscope was first invented in the 1950s by M. Minsky and was improved from that time on until today.[32]

The universal application of CLSM is caused by the advantages of the method. High resolution images and relatively high frame rates are among the main features of CLSM.[31,33,34] The main advantage is 3D sectioning. Confocal laser scanning microscopy can visualize details of fluorescently labeled probes in a 3D image: details, that previously were only seen in very thin samples with the conventional epifluorescence microscopes. In thick samples the fluorescence background overwhelmed the focal plane signal.[31] In contrast to standard epifluorescence microscopy, CLSM images only show the focal plane. The principle (Figure 5) is based on scanning the sample point by point using a laser beam that is focused into the sample. The laser light is scanned across the sample and the fluorescence signal is collected using the single objective lens. With a lens of 1.4 numerical aperture (NA) the theoretical lateral resolution is 0.14 µm and the vertical resolution is 0.23 µm.[31] Additionally, a spatial filter (pinhole) is needed to remove unwanted fluorescence light coming from the background.[31,34] The signal is detected by a photodetector, like a photomultiplier tube (PMT) or Avalanche photodiode (APD), behind the pinhole. Only light focused at the pinhole and therefore coming from the focal plane within the sample is detected. A stepper motor or piezo-drive is used to go small steps along the z-axis to obtain three-dimensional information and images.[34]

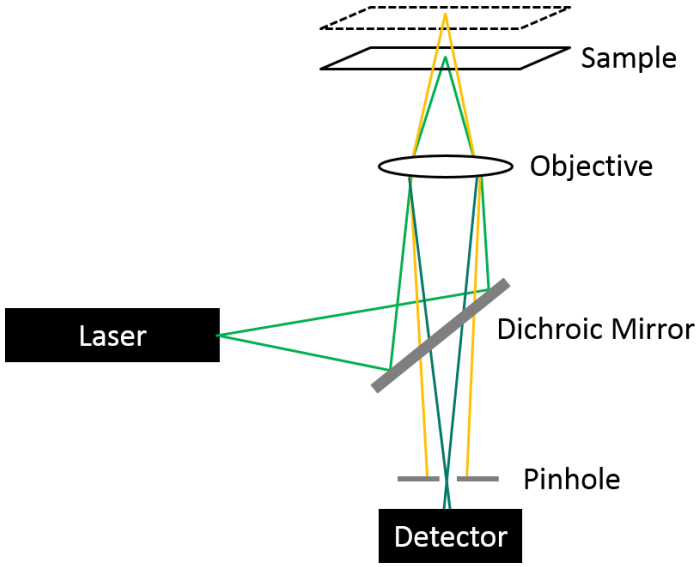

Figure 5: Schematic setup of a confocal laser scanning microscope. The sample is illuminated with a focused laser beam, which passes a dichroic mirror and the objective lens. The laser beam is scanned across the sample and the fluorescence signal is collected using an objective lens and the dichroic mirror. A pinhole is placed in front of a detector to remove unwanted fluorescence from areas around the focus point.

There exist different types of CLSM, which can be classified by the scanning process. 3D images can either be taken by stage-scanning or beam-scanning. The latter process is more suitable for biological probes, because image acquisition times are faster.[31]

Confocal laser scanning microscopy is used in many disciplines, such as biology, medicine, chemistry, physics and material sciences. The CLSM method itself is already a frequently used analysis tool, but CLSM is also the basic concept for many other methods, such as fluorescence correlation spectroscopy (FCS, described in the next section) or fluorescence lifetime imaging microscopy (FLIM).

2.5 Fluorescence Correlation Spectroscopy

Fluorescence correlation spectroscopy (FCS) was first introduced by Madge, Elson and Webb in the 1970s and became more and more interesting for researchers, especially in the fields of physical chemistry or biophysics.[35–46] FCS investigates the dynamics of fluorescent or fluorescently labeled molecules, nanoparticles or macromolecules and is compatible with a variety of solvents. This allows to study the dynamical behavior of fluorescent molecules in various environments.[46]

Different from conventional fluorescence spectroscopy studies, the principle of FCS is based on the small statistical fluctuations of the light intensity of a fluorescent species diffusing through a very small observation volume.[36] This observation volume is determined by the focus of a confocal microscope and typically has a volume of around 1 μm^3. The intensity fluctuations are correlated to analyze the dynamics of the sample system. Therefore, diffusion coefficients, hydrodynamic radii, aggregation behavior or chemical reactions can be observed by fluorescence correlation spectroscopy.[38] Due to fluorescence, this technique is very sensitive, and individual molecules can be analyzed.[36] FCS also has a high selectivity. Different from dynamic light scattering techniques, FCS only detects fluorescent probes. So, it is possible to selectively label single component of the measured system. Another advantage is the short measurement time, which is usually a few seconds, enabling the investigation of time-dependent processes.

The FCS setup is based on a confocal microscope as shown in Figure 6. A laser is used as light source to excite the fluorescent sample. The wavelength needs to match the excitation wavelength of the fluorescent species. Commonly used lasers are argon ion lasers or helium-neon lasers. The laser light passes a dichroic mirror before it is focused by the objective into the sample. As soon as the fluorescent molecules diffuse inside the observation volume, they are excited by the laser light and emit light, which passes back

through the objective, the dichroic mirror, an emission filter and the pinhole, before it arrives at the detector. Often Avalanche photodiode (APD) detectors are used in FCS setups.

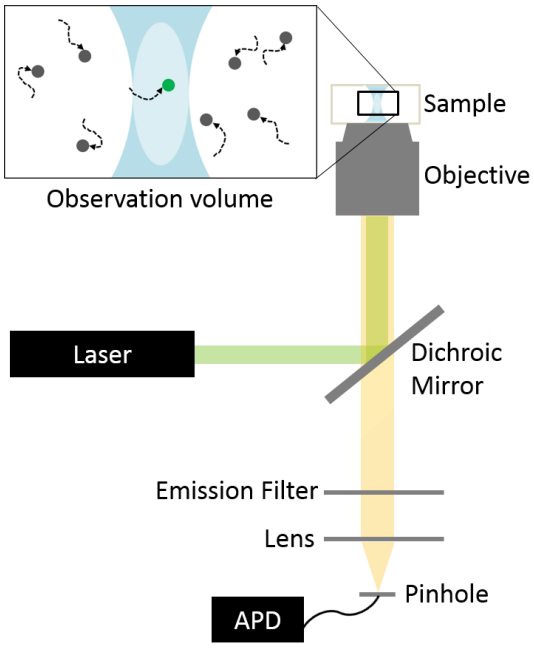

Figure 6: Fluorescence correlation spectroscopy (FCS) setup, based on a confocal microscope. A laser is used as light source to excite the fluorescent sample. The laser light passes a dichroic mirror before it is focused by the objective into the sample. Fluorescent molecules are excited by the laser light and emit light, which passes back through the objective, the dichroic mirror, an emission filter and the pinhole, before it arrives at the detector.

Even though many solvents can be used for FCS experiments, mainly samples are dissolved in aqueous solutions. The ideal concentration of the fluorescent species is around 10 nM to observe in average one molecule that is diffusing through the observation volume at a time. The observation volume V_{obs} shows a Gaussian profile and can be described by its radial r_0 and axial z_0 dimensions:[45]

$$V_{obs} = \pi^{\frac{3}{2}} \cdot r_0^2 \cdot z_0 \tag{5}$$

The fluorescent molecules diffuse into and out of the observation volume, because of Brownain motion and cause a variation in the light intensity, which is detected by the APD. This signal is a time trace as depicted in Figure 7 (left).

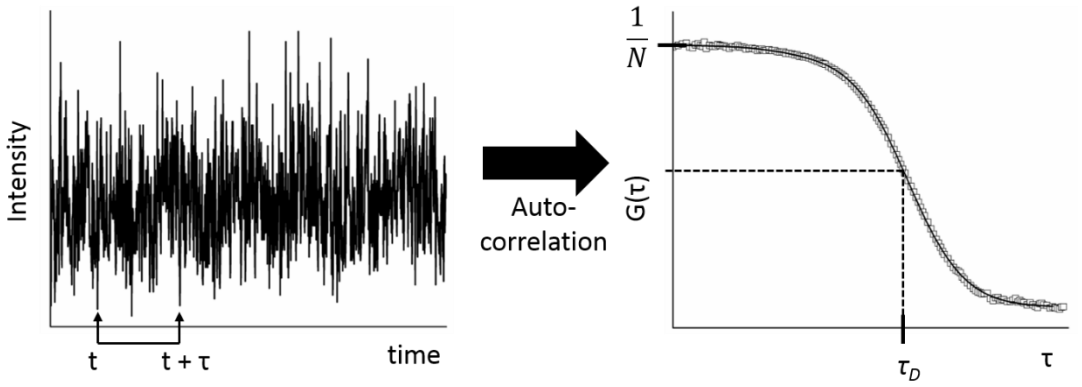

Figure 7: Principle of fluorescence correlation spectroscopy (FCS) measurements: Intensity fluctuations from the excited fluorescent species (left) are transferred into an autocorrelation function (right) and fitted with an appropriate model function to gain information about the diffusion time τ_D and the number of particles *N* in the observation volume. Adapted from [44,45].

The fluorescence intensity signal *F(t)* is fluctuating around a temporal average:[36,45,46]

$$F(t) = \langle F(t) \rangle + \delta F(t). \tag{6}$$

To gain information out of the light intensity fluctuation signal it is necessary to auto-correlate the signal for any delay time τ^*, in order to obtain the normalized fluctuation autocorrelation function *G(τ*)* (Figure 7):[36,45,46]

$$G(\tau^*) = \frac{\langle \delta F(t) \delta F(t+\tau^*) \rangle}{\langle F(t) \rangle^2} \tag{7}$$

To extract parameters as the diffusion coefficient *D* or the concentration *c*, experimental autocorrelation must be fitted with a mathematical model function. Therefore, the approximation is made for measurements in solution: the detection volume can be seen as a three-dimensional Gaussian profile, as described in equation 5. If the fluorescence fluctuations are cause by only one type of molecules, which is significantly smaller than the observation volume, and if the molecules are able to diffuse freely in three dimensions, the autocorrelation function is describes as:[44–46]

$$G(\tau^*) = 1 + \frac{1}{N} \frac{1}{\left(1+\frac{\tau^*}{\tau_D}\right)} \frac{1}{\sqrt{1+\frac{\tau^*}{S^2 \tau_D}}} \tag{8}$$

The autocorrelation function in three dimensions contains the number of particles N in the observation volume and the structural parameter S, which is the ratio of the axial z_0 to the radial r_0 dimension, describing V_{obs}. Equation 8 depends on the diffusion time τ_D of the fluorescent species, which is the decay time of the correlation curve. It can be calculated from the diffusion coefficient D:[44,46]

$$\tau_D = \frac{r_0^2}{4D} \tag{9}$$

The Stokes-Einstein equation (10) describes the relation between the hydrodynamic radius R_H of the molecule and its diffusion coefficient D taking the temperature T, the Boltzmann constant k as well as the viscosity of the solution η into account.

$$R_H = \frac{kT}{6\pi\eta D} \tag{10}$$

Fluorescence correlation spectroscopy is frequently used in the study of nanoparticle systems for drug delivery. Examples of FCS studies in different cooperation projects are shown in chapter 6 of this thesis.

3 Polymer Gel-Assisted Formation of Giant Unilamellar Vesicles

Every single human being consists of trillions of cells[47] – our smallest living building units. Even though there exist different types of cells, such as eukaryotic and prokaryotic cells, they all have a protection against their direct environment - the cell membrane. This membrane consists of a lipid double layer, also called bilayer.[48] It consists mostly of phospholipids, which have an amphiphilic character, and therefore form the characteristic double layer. In case of eukaryotic cells, the lipid double layer contains other components, such as proteins or protein channels.[49] Because of the complexity of cells and cell membranes, it is very important to understand our smallest building units. Hence, cell membrane model systems are used in biological, medical or biochemical studies.[49,50] There are different types of models, for example black lipids membranes, solid supported bilayers or vesicles.[51–56] Probably the most relevant among these model systems are giant unilamellar vesicles (GUVs). They resemble the basic structure of all living cells, mimicking the closed cell membrane.[53,57–61] GUVs and their preparation are well known, but still the size-controlled formation is missing. Desirably, hundreds of vesicles with defined diameters can be prepared in an easy and comparably low-priced way. To address this problem, a polymer gel-based system was used in this project to create uniform and well-defined giant unilamellar vesicles.

3.1 Chemical Concepts and Methods

The theoretical concepts of cell membrane models as well as the chemical background of the polymer hydrogel, used in this work, is explained in this chapter. Confocal laser scanning microscopy and fluorescence correlation spectroscopy as the analytical methods of choice for this work, are explained in section 2.4 and section 2.5.

3.1.1 Giant Unilamellar Vesicles

The word vesicle describes a structure of one or more spherical bilayers that enclose a small aqueous volume.[57–61] The bilayers consist of amphiphilic molecules that self-assemble into the vesicle structure. The amphiphiles contain a hydrophilic part, which is in contact with the aqueous solution, and a hydrophobic part, which interacts to form the inner part of the bilayer.[62] In case of vesicles that have lipids as amphiphiles, they are called liposomes. These lipids are often phospholipids, which have hydrophobic, non-polar hydrocarbon chains and a hydrophilic, polar phosphate head group.[49,63]

A variety of phospholipids is existing. One prominent example is 1,2-dioleoyl-*sn*-glycero-3-phosphocholine (DOPC, Figure 8A) that belongs to the phosphatidylcholines, a major component of biological cell membranes. This phospholipid is the main lipid component used for vesicles formation in this work. Two other phospholipids were also used: 1,2-dioleoyl-*sn*-glycero-3-phosphoserine (DOPS, Figure 8B) belongs to the group of phosphatidylserines, which play an important role in blood coagulation.[64] 1,2-dioleoyl-*sn*-glycero-3-phosphoethanolamine (DOPE, Figure 8C) is a phosphatidylethanolamine and can mainly be found in the cytoplasmic side of the membrane bilayer.[65]

If a vesicle consists of a single bilayer, it is called unilamellar.[57] Multilamellar vesicles are formed from multiple bilayers. Unilamellar vesicles can be differentiated by their sizes. Small unilamellar vesicles (SUVs) show diameters below 100 nm, often even below 50 nm. Sometimes they are also called sonicated unilamellar vesicles, because they are formed upon applying an external sonication energy.[57] The diameter of large unilamellar vesicles (LUVs) ranges from 100 nm up to 10 µm.[53,57] They can be prepared by an extrusion process.[66]

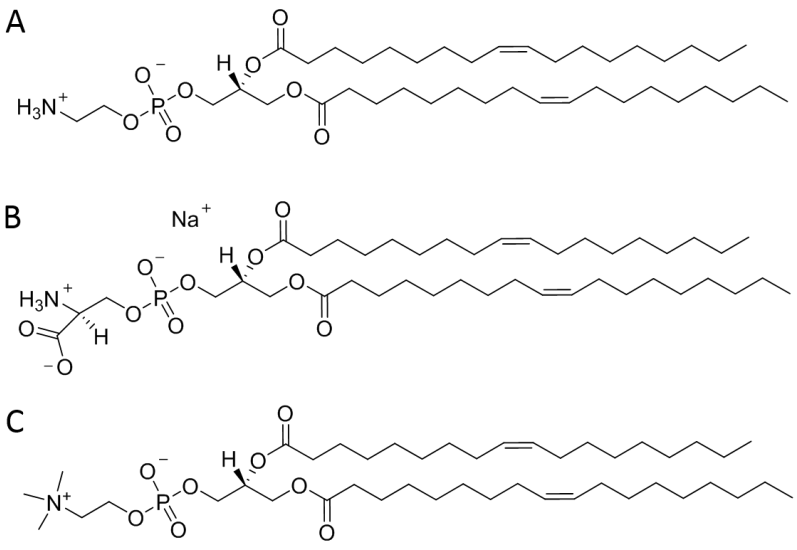

Figure 8: Chemical structures of the phospholipids used in this work for vesicle preparation: A: 1,2-dioleoyl-*sn*-glycero-3-phosphocholine DOPC, a phosphatidylcholine and the main component of the vesicles prepared in this work. B: 1,2-dioleoyl-*sn*-glycero-3-phosphoserine DOPS, a phosphatidylserine. C: 1,2-dioleoyl-*sn*-glycero-3-phosphoethanolamine DOPE, a phosphatidyl-ethanolamine.

Vesicles with a single double layer and with dimeters between 10 – 200 µm are called giant unilamellar vesicles (GUVs, Figure 9).[57,67] Due to their properties, giant unilamellar vesicles (GUVs) are perfect candidates for cell membrane models.[68] Their size is in the same range as the sizes of biological cells and the unilamellar character perfectly fits to biological cell membranes. Similar to cells, GUVs are flexible. All these characteristics make them ideal models for an easier understanding of membrane processes. GUVs cannot only be used as membrane models, but also as cell models. They were already used in different studies, such as the imitation of

cytological processes, studying the dynamics of lipid membranes or gene expression.[44,69–71]

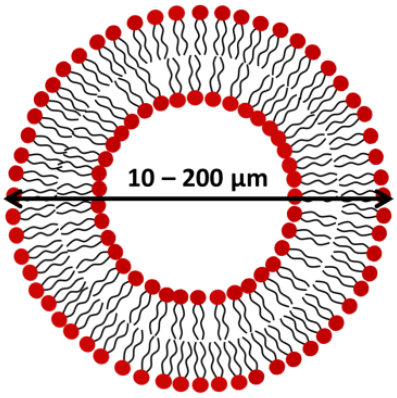

Figure 9: Schematic image of a giant unilamellar vesicle (GUV), consisting of one bilayer of self-assembled amphiphilic (phospho-)lipids. The diameter of GUVs ranges from 10 to 200 µm.

The advantage of GUVs compared to other membrane models, especially to supported bilayers is their shape. The vesicle form is comparable to the cells, whereas the planar supported bilayers are not flexible. Membrane stacks as membrane models are also not perfect, because of their geometry and because they contain more bilayers than biological cells.[52]

3.1.2 Common Methods for Preparing Giant Unilamellar Vesicles

The preparation of giant unilamellar vesicles (GUVs) is possible using many different procedures and is studied since the 1960s.[72]

The most widely used technique is the electroformation.[73] This method uses an externally applied electric field for the formation of GUVs. Therefore, the lipids are deposited from an organic solution on a conductive surface.[57] This can be a buffer-filled chamber with conductive slides. An (alternating) electric field starts the hydration of the lipids into GUVs.[58] There are several advantages of the electroformation method. The first factor is the speed of the vesicle formation, which is a few hours or even minutes. A second factor is the good quality of the GUVs. Their hydration can be easily controlled by adjusting the electric field. Another advantage lays in the direct observation

of the formed vesicles under a microscope, if suitable chambers are used in the process. The reproducibility of the process is high and results in unilamellar and spherical vesicles.[57,74,75] But there are also disadvantages in the electroformation technique: For this process a special equipment is needed. The formation is very sensitive to charged lipids and may not work if too many charged lipids are present. Furthermore, this procedure forms interconnected vesicles, which may exchange their lipids with their neighbors.[57,74] The formation process in shown in Figure 10. The procedure is also possible without an electric field. In this case, the method is called gentle hydration. The procedure is similar to electroformation: lipids are deposited on a solid surface, but here the vesicles form by spontaneous swelling and not from the influence of an electric field. The addition of water or solvent to the already pre-organized lipids (into bilayers) results in swelling of the bilayers. Upon disturbance (e.g. mechanical shaking) parts of the bilayer release to the bulk solution and self-close.

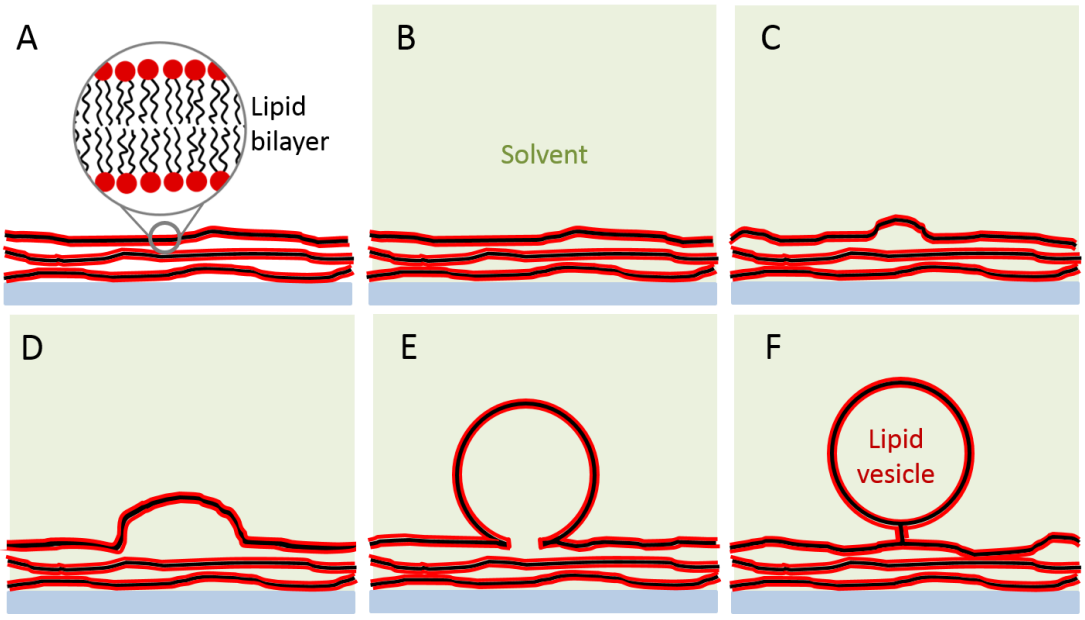

Figure 10: Scheme of the preparation of giant unilamellar vesicles by lipid film hydration on a solid surface. The process starts from (A) a multilayer stack of lipid bilayers that is (B) hydrated by a solvent and grows (C-E) into (F) a self-closed vesicle. In case of electroformation, the solid surface is conductive and an electric field is applied, whereas the method is called gentle hydration when there is no electric field present. Adapted from [57,59,76].

The advantages of the gentle hydration are the simplicity, because no special equipment is needed, and the possibility to use charged lipids for the GUV preparation. Disadvantageously, the formation is difficult to control and takes a few days.[57,74] Both processes, electroformation and gentle hydration, are lipid film hydration methods and were optimized and improved in the last decades. The control of the vesicles' size is a challenge in lipid film hydration methods. Tao *et al.* found a way for preparing GUVs via electroformation with low polydispersity by adding Ca^{2+} or $CaCO_3$ to the lipid film surface.[77] But the presence of these ions or molecules may influence the membrane behavior.

Another possibility for GUV formation is the fusion or coalescence of small vesicles. In one method, small vesicles are stored in suspension for several days to form GUVs.[57,78] The reasons for their coalescence could be the usage of oppositely charged lipids, the addition of fusogenic peptides or additional polyethylene glycol (PEG).[79–81] This technique is simple, does not need special equipment and is free from organic solvents, but the vesicle size and the lamellarity are not controllable. Furthermore, this method is not suitable for every type of lipids.

The formation of GUVs is also possible from a micellar lipid solution. In this process, the lipids are forces into micellar structures due to a high amount of micelle-forming surfactants, which are present in the lipid solution. When the surfactant is removed, the micelles form into giant vesicles.[82] This method is simple and does not require special equipment. But it does not control of the vesicles' size and is limited to certain lipids.[57]

3.1.3 Gel-Assisted Formation of Giant Unilamellar Vesicles

Besides the commonly used GUV preparation methods such as electroformation or gentle hydration, which are performed on a solid surfaces from lipid bilayers, other methods were established in the last years.

In 2008 *Horger et al.* improved the gentle hydration technique. They used a layer of agarose gel on glass to form the vesicles on a gel substrate. For this process, three steps were relevant. First, a film of an ultralow melting agarose was deposited on a glass slide. Second, lipids were added to generate an agarose-lipid hybrid film. And third, the film was hydrated, so vesicles are forming. This method has many advantages, especially compared to the gentle formation on solid substrates. With the agarose gel-assisted GUV formation process, it was possible to work in the presence of physiological buffer, such as phosphate buffered saline (PBS). The vesicles formed within minutes in remarkably high yields. Furthermore, no special equipment or an electric field was needed and no additional pre-hydration step required. This method works for a variety of lipids and lipid mixtures. Besides all the advantages of this method, there still remain some problems. The agarose can dissolve in the aqueous solution and ended up inside in the giant vesicles. Additionally, this procedure generated unilamellar as well as multilamellar giant vesicles.[83]

To improve the gel-assisted GUV formation, *Weinberger et al.* changed the agarose gel by a fully hydrolyzed high-molecular weight polyvinyl alcohol (PVA). This polymer was used as a dry but swellable film on a glass substrate. The lipids for the vesicle formation were spread on this gel surface and hydrated in an aqueous (buffer) solution. GUVs formed very fast from a film, which was composed of lipids in the fluid state. From this process, many unilamellar vesicles can be prepared within two minutes. Small vesicles as well as large ones can be obtained from (Figure 11). During the growing process, small vesicles fused into large vesicles.

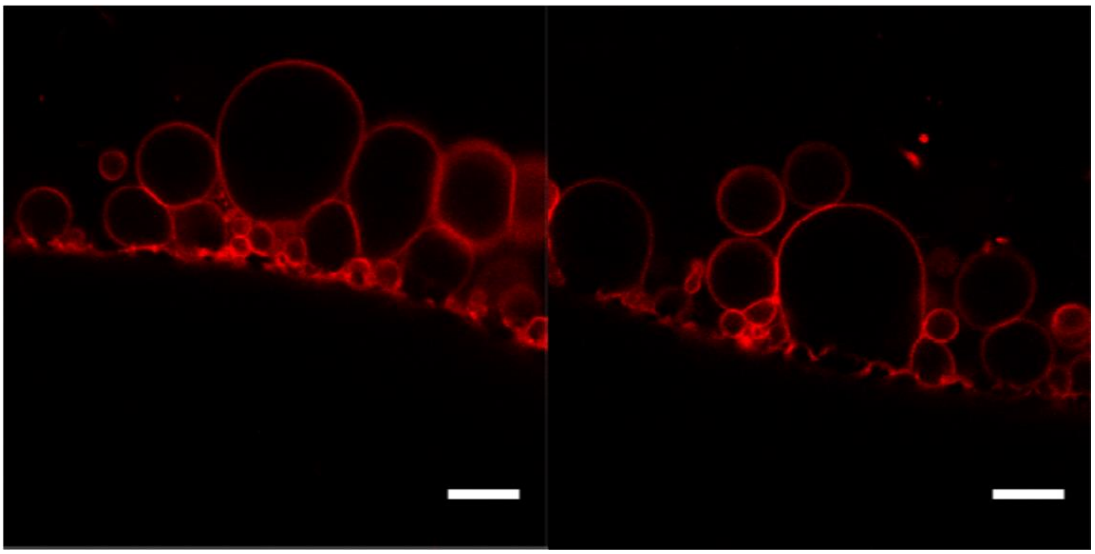

Figure 11: Confocal laser scanning images (XZ plane) of DOPC-GUVs labeled with 0.5 mol% RhodamineB-PE, grown on unlabeled PVA film. Scale bars are 20 µm. Reprinted from [59].

The mechanism of the GUV formation is not fully understood, yet. *Weinberger et al.* described the possible pathway for GUV formation on solid (glass) substrate and gel substrate as the following: The water penetration on glass into pre-ordered lipid bilayers has two main water transport ways. On the one hand, water approaches the interlamellar regions from the edges and swells the bilayer stack. On the other hand, water can permeate the bilayer directly, because a phospholipid bilayer has a certain water permeability (Figure 12A). In the case of GUV formation on a gel surface, the same water transport modes occur, but there is an additional pathway from the gel side. The PVA gel takes up water and creates a chemical potential gradient between the dry gel and the outer region. This circumstance drives water across the membrane stack (Figure 12B).[59]

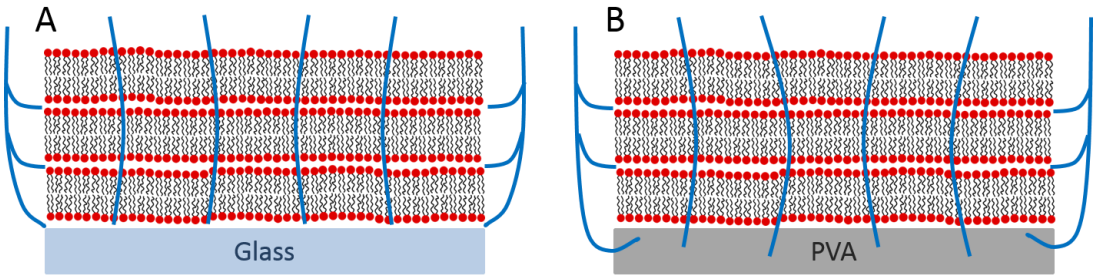

Figure 12: Water penetration pathways (blue lines) through a lipid bilayer stack deposited on (A) glass and (B) PVA gel. Adapted from [59].

The PVA gel-assisted method has the advantage that it is even faster than the electroformation and it avoids the risk that lipids degrade. Furthermore, the GUVs are free of polymer, which is a great advantage compared to the agarose gel-assisted process. Therefore, it is possible to encapsulate biomolecules, such as drugs, or other species in the GUVs with this method. Numerous lipids or lipid mixtures can be used in the PVA gel-assisted GUV formation to obtain defect-free vesicles.[59]

Even though the gel-assisted GUV formation methods already have many advantages compared to other methods, some problems remain. In case of the agarose gel-assisted method the substrate dissolves and remains in the vesicles. This is not the case for PVA as substrate, but with this method the size of the vesicles is not controllable. Giant vesicles are formed, especially when small vesicles fuse to larger ones, but the diameter of the GUVs ranges between 5 and 50 µm. For specific cell model experiments it would be helpful to generate GUVs, that have a defined diameter. Furthermore, the PVA gel is a physically cross-linked gel and does not stick to the glass surface. So the substrate cannot be used again. Ideally, the gel-assisted GUV formation could be done with a gel that is attached to the glass surface and shows all the advantages that the gel-assisted methods already have. As it is shown in the following, such a gel could be a polymer hydrogel, that is based on poly(*N*-isopropylacrylamide) (PNIPAAm).

3.1.4 Poly(*N*-isopropylacrylamide)

Poly(N-isopropylacrylamide), or short PNIPAAm, is one of the most widely used and known thermos-responsive polymers. Research on PNIPAAm deals with its solution properties, phase transitions or functionalization and its applications.[84–87] A simple search for this polymer in the chemical reaction database SciFinder results in 14687 references containing poly(N-isopropylacrylamide) (status January 18, 2018). Many research areas are interested in the molecule, so the studies and publications about PNIPAAm increased in the last decades, as summarized in Figure 13.

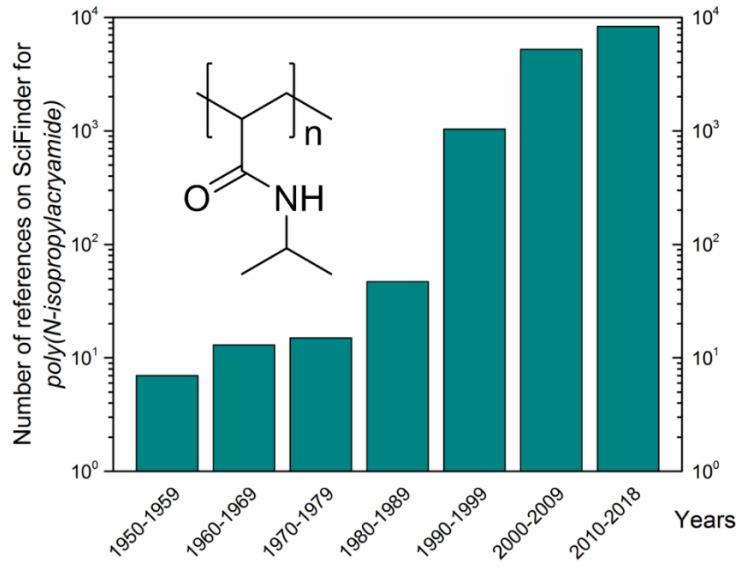

Figure 13: Number of references found for poly(*N*-isopropylacryamide) on the database SciFinder for the decades from 1950 until today, increasing exponentially (y-axis in logarithmic scale). The chemical structure of PNIPAAm is presented within the graphics.

To understand why PNIPAAm is so interesting, it is necessary to take a look at its chemical structure (Figure 13). PNIPAAm is a polymer that is composed of the monomer unit *N*-isopropylacrylamide (NIPAAm), which is an N-substituted acrylamide with an isopropyl group at its nitrogen atom. PNIPAAm is a hydrophilic polymer with a special property. It has a transition temperature close to the physiological temperature. The structure of PNIPAAm in aqueous solutions changes rapidly from a more hydrophilic to a more hydrophobic behavior between 30 and 35°C, which defines its lower

critical solution temperature (LCST).[86–89] In this transition, the hydrophobic isopropyl groups of the polymer and their local environment play the most important role. In water or other aqueous solutions, which are able to form strong hydrogen bonds, PNIPAAm is soluble. Temperature dependent interactions between the polymer and the solvent arise because of changes in the local environment around the hydrophobic isopropyl domains. Below the LCST, only water molecules surround the isopropyl groups, building hydrogen bonds, whereas above the LCST the isopropyl groups interact with the water molecules and with the polymer chain segments. Hence, above 35°C the hydrogen bonds are repealed and PNIPAAm phase separates and precipitates. PNIPAAm is a thermo-responsive polymer that shows inverse solubility upon heating.[86–89]

Poly(*N*-isopropylacrylamide) is known since the 1950s, when its monomer unit *N*-isopropylacrylamide (NIPAAm) was first synthesized and polymerized.[87,90] PNIPAAm can be synthesized by various methods, but the most widely used synthesis procedure is free radical polymerization.[87] In this procedure, the monomer NIPAAm is dissolved in an organic solvent and the reaction is started with an initiator molecule upon heating. Here, the initiation reaction generates free radicals, which are the active center from which the polymer chain is growing (propagation) by adding one monomer after the other to the radical chain. The polymer chains do not start simultaneously. The growing of the polymer chains can be stopped by recombination, disproportionation or conversion.[91]

The thermo-responsive PNIPAAm is of high interest for many research areas and a variety of applications. Depending on the architecture of the polymer, different studies have been published. If PNIPAAm is used as a solid it can be coated onto glass surfaces, which should then absorb and release water vapor as humidity sensors or for use in greenhouses.[87] In the biological field, PNIPAAm chains in solution could be used as immunoassay technology because of its thermos-responsive behavior in the physiological temperature regime.[92] The combination of PNIPAAm and polystyrene (PS) can give a fully reversible thermo-responsive block copolymer membrane.[93] Furthermore,

PNIPAAm can also occur in a micellar form. Together with polylactic acid PNIPAAm can control drug delivery from core-shell nano-sized micelles.[94]

As already mentioned in some of the application examples, the thermo-responsive property of PNIPAAm is often combined with the properties of another polymer unit. Hence, it is possible to combine two or more polymers to a copolymer. This can be a block copolymer, a grafted polymer or a statistical copolymer. One interesting candidate is a PNIPAAm-based terpolymer (polymerized from three different monomers), which is already used for a few years in different studies.[95,96] It is a statistical copolymer and the main part of this terpolymer is NIPAAm, to retain the temperature-responsive solubility behavior. The second monomer is methacrylic acid (MAA). This ionizable function is needed for a higher hydrophilicity. The polar MAA groups increase the swelling ratio and ensure a homogeneous swelling behavior.[95] The third part in the terpolymer is the hydrophobic molecule 4-methacryloyloxybenzophenone (MABP). The benzophenone group is needed to cross-link the terpolymer. MABP is photo-reactive, so aliphatic groups from the polymer chain react with the benzophenone moieties under UV (365 nm) irradiation.

Figure 14 shows the cross-linking mechanism: Through UV irradiation a photon absorbs and promotes one electron on the oxygen from a nonbonding sp^2-like n-orbital to the antibonding π^*-orbital of the carbonyl. The n-orbital on the oxygen is electron-deficient and interacts with the weak C-H σ-bonds. This results in hydrogen abstraction. The two new radicals rapidly recombine and form a new C-C bond and cross-link the two polymer chains.[97]

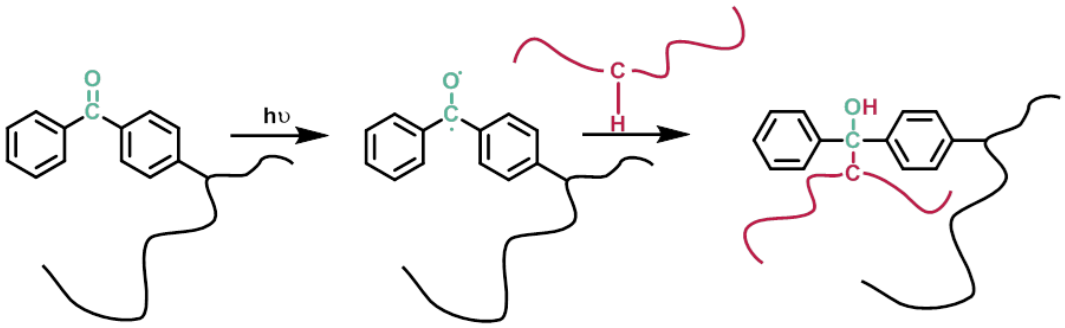

Figure 14: Photochemical cross-linking mechanism of benzophenone units by UV irradiation with 365 nm. UV light promotes one electron on the oxygen from a nonbonding sp^2-like n-orbital to the antibonding π^*-orbital of the carbonyl. The n-orbital on the oxygen interacts with the weak C-H σ-bonds, resulting in hydrogen abstraction. The two new radicals rapidly recombine and form a new C-C bond and cross-link the two polymer chains. Adapted from [97,98].

Once the terpolymer is irradiated with UV light, the benzophenone units of the MABP moiety react with the aliphatic groups and form a chemically cross-linked polymer network. This network can absorb a high amount of water by swelling into a hydrogel. Hydrogels are defined as materials that have the ability to swell in water and keep a high amount of water within their network structure due to the presence of high amounts of hydrophilic groups in the structure.[99] The PNIPAAm terpolymer has exactly this behavior. The network structure arises from the cross-linked benzophenone groups and the NIPAAm groups as well as the MAA groups are hydrophilic to retain the water inside the polymer. PNIPAAm hydrogels and many other hydrogels are often used in biomedical applications or bioscience studies, because their high water content leads to a good biocompatibility.[100–103]

3.2 Experiments und Materials

In this section, the chemicals and materials as well as the analytical setups that were used for this work are summarized. Furthermore, the chemical reactions and the experiments with all important parameters are described in detail.

3.2.1 Materials

4-Hydroxybenzophenone (98 %), anhydrous dichloromethane (DCM, ≥ 99.8 %), methacryloyl chloride (≥ 97 %), trimethylamine (TEA, ≥ 99 %), diethyl ether (≥ 99.7 %), sodium sulfate (Na_2SO_4, ≥ 99 %), anhydrous hexane (99 %), azobisisobutyronitrile (AIBN, 98 %) and anhydrous 1,4-dioxane (99.8 %) were purchased from Sigma-Aldrich and used as received. Ethanol (≥ 99.8 %) was purchased from VWR Chemicals and chloroform (≥ 99 %) from Acros Organics. Methanol (≥ 99.8 %) was purchased from Alfa Aesar. All solvents were used as received. Phosphate buffered saline (PBS), *N*-isopropylacrylamide (NIPAAm) and methacrylic acid (MAA) were purchased from Sigma-Aldrich. PBS was received as powder and dissolved in deionized water to obtain a 0.01 M solution with a pH of 7.4. *N*-isopropylacrylamide (NIPAAm) was recrystallized from toluene/hexane 1:1 and MAA was distillated before use. Phospholipids were purchased from Sigma-Aldrich as powders. 1,2-dioleoyl-*sn*-glycero-3-phosphocholine (DOPC) and 1,2-dioleoyl-*sn*-glycero-3-phosphoserine (DOPS) were dissolved in chloroform (c = 1 g/L). As fluorescent markers Atto488- and Atto633-labeled 1,2-dioleoyl-*sn*-glycero-3-phosphoethanolamine (Atto488-DOPE and Atto633-DOPE) were used and dissolved in DCM and methanol 4:1 (c = 1 g/L). Erythrosine was purchased from Sigma-Aldrich as a powder and diluted in PBS to a concentration of 50 µM. The synthesis of benzophenone triethoxysilane was performed by G. Kircher (MPI-P) according to the literature.[98]

3.2.2 4-Methacryloyloxybenzophenone (MABP)

10 g (50 mmol) of 4-hydroxybenzophenone were dissolved in 100 mL of DCM, the mixture was cooled in an ice bath and a solution of 5.1 mL (53 mmol) of methacryloyl chloride and 7.7 mL (56 mmol) of TEA in 20 mL of dry DCM were added dropwise. The reaction was stirred at room temperature for 4 h. The solvent was evaporated and the residue was dissolved in diethyl ether. The non-soluble triethylammonium salt was removed by filtration. The organic phase was washed with water three times and afterwards dried over Na_2SO_4. The solvent was evaporated and the crude product was chromatographed over DCM/hexane 7:3. The product was recrystallized from a mixture of DCM and hexane (1:4).

^{1}H NMR (CDCl3, δ): 2.01 (3 H, s), 5.74 (1 H, q), 6.32 (1 H, t), 7.15–7.22 (2 H, m), 7.37–7.48 (2 H, m), 7.48–7.57 (1 H, m), 7.69–7.76 (2 H, m), 7.76– 7.85 (2 H, m).

3.2.3 Functionalization of the Glass Substrates

Round microscope cover slides (diameter: 25 mm, thickness: 160 µm) were used as substrates for the polymer films. The glass slides were cleaned in an ultrasound bath, 4x 15 min (i) in a 2 vol% Hellmanex solution (Hellmanex® II, Hellma GmbH, Müllheim), (ii) in ultrapure water (Milli-Q water, 18.2 MΩ·cm) and (iii) 2x in ethanol. Afterwards the glass slides were stored for at least 24 h in a 6 % solution of benzophenone triethoxysilane in ethanol under argon in the dark. Finally, the slides were washed with ethanol and dried under vacuum for 1 h at 50 °C.

3.2.4 Poly(*N*-isopropylacrylamide) Based Terpolymer

10 g (88 mmol) NIPAAm, 380 mg (0.37 mL, 4.4 mmol) MAA and 235 mg (0.88 mmol) MABP were dissolved in 68 mL dioxane. Argon was flown

through the solution for 1 h. 67 mg (0.41 mmol) AIBN were added to the solution and the reaction was stirred at 60 °C under argon for 48 h. For purification, the reaction solvent was evaporated and the product precipitated from methanol in ice cold diethyl ether. The molecular weight of the product was M_w = 221 kg/mol and the polydispersity index is *PDI* = 1.55, as obtained from gel permeation chromatography.

3.2.5 Preparation of the Polymer Template

Polymer films were prepared from a 10 wt% PNIPAAm terpolymer solution in ethanol. The solution was spin-coated at room temperature onto the pre-functionalized round microscope glass substrates at a spinning speed of 2500 rpm for 30 s. After spin-coating the samples were solvent vapor annealed for 1 h in ethanol vapor and afterwards temperature annealed for 1 h at 170 °C in vacuum. Then, the samples were dried for 24 h at 50 °C under vacuum. The polymer was cross-linked and anchored to the glass substrate by irradiation with UV light (365 nm), using an LED (LCS-0365-02-22 High-Power LED Collimator Source, 365nm, 13W, 22mm aperture, Type-B). The distance between the light source and the sample was always kept to 13 cm. To homogenize the light, a glass diffuser (DGUV10-1500, Thorlabs, Newtown, USA) and a 12 cm tube were mounted between the LED and the sample holder. With this setup, 1 min illumination time corresponds to an energy dose of 1.68 J/cm² at the sample position.

For micro-patterning different photolithography masks (Table 2) with appropriate structure were positioned onto the samples.

The total irradiation energy dose for the cross-linking was 4.2 J/cm², 0.28 J/cm² without and 3.92 J/cm² with photolithography mask. Subsequently, the samples were rinsed with pure ethanol and dried at 50 °C for 1 h under vacuum.

3.2.6 Giant Unilamellar Anchored Vesicle (GUAV) Formation

Lipid solutions were stored at -20 °C before use. The final lipid solution for GUV formation was prepared from DOPC solution with 20 % DOPS and 0.5 % Atto488-DOPE. 30 µL of the lipid solution were added to the polymer sample. After evaporation of chloroform, 600 µL PBS were used to grow GUVs.

3.2.7 Confocal Laser Scanning Microscopy

Confocal laser scanning microscopy CLSM experiments were performed with a commercial setup (Carl Zeiss, Jena), consisting of an inverted microscope model Axiovert 200, the module LSM510 and a Zeiss C-Apochromat 40×/1.2 W water immersion objective. The Atto488-labelded lipids were excited with an argon ion laser with a wavelength of 488 nm. The samples were measured in Attofluor cell chambers at room temperature.

3.2.8 Determination of the Lipids Diffusion Coefficient via FCS

To the mixture of phospholipids for the GUAV formation 0.05 % Atto633-DOPE were added and the GUAVs were prepared as describes before. FCS experiments were performed on an LSM 880 (Carl Zeiss, Jena, Germany) setup. Excitation laser light was focused on the samples using a Zeiss C-Apochromat 40×/1.2 W water immersion objective. Emission was collected with the same objective and, after passing through a confocal pinhole, directed to a spectral detection unit (Quasar, Carl Zeiss). In this unit, emission is spectrally separated by a grating element on a 32 channel array of GaAsP detectors operating in a single photon counting mode. A HeNe laser (λ = 633 nm) was used for excitation of Atto633-labeled lipids and emission in the range from 650 to 696 nm was detected. An AttoFluor metal chamber was used as a sample cell. For each sample, 10 measurements (30 seconds

each) were performed. Obtained experimental autocorrelation curves were fitted with a theoretical 2D model function.[44]

3.2.9 Photo-Oxidation

For imaging an LSM 880 confocal laser scanning microscope (Carl Zeiss, Jena, Germany) was used. Atto488-DOPE lipids were excited by an argon ion laser with a wavelength of 488 nm. Excitation laser light was focused on the sample using a Zeiss C-Apochromat 40×/1.2 W water immersion objective. Emission light was collected with the same objective and, after passing through a confocal pinhole, directed to a spectral detection unit (Quasar, Carl Zeiss). In this unit, emission is spectrally separated by a grating element on a 32 channel array of GaAsP detectors operating in a single photon counting mode. For irradiation of the photo-oxidizer erythrosine a mercury lamp (HXP 120 C, FSet43wf) was used. Image analyzation was performed with the software ImageJ.

3.3 Results and Discussion

As explained above, the gel-assisted formation of giant unilamellar vesicles (GUVs) is a new, promising method that offers numerous advantages compared to classical methods. It is faster than the most widely used methods, such as electroformation, and does not require special and expensive equipment. Furthermore, a variety of different lipids can be processed to defect-free GUVs. The vesicles are free of gel polymer molecules, while various biomolecules can be purposefully encapsulated. However, this method has two main disadvantages: (i) the physical polymer gel is not permanently attached to the glass substrate and thus can be only used once and (ii) the formed GUVs are polydisperse, their size can not be controlled or tuned. The following section describes a PNIAAm-based hydrogel system that overcomes both disadvantages and can be used for the preparation of uniform giant unilamellar vesicles with pre-defined size.

3.3.1 Preparation of Flat PNIPAAm Terpolymer Films

The PNIPAAm terpolymer was synthesized by free radical polymerization with the initiator AIBN using 94 % NIPAAm, 5 % MAA and 1 % MABP (Figure 15) with a yield of 80 %. The synthesis via free radical polymerization resulted in a statistical polymer whose monomer units are randomly distributed.

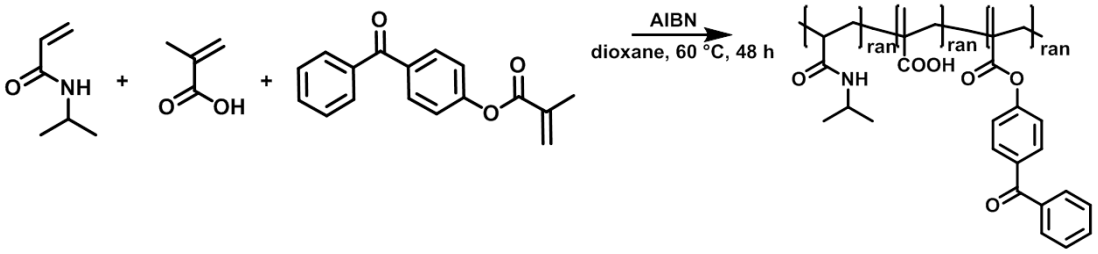

Figure 15: Free radical polymerization scheme of NIPAAm, MAA and MABP copolymerized in dioxane at 60°C for 48 h, using AIBN as initiator. The product is a PNIPAAm-based terpolymer.

The amount of the cross-linking unit MABP is only 1 %, meaning that the molecular weight of the final polymer needed to be higher than 113 kg/mol to ensure that at least ten cross-linking units were present in each polymer chain to obtain a sufficient network as soon as the polymer was cross-linked. The polymer was synthesized with M_w = 221 kg/mol and a polydispersity index *PDI* of 1.55. This molecular weight was high enough to build a sufficient network after cross-linking, because statistically around 20 cross-linking units are present in each polymer chain.

This work was based on the previously published gel-assisted methods for giant vesicle formation and had the goal to improve them.[59,83] These methods were based on gel-films on glass substrate. In this work, the PNIPAAm terpolymer was spin-coated from a 10 wt% solution in ethanol on glass substrates to gain a polymer film with a thickness of about 1 µm.

In contrast to the existing gel-assisted methods, the PNIPAAm hydrogel was anchored to the supporting glass substrate. To this end, the glass substrates were functionalized before usage. The functionalization was needed to covalently bind the polymer chains to the functional groups on the glass support upon UV irradiation.[104,105] The glass surface was coated with benzophenone units, which react with the polymer chains trough UV light activation as described in section 3.1.4. The glass surface was covered with a benzophenone-functionalized silane through self-assembly, resulting in replacement of the alkoxy groups of the silane by the hydroxyl groups of the glass, forming covalent Si-O-Si bonds.[98] This process was easily done by placing cleaned glass substrates in an ethanolic solution of benzophenone silane. Numerous glass substrates were functionalized in one step.

After spin-coating the PNIPAAm films to the functionalized glass substrates, one more step was required: solvent vapor annealing. Laying the sample in a closed chamber with ethanol vapor, resulted in partial re-solubilization of the film and flattening of the surface. The solvent vapor annealing process was of high importance to reduce the roughness and to gain a flat film surface, because it was necessary for the subsequent procedure: The UV light in the cross-linking step should arrive perpendicular to the film surface

and the application of the lipids required a very flat surface for a plain lipid distribution. After solvent vapor annealing, the PNIPAAm terpolymer film was temperature annealed to obtain a completely dry and homogeneous sample.

The film preparation procedure was finalized with the cross-linking step. Irradiation of the polymer film with UV light activated the benzophenone groups (Figure 14, section 3.1.4) both in the polymer chain and on the functionalized glass, resulting in cross-linked polymer chains and anchoring the polymer to the glass. The cross-linking steps generated a chemically cross-linked and anchored polymer network, improving the GUV formation method that was based on the physically cross-linked PVA gel that loosens from the glass substrate.

The addition of water to the cross-linked PNIPAAm terpolymer film led to swelling into a hydrogel. In general, the swelling behavior depends on the amount of water or aqueous solution, which the polymer network can hold and therefore depends on its cross-linking density. Since the gel was anchored to the glass surface, the hydrogel stayed in the exact position on the glass.

3.3.2 Properties of Flat PNIPAAm Terpolymer Films

The PNIPAAm based terpolymer film, consisting of 94 % NIPAAm, 5 % MAA and 1 % MABP, was cross-linked via UV irradiation to a chemically cross-linked polymer network. The polymer film was colorless and had a thickness of h_d = 1.1 µm in the dry state. An important step in the film preparation procedure was the solvent vapor annealing of the film surface, as explained in section 3.3.1. Without this solvent annealing the surface of the polymer film showed a high roughness with height difference up to 0.35 µm, which were more that 30 % of the film thickness (Figure 16A). After the solvent annealing process (Figure 16B) the surface was much smoother and the height difference was less than 0.09 µm (< 8 % of the film thickness).

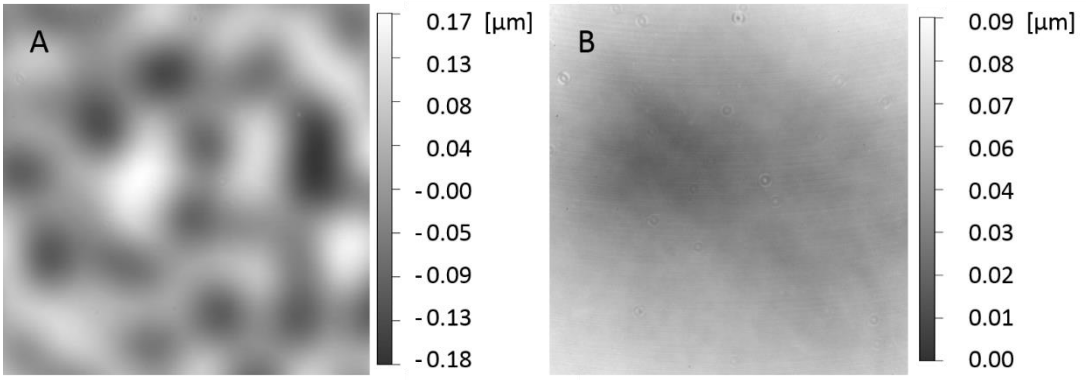

Figure 16: Surfaces of PNIPAAm terpolymer films, prepared (A) without and (B) with solvent vapor annealing. Images (320x320 µm) were taken with a white light confocal microscope based profilometer (NanoFocus®, µSurf®, NanoFocus AG, Oberhausen).

By the addition of water or aqueous solutions to the polymer film, the system swells into a hydrogel and absorbs the added water inside the polymer chain network, whereas the whole network extends (Figure 17).

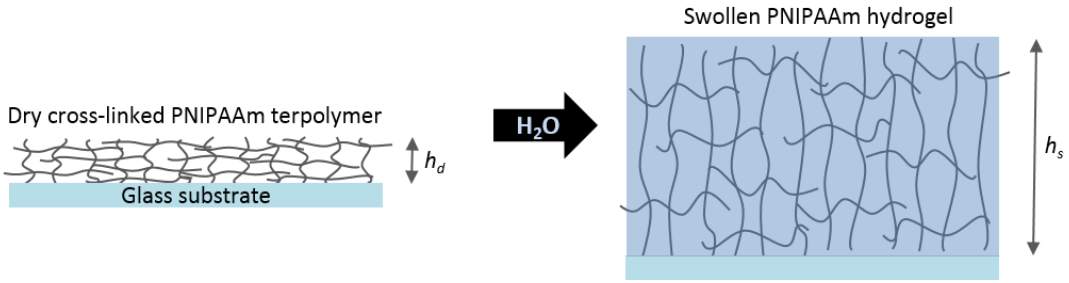

Figure 17: Swelling scheme. The dry terpolymer film with a thickness h_d was anchored to the glass substrate and swelled into a hydrogel upon addition of water. The polymer chains extended to absorb the water inside the network with the thickness h_s of the swollen polymer film.

Since the polymer is cross-linked to the glass substrate, the dry film as well as the hydrogel were anchored to the glass. Therefore, the swelling process was mainly in one direction: vertically upwards. On the bottom the gel swelling was hindered by the glass. In the horizontal direction the swelling was hindered, because the polymer chains are fixed to the glass and the gel can only extend little. The anchored parts of the polymer confined it in the swelling process.

The energy dose that was used to cross-link the polymer can vary, resulting in different cross-linking degrees and therefore in different swelling behavior

of the hydrogel. The less the polymer chains were cross-linked (low energy dose), the weaker was the network, the more the gel could swell. The thickness of the swollen polymer h_s was determined by z-scans performed on a confocal microscope (LSM510, Zeiss, Jena) in the fluorescence mode. Therefore, the fluorescent tracer dye Rhodamine 6G was added to the hydrogel. This weakly hydrophobic dye interacted with the hydrophobic segments on the polymer chains of the hydrogel and partitions more into the gel than in the supernatant water above it.[96] By z-scanning from the glass surface through the gel, into the supernatant aqueous solution, there was a visible difference in fluorescence intensity and the thickness h_s of the gel could be determined. The ratio between the thickness h_s in the swollen state and the thickness in the dry state h_d is defined as the swelling ratio R_s. The polymer films were cross-linked with various energy doses to obtain different swelling ratios (Figure 18). The minimum energy dose v that was needed for this polymer to anchor it to the glass and to create a chemically cross-linked network was $v \approx 0.2$ J/cm². In this case, the hydrogel was weakly cross-linked and it is not possible to determine the hydrogel thickness, because the Rhodamine 6G concentration difference between the gel and the supernatant was not observable anymore. But, it is proved that the polymer was cross-linked, because it was already attached to the glass and could not be removed by rinsing with ethanol, which would be the case for non-cross-linked polymer. And if this low energy dose activated the benzophenone units on the glass surface it also activated the benzophenone units in the polymer. Below the energy dose of $v \approx 0.2$ J/cm² the polymer was completely removed from the glass by rinsing with ethanol. The lowest swelling ratio for this terpolymer hydrogel is 2.4. It needed an energy dose of $v \approx 84.6$ J/cm². In this state, the polymer network was as dense as possible.

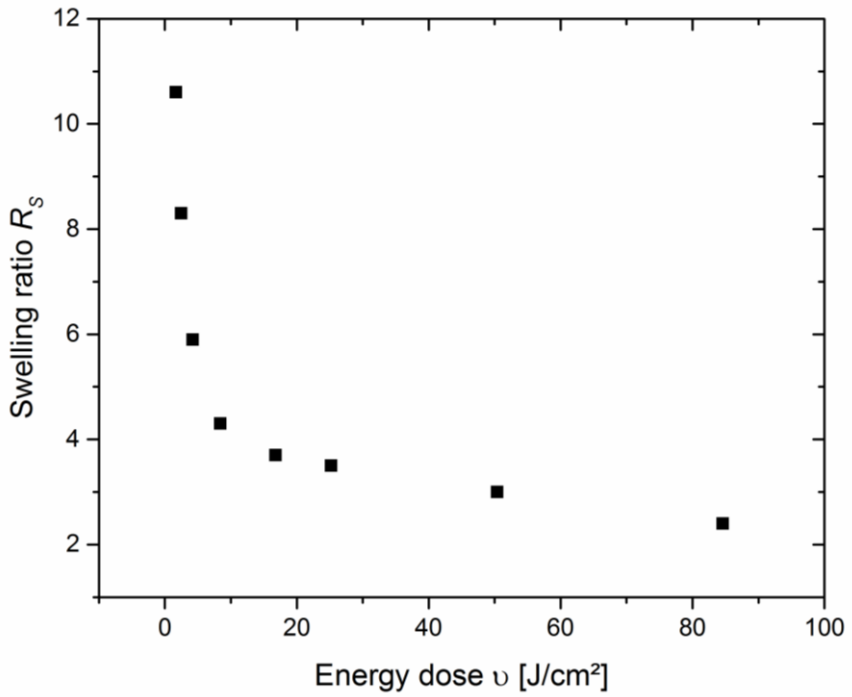

Figure 18: Swelling ratios R_s for flat PNIPAAm terpolymer hydrogel films at different cross-linking energy doses v. Below 5 J/cm² a linear dependency was observed, caused by a fast consumption of benzophenone units and efficient cross-linking. Above 5 J/cm² less benzophenone units remained for cross-linking and further cross-linking was less efficient.

In the low energy range (v < 5 J/cm²) was a linear dependency of the swelling ratio on the energy dose, caused by a fast consumption of benzophenone units and efficient cross-linking. This linear dependency in the lower energy regime was also described in the literature.[106] In the higher energy range (v > 5 J/cm²), less benzophenone units remained for cross-linking, resulting in slower and less efficient further cross-linking.

Table 1 summarizes the energy dose that was used for cross-linking and the resulting swelling ratios and polymer volume fractions ($\varphi = 1/R_s$) of the PNIPAAm terpolymer films.

Table 1: Energy doses *v*, that were used for the cross-linking of PNIPAAm terpolymer films, resulting swelling ratios R_s and polymer volume fractions φ.

Energy dose v [J/cm²]	Swelling ratio R_s	Polymer volume fraction φ
1.7	10.6	0.09
2.5	8.3	0.12
4.2	5.9	0.17
8.4	4.3	0.23
16.8	3.7	0.27
25.2	3.5	0.29
50.4	3.0	0.33
84.6	2.4	0.42

With the PNIPAAm based terpolymer hydrogel there was already a huge variety in the swelling behavior. It was tuned by adjusting the energy that was used in the cross-linking step. To change the cross-linking density even more, another possibility could be to polymerize more benzophenone units into the terpolymer. The more cross-linking units are present, the denser the network would be. This was not necessary for this work, so no further studies were performed in this direction, but it is a possibility for other purposes.

3.3.3 GUV Formation on Flat PNIPAAm Terpolymer Films

For the preparation of giant unilamellar vesicles via a gel-assisted method, a solution of lipids was essential. Within this work the main lipid component was 1,2-dioleoyl-*sn*-glycero-3-phosphocholine (DOPC, see Figure 8A). The second lipid type that was used in this work is 1,2-dioleoyl-*sn*-glycero-3-phosphoserine (DOPS, see Figure 8B). These types of lipids were used, because they are major components of biological cell membranes. To make the lipids and GUVs visible for confocal laser scanning microscopy (CLSM), a third kind of lipids was added – an Atto488-labeled 1,2-dioleoyl-*sn*-glycero-3-phosphoethanolamine (Atto488-DOPE). This is a commercially available labeled lipid and perfectly suitable for CLSM imaging. The lipids were used from a chloroform solution with 80 % DOPC and 20 % DOPS. The amount of labeled lipids was 0.5 %.

To generate GUVs, the first step was to add the lipids by dropping 30 µL lipid-chloroform solution to the polymer surface. The chloroform drop evaporates very fast and a layer of lipids is created on the surface. The second step is the addition of an aqueous solution and leads to self-assembling of the lipids into bilayers, to the swelling of the polymer gel and to the formation of GUVs. As hydration solution phosphate buffered saline (PBS) is used instead of water to simulate physiological conditions, which are important when dealing with cell membrane models. The generated GUVs can be observed by CLSM imaging as shown in Figure 19.

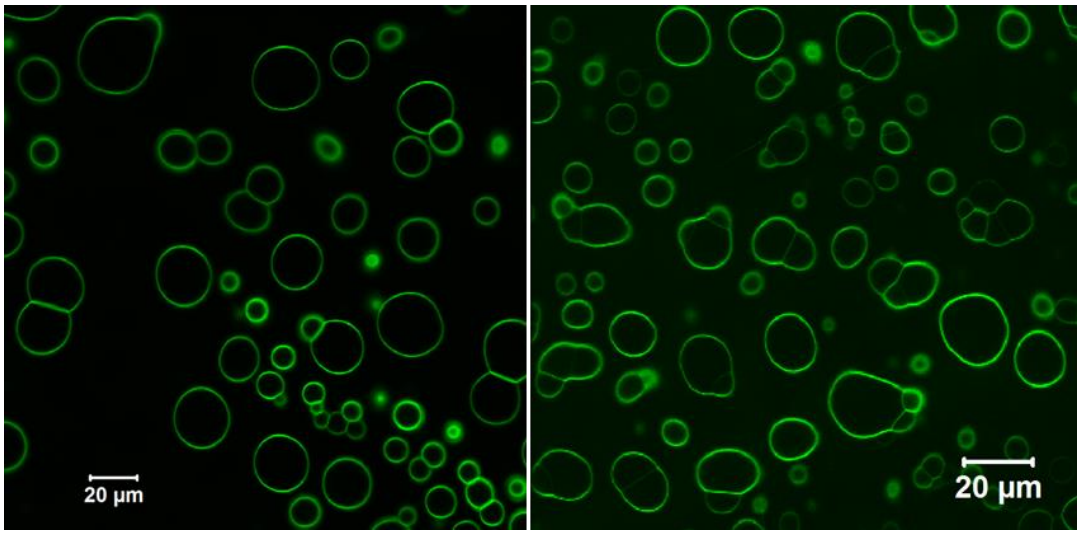

Figure 19: Confocal laser scanning microscopy (CLSM) images of DOPC/DOPS-GUVs labeled with 0.5 % Atto488-DOPE, grown on PNIPAAm terpolymer films.

The vesicles grow within less than 5 minutes to diameters between 5 µm and 25 µm. If they are fully grown, they have a spherical shape, but it is clearly observable in Figure 19 that some vesicles are in contact with others and in some cases, they merge to one big vesicle. The vesicles are unilamellar, because in the CLSM studies the intensity of the lipid membranes are always the same, which would not be the case if there were mono-, bi- or multilamellar membranes.

Compared to previous studies about gel-assisted GUV formation, the prepared GUVs are comparable in size and growing speed.[59,83] The advantage here is the chemically cross-liked hydrogel, because it does not

dissolve in the buffer solution and stays exactly at its position on the glass substrate. The PNIPAAm terpolymer represents a perfect template to prepare GUVs, because it is a chemically cross-linked and anchored hydrogel, on which the formation of GUVs is easy and fast.

The PNIPAAm terpolymer gel enables the formation of GUVs, but their formation and especially their size strongly depend on the cross-linking density of the polymer gel (Figure 20). When GUVs are formed on polymer gel with a low cross-linking density (energy dose: 4.5 J/cm²), the GUVs show sizes between 3 µm and 20 µm (Figure 20A). Higher cross-linking density (60 J/cm²) results in much smaller vesicles with diameters between 1 µm and 3 µm (Figure 20B).

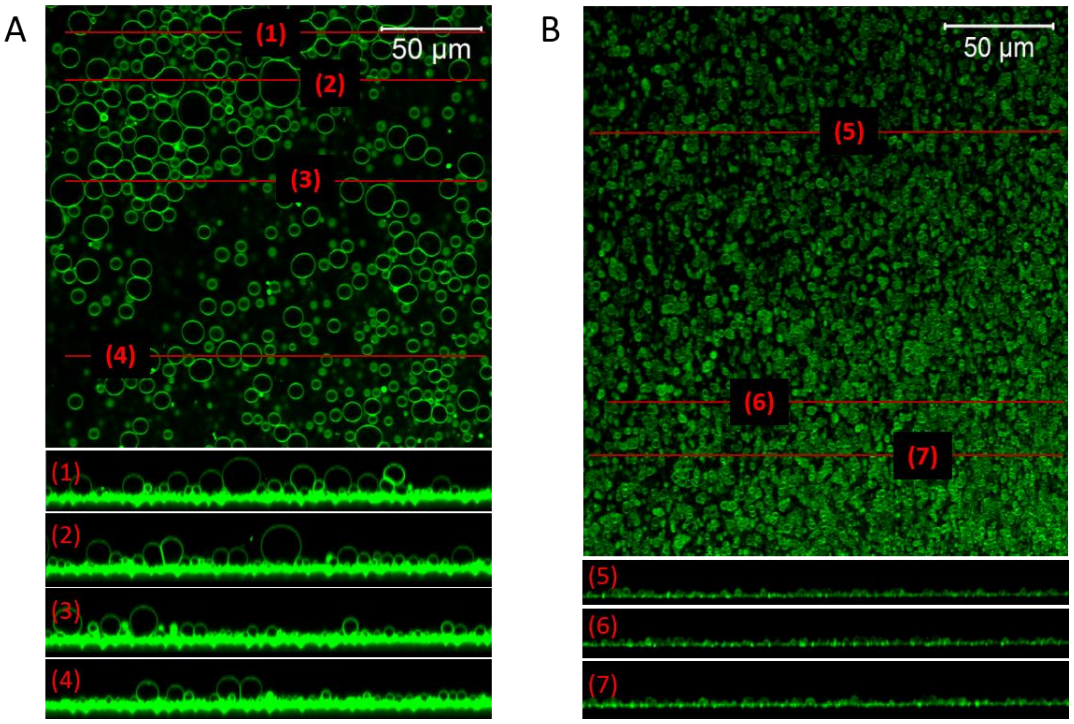

Figure 20: CLSM images of GUVs, formed on differently cross-linked PNIPAAm terpolymer gels. (A) Cross-linked with an energy dose of 4.5 J/cm². Resulting GUV diameters are between 3 µm and 20 µm. x-z-plane images were taken at several positions (1)-(4). (B) Cross-linked with an energy dose of 60 J/cm². Resulting GUV diameters are between 1 µm and 3 µm. x-z-plane images were taken at several positions (5)-(7).

A possible reason for the different GUV diameters could be, that the lipids are able to diffuse inside the polymer gel. The mesh size of the polymer network is large for weakly cross-linked polymer. The polymer volume

fraction is around 10 % for the sample from Figure 20A, so the amount of aqueous solution is very high and the network very wide. Hence, the lipids have enough space to diffuse into the gel. The less lipids remain on the polymer surface, the less material remains for the vesicle formation, so the vesicles grow larger. The lipids inside the gel are also the reason why the polymer gel looks green in x-z-CLSM images. The polymer is not labeled, but the lipids are and they are inside the polymer gel.

3.3.4 Preparation of Patterned PNIPAAm Terpolymer Films

As already discussed, the PNIPAAm-based method to prepare GUVs is very successful and exhibits advantages to other methods. The aim of this work was the size-defined formation of GUVs. If GUVs are used as cell membrane models, it would be very advantageously if the size of the vesicles can be defined during the preparation process. This could be achieved by growing the vesicles on a patterned polymer gel.

Therefore, the PNIPAAm terpolymer film is prepared as described in section 3.3.1: a thin film is generated by spin-coating an ethanolic PNIPAAm terpolymer solution on a functionalized glass substrate. The difference lies in the cross-linking step. A pattern is generated on the polymer film by micro-patterning via structured illumination with a photolithography mask. For this procedure the before mentioned solvent annealing step is even more important. Because for the photolithography, the mask is laying directly on the polymer surface. It is important that the film is completely flat, so that the photolithography mask is in full contact with the polymer. Only if this is the case, the UV light illuminates only the parts of the film, which are not covered by the mask.

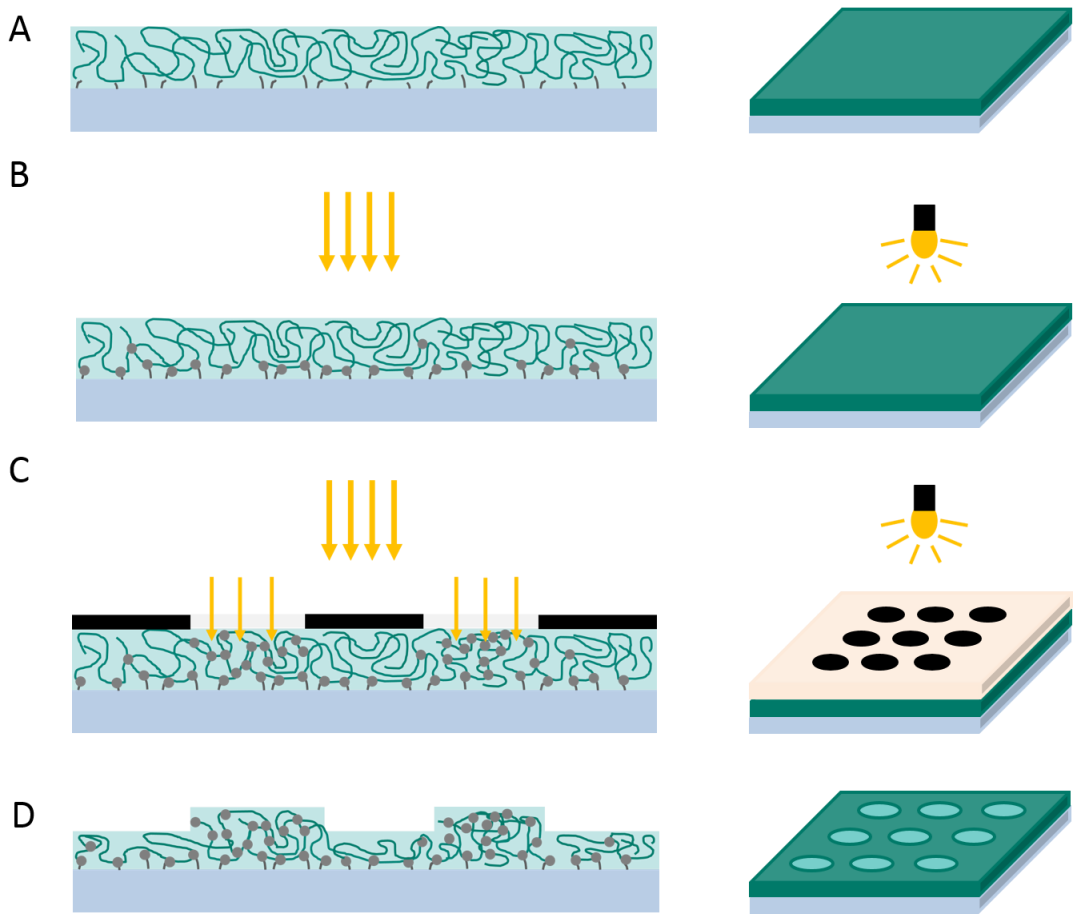

Figure 21: Schematic micro-patterning procedure via photolithography of PNIPAAm terpolymer films. (A) PNIPAAm terpolymer film on a functionalized glass substrate. (B) Anchoring of the PNIPAAm terpolymer film to the glass substrate and weak cross-linking via UV irradiation (365 nm, 0.28 J/cm²). (C) Patterning by UV irradiation through the non-covered glass of a photolithography mask (365 nm, 3.92 J/cm²). Polymer chains below the mask do not cross-link further, but illuminated polymer chains cross-link further via their benzophenone units. (D) Rinsing with ethanol removes non-cross-linked polymer, leading to a PNIPAAm terpolymer film with a defined hole pattern.

First, the polymer film is illuminated with UV light for a short period of time or a low energy dose, respectively. The energy dose is $\upsilon \approx 0.28$ J/cm², which is high enough to cross-link a few benzophenone units within the polymer and to anchor the polymer to the glass (Figure 21B). In the next step, the pattern is created by illumination with the same light source through a photolithography mask (Figure 21C). This mask covers the parts of the polymer film, which do not need further illumination and cross-linking. Therefore, an energy dose of $\upsilon \approx 3.92$ J/cm² is needed. The non-covered parts are illuminated further, to cross-link the polymer even more and therefore

create areas in the polymer film with different cross-linking densities. After the illumination all uncross-linked and not anchored polymer is removed by rinsing the film with ethanol. This process results in a polymer film with holes in a defined pattern with defined diameters (Figure 21D).

The procedure to form the patterned PNIPAAm films is straight forward and not very time consuming. The UV illumination step takes around three minutes and the rinsing with ethanol to remove non-cross-linked parts of the film take three more minutes. To dry the film completely one hour in the vacuum oven is necessary, but then the film is ready to be used. The final patterned PNIPAAm terpolymer sample shows a defined pattern with holes in the dry film that have a weakly cross-linked polymer layer on the bottom (Figure 22).

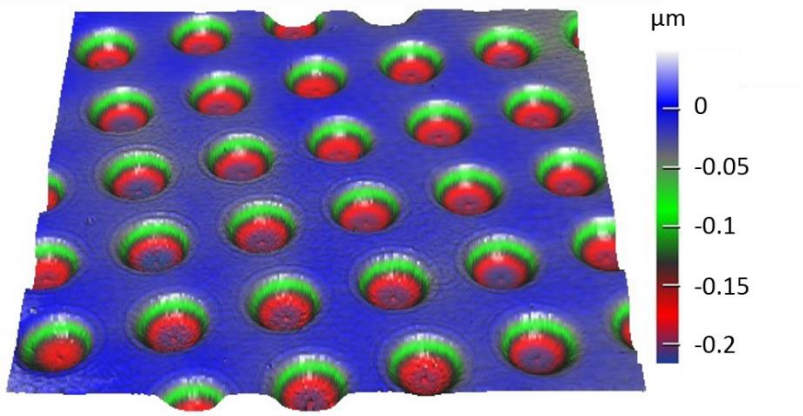

Figure 22: 3D image of a PNIPAAm terpolymer film that was micro-patterned via photolithography with a special photolithography mask. Images were taken with a white light confocal microscope based profilometer (NanoFocus®, µSurf®, NanoFocus AG, Oberhausen).

The PNIPAAm terpolymer is ideal to create GUVs on flat films, but due to the possibility to cross-link it chemically, a pattern can be created. This is a great advantage compared to previous gel-assisted GUV formation methods.

3.3.5 Properties of Patterned PNIPAAm Terpolymer Films

In general the properties of the patterned polymer film are comparable to the flat film. The PNIPAAm terpolymer film consists of 94 % NIPAAm, 5 % MAA and 1 % MABP and was cross-linked via UV irradiation. The polymer film was colorless, attached to a round glass substrate (diameter 2.5 cm), had a round shape with a diameter of 1 cm and had a thickness of h_{df} = 1.1 µm in the dry state. But the important property and difference to the flat film is the pattern on the surface of the polymer film. As shown in Figure 22, the film had a defined pattern with round shaped holes. These holes had a depth of 0.4 µm in the dry state, or a remaining film thickness of h_{dh} = 0.7 µm.

The thickness was not the only difference. Due to the short term cross-linking in the beginning of the micro-patterning procedure, the cross-linking densities were different in the holes compared to the rest of the film. The difference in cross-linking, resulted in different swelling behavior. Because of the pattern in the polymer film and in this regard because of the different areas of cross-linking density, the hydrogel swelling was predestinated by the pattern. The highly cross-linked areas of the film showed a weaker swelling then the less cross-linked parts (defined as holes in the dry state of the polymer film). In the state of a completely swollen gel, the predefined pattern was vice versa. The parts, that had been holes in the dry film pattern, were pillars in the hydrogel (Figure 23). This treatment resulted in a swelling ratio of $R_{S,\,film} \approx 8$ for the stronger cross-linked polymer film and a swelling ratio of $R_{S,\,pattern} \approx 20$ for the weaker cross-linked pattern.

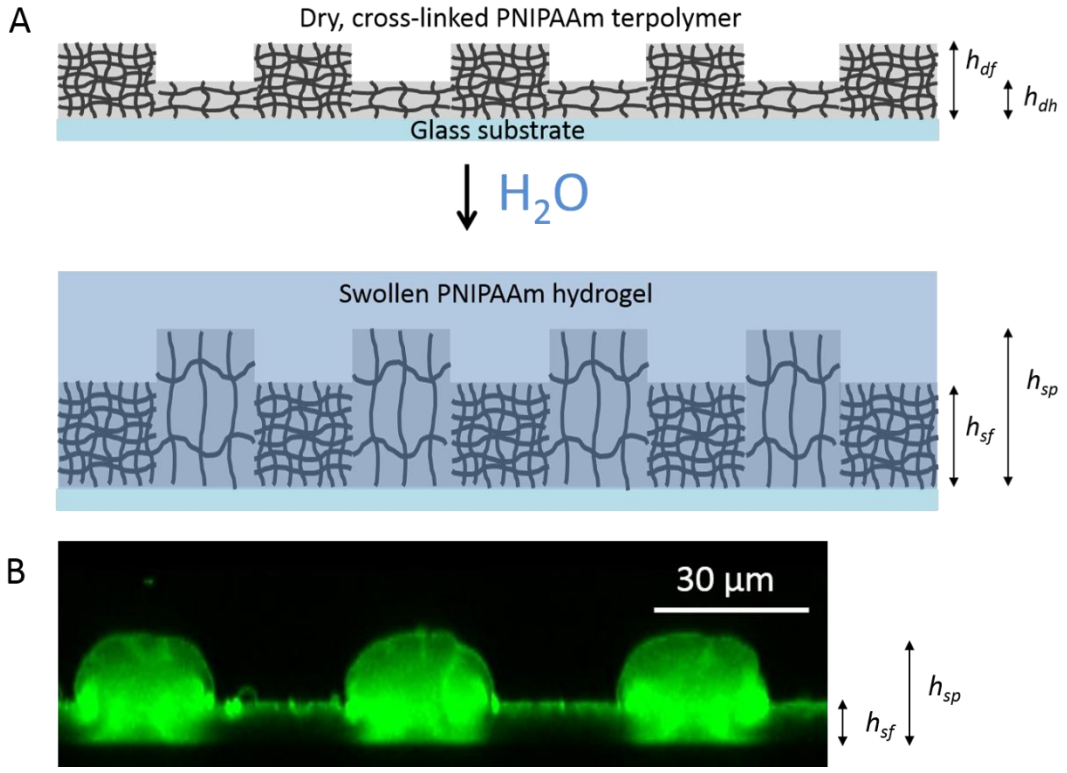

Figure 23: (A) Scheme of the swelling behavior of the micro-patterned PNIPAAm terpolymer film. Strongly cross-linked areas (h_{df} – height of the dry film) swell less (h_{sf} – height of the swollen film) upon addition of water compared to weakly cross-linked areas (h_{dh} – height of the polymer layer below the dry holes), which swell into a pillar pattern (h_{sp} – height of the swollen pillar). (B) CLSM image (x-z-plane) of a swollen patterned PNIPAAm terpolymer film in PBS, labeled with Atto488-dye. The swelling ratio of the film is $R_{S,f}$ = 8 and the swelling ratio of the pillars is $R_{S,p}$ = 20.

The principle that is pictured in Figure 23A was working as shown in Figure 23B. The weakly cross-linked parts (bottom of the holes in the dry state) swelled much more compared to the rest of the film. The shape of the forming pillars was not perfect cylindrical, but behaved as expected and was suitable to generate vesicles.

3.3.6 GUV Formation on Patterned PNIPAAm Terpolymer Films

The giant unilamellar vesicles (GUVs) were formed from DOPC and DOPS lipids, labeled with Atto488-DOPE lipids as described in section 3.3.3. The lipid application procedure was the same and the polymer together with the dried lipids was swollen with PBS. The idea was to grow vesicle on top of the

patterned polymer gel, on the areas that swell into pillars and remain in the same size as the pillar diameter. Experiments on flat PNIPAAm terpolymer film showed, that GUVs grow better on weakly cross-linked gel areas with swelling ratios above 10. Therefore, the GUVs formed on the weakly cross-linked pillars. Their size defined the maximum size of the vesicles. Within 5 min the gel swelled to a thickness of around 9 µm with a pillar size of about 15 µm and numerous vesicle formed (Figure 24). Vesicle formation speed was comparable to that observed on PVA-gels or agarose substrate.[59,83]

With the patterned PNIPAAm terpolymer films it was possible to generate hundreds of uniform GUVs with a diameter size that was defined by the polymer pattern (Figure 24A). The vesicles grew on the polymer pillar top and their growing was restricted by the pillar diameter. Hence, every polymer pillar hosted one GUV (Figure 24B/C). A few small vesicles also grew on the film surface and on the pillar side surface. These vesicles were very small compared to the GUVs and are in the size range of LUVs. The GUVs on the pillars showed diameters that were comparable to the pattern sizes. When the pattern diameter of the photolithography mask was 30 µm, the formed vesicles had a diameter of 30.9 ± 2.4 µm. This PNIPAAm-based technique can create GUVs with desired diameters to use them as cell membrane models. The advantage of this method is not only the fast, easy and size-defined preparation of GUVs, but also the fact, that the vesicles were anchored to the polymer substrate. The so-called giant unilamellar anchored vesicles (GUAVs) did not need to be immobilized for further studies, because they were already attached to the polymer during the formation. With an array of hundreds of vesicles different studies could be performed simultaneously (see section 3.3.8).

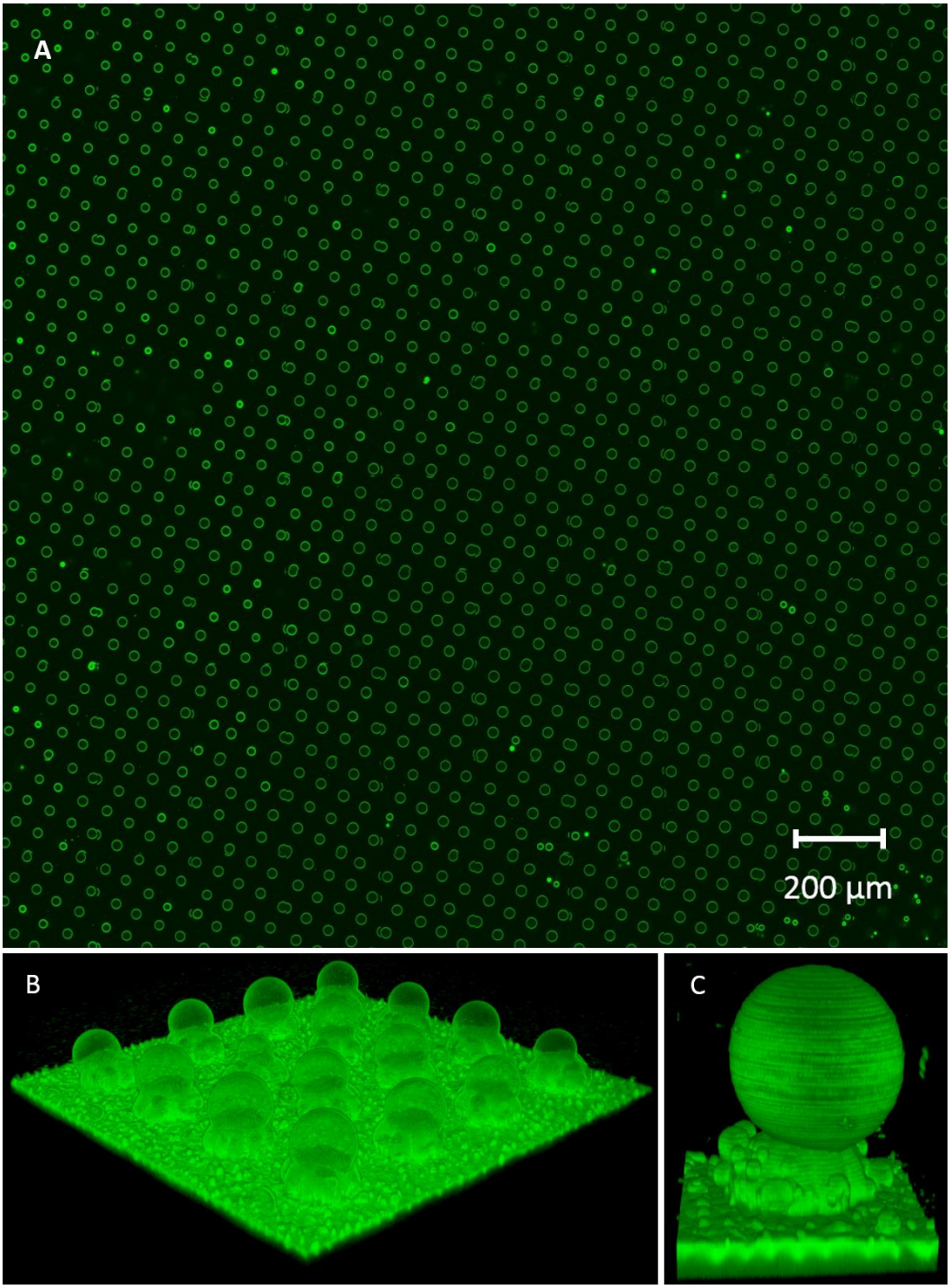

Figure 24: CLSM images of DOPC/DOPS GUVs formed on micro-patterned PNIPAAm terpolymer films. (A) 2D image of an array of hundreds of uniform GUVs. (B) 3D image of a 4x4 array of swollen PNIPAAm terpolymer pillars with GUVs formed on the top of the pillars. (C) 3D image of a single GUV on a PNIPAAm hydrogel pillar.

3.3.7 Size Control

The diameter of the vesicles was defined by the micro-patterned PNIPAAm terpolymer film. The growing process was limited to the surface area of the pre-defined pattern, which was the top of the pillars. Consequently, the size of the swollen polymer pattern defined the size of the GUVs. Within this study, three different pattern sizes and vesicle diameters were prepared. The diameters were chosen in the range of cell and cell membrane sizes to obtain ideal models for cell membrane experiments. Defined by the photolithography mask, the pattern diameters were 15 µm for mask 1, 30 µm for mask 2 and 50 µm for mask 3 (see Table 2). The distances between the centers of the patterns were 40 µm for mask 1, 60 µm for mask 2 and 100 µm for mask 3. For every pattern GUVs were prepared. The mean diameter for GUVs on the 15 µm pattern was 17.6 ± 2.9 µm, on the 30 µm pattern it was 30.9 ± 2.4 µm and on the 50 µm pattern it was 46.4 ± 2.4 µm. Figure 25 shows the results of the new method for PNIPAAm gel-assisted formation of GUVs. Their size was comparable to the pattern size, giving the ability to create vesicles that are uniform and have a desired size between 15 and 50 µm.

Table 2: Specifications of the photolithography masks for micro-patterning of the PNIPAAm terpolymer films.

Mask	Pattern diameter *a* [µm] 	Pattern distance *d* [µm] 
1	15	40
2	30	60
3	50	100

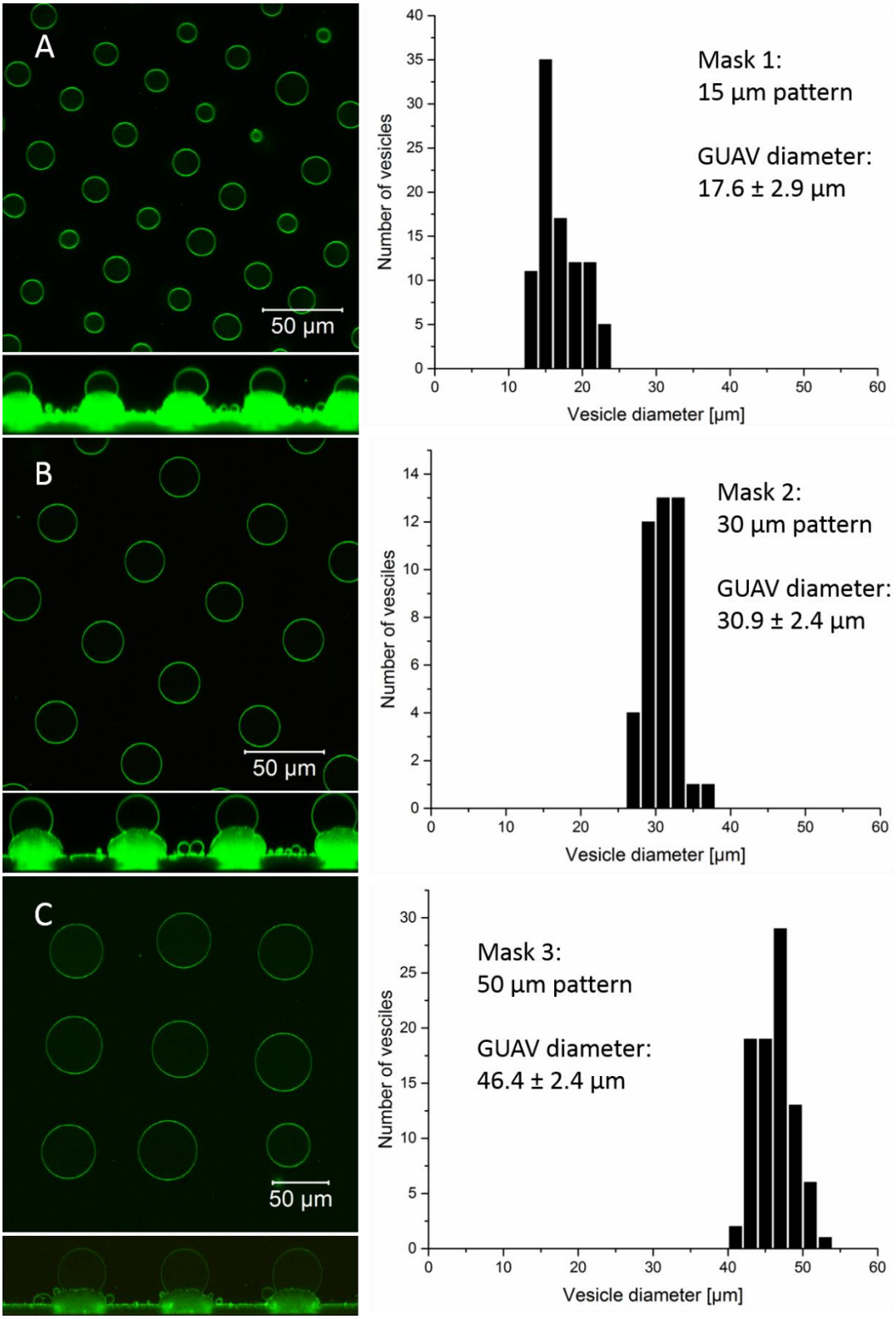

Figure 25: Left: CLSM images (x-y-plane and x-z-plane) of uniform giant unilamellar vesicles prepared by PNIPAAm gel-assisted swelling for (A) 15 µm, (B) 30 µm and (C) 50 µm pattern size. Right: Histograms of the vesicle size distribution.

The PNIPAAm gel-assisted formation of GUVs has several advantages compared to other methods. As already explained, the polymer film cannot dissolve in the solvent, because it is an anchored network. That means there is no freely diffusing polymer inside the GUVs as it was the case for GUV preparation with agarose gel. Furthermore, this method enables the formation of hundreds of uniform and size defined vesicles within a few minutes. The next advantage of this technique is the immobilization of the vesicles. Usually the immobilization of GUVs as cell models is a big challenge, but with this method, the vesicles were already in a controlled position, anchored to the PNIPAAm substrate. This new type of giant unilamellar anchored vesicles (GUAVs) easily enables further investigations on an array of hundreds of vesicles simultaneously.

3.3.8 Applications

With the PNIPAAm gel-assisted method, size-defined giant unilamellar anchored vesicles were prepared. Hundreds of vesicles were in a defined and controlled position. The GUAVs did not move or flow in the solution, which is an advantage compared to cell-mimicking GUVs that were prepared with other methods, such as electroformation. These GUVs needed to be immobilized after their preparation of perform further experiments.

This chapter shows two different application examples for giant unilamellar anchored vesicles (GUAVs). The first application used the advantage that the vesicles were immobilized and did not move from their position. Hence, fluorescence correlation spectroscopy measurements could easily be performed to determine the diffusion coefficient of the lipids in the membrane. The second example used the advantage to have tens or hundreds of GUAVs immobilized and together in order to investigate the photo-oxidation behavior of the lipids in the membrane.

Application 1: Investigating the Diffusion of DOPE lipids in Giant Unilamellar Anchored Vesicles

Biological membranes are not only a barrier between the exterior and interior of cells, but also segregate into specialized functional domains.[107,108] The membrane forms a structural matrix, providing mechanical stability.[107] Already in 1972 Singer and Nicolson described the importance of understanding the dynamics of cell membranes.[109] The diffusion coefficient of membrane lipids belongs to the most important parameters regarding the dynamical studies, because it is closely related to the structure of the biological membrane.[107] To characterize the diffusion of lipids in biological membranes or membrane models, various experimental techniques are useful. Mainly, fluorescence correlation spectroscopy is used, but fluorescence recovery after photobleaching, single particle tracking or nuclear magnetic resonance measurements are other possible methods.[107,110]

Herein, fluorescence correlation spectroscopy (FCS) measurements were used to investigate the dynamics of the GUAV lipid bilayer that represents the cell membrane.[44] For these measurement 0.01 % of fluorescently labeled lipids (Atto633-DOPE: Atto633-1,2-dioleoyl-*sn*-glycero-3-phosphoethanol-amine) were added to the standard lipid mixture that was used for the GUAV formation. Via confocal laser scanning microscopy and *z*-scanning in the fluorescence mode, the laser beam was focused on the membrane. Once the focus was fixed, measurements could be performed for several minutes in the same position, because the vesicle membrane did not move and the only diffusion was coming from the lipids inside the membrane. Measurements were done in three different samples and 12 different vesicles. Figure 26 represents an autocorrelation (AC) curve of the DOPE lipid diffusion in the GUV membrane, as determined by FCS measurements. The experimental autocorrelation curve was fitted with a single component model, showing only one type of species diffusing in the membrane. The diffusion coefficient of this species was found to be $D = 1.01 \cdot 10^{-11} \pm 0.14 \cdot 10^{-11}$ m^2/s, which is in the same order of magnitude as described in the literature for comparable systems.[107,111,112]

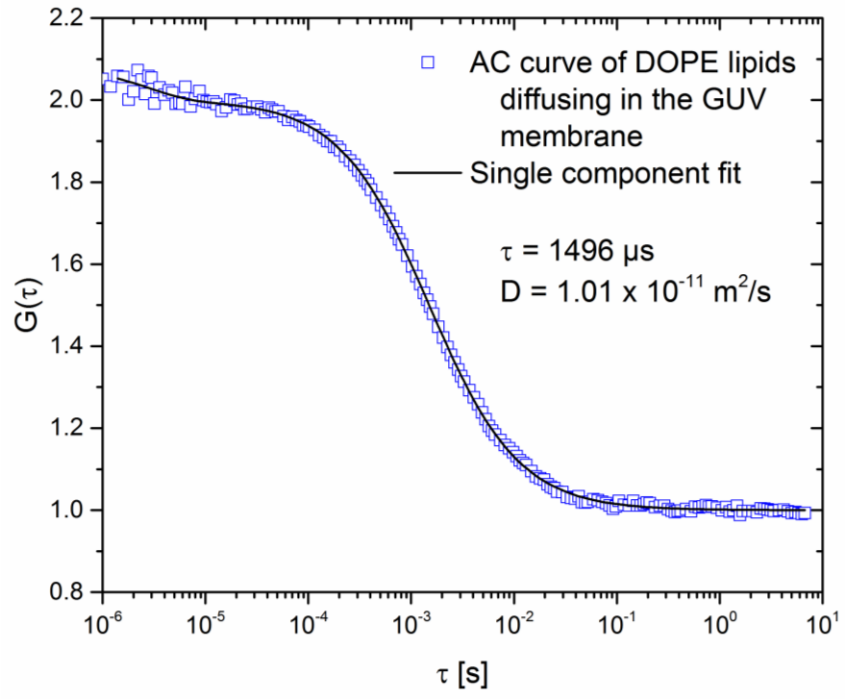

Figure 26: Autocorrelation curve of Atto633-labeled DOPE lipids in GUV membrane, fitted with a single component model fit. Resulting diffusion coefficient is $D = 1.01 \cdot 10^{-11}$ m²/s.

Fluorescence correlation spectroscopy measurements could be easily done once the GUVs were formed on the patterned PNIPAAm gel. No further step was necessary. The vesicles were already anchored and in a physiological medium (PBS).

Whereas this first application example of GUAVs showed the advantage of anchored vesicles, the second application example will show the benefit of hundreds of uniform anchored vesicles. In a single experiment, studies on plenty of vesicles were performed at the same time.

Application 2: Photo-oxidation in the vesicle membrane

Oxygen is not only important, but essential for life and the reason for oxidation processes. Reactive oxygen species can exhibit enough energy for oxidative damage to the DNA or proteins or they can initiate the peroxidation of the lipids in biological membranes.[113,114] Oxygenation in the cell membrane is not generally bad. For cell functions, such as signaling, cell apoptosis or maturation, a certain amount of oxidized lipids is required.[115]

Nevertheless, uncontrolled oxidation of lipids can lead to diseases, such as Parkinson or Alzheimer.[115] Therefore, the investigation of the photo oxidation process in the membrane is of high importance.

In this study, the oxidation of lipids in the vesicles membrane was investigated and monitored using confocal laser scanning microscopy. This study was based on the hydroperoxidation of the double bonds in the lipids tails by inserting OOH groups, that led to changes in the chain conformation and therefore to an increase of the area per lipid inside the vesicles. To generate hydroperoxide groups, the photo-oxidizer molecule erythrosine was used. Irradiation of erythrosine at 547 nm created singlet oxygen, that reacted with the unsaturated lipid bonds to hydroperoxide.[116,117]

GUAV were formed on patterned PNIPAAm gels as describes before. A 50 µM solution of the photo-sensitizer molecule erythrosine in phosphate buffered saline (PBS) was used for the GUAV formation. After the formation process, the area increase of the vesicles was studied without further preparation. The area increase occurred upon irradiation of erythrosine and subsequent hydroperoxidation of the lipids. The area increase was monitored by confocal laser scanning microscopy (CLSM) at the equator of the GUAVs after different irradiation times and irradiation doses, respectively. The results are shown in Figure 27: an increase in radius and area of the vesicles as well as a deformation of the round shape was observed. The more energy was used, the more singlet oxygen was generated by the erythrosine molecules. This led to the deformation and area increase of the GUAVs. Before the irradiation the vesicles were uniform and completely round shaped. After 1 min or 3.1 kJ/cm^2 irradiation of the photo-oxidizer erythrosine, the GUAVs were larger, deformed and moved from their positions. After 3 min (9.3 kJ/cm^2) the GUAVs grew even larger and even more of them deformed or moved from their position. After 11 min (33.9 kJ/cm^2) the GUAVs reached their final size and most of them have moved from their initial position. The CLSM images in Figure 27 clearly show the advantage of this GUAV formation method: The sample can be used for further studies directly after GUAV preparation and gives the ability to monitor and analyze the behavior of dozens of vesicles simultaneously.

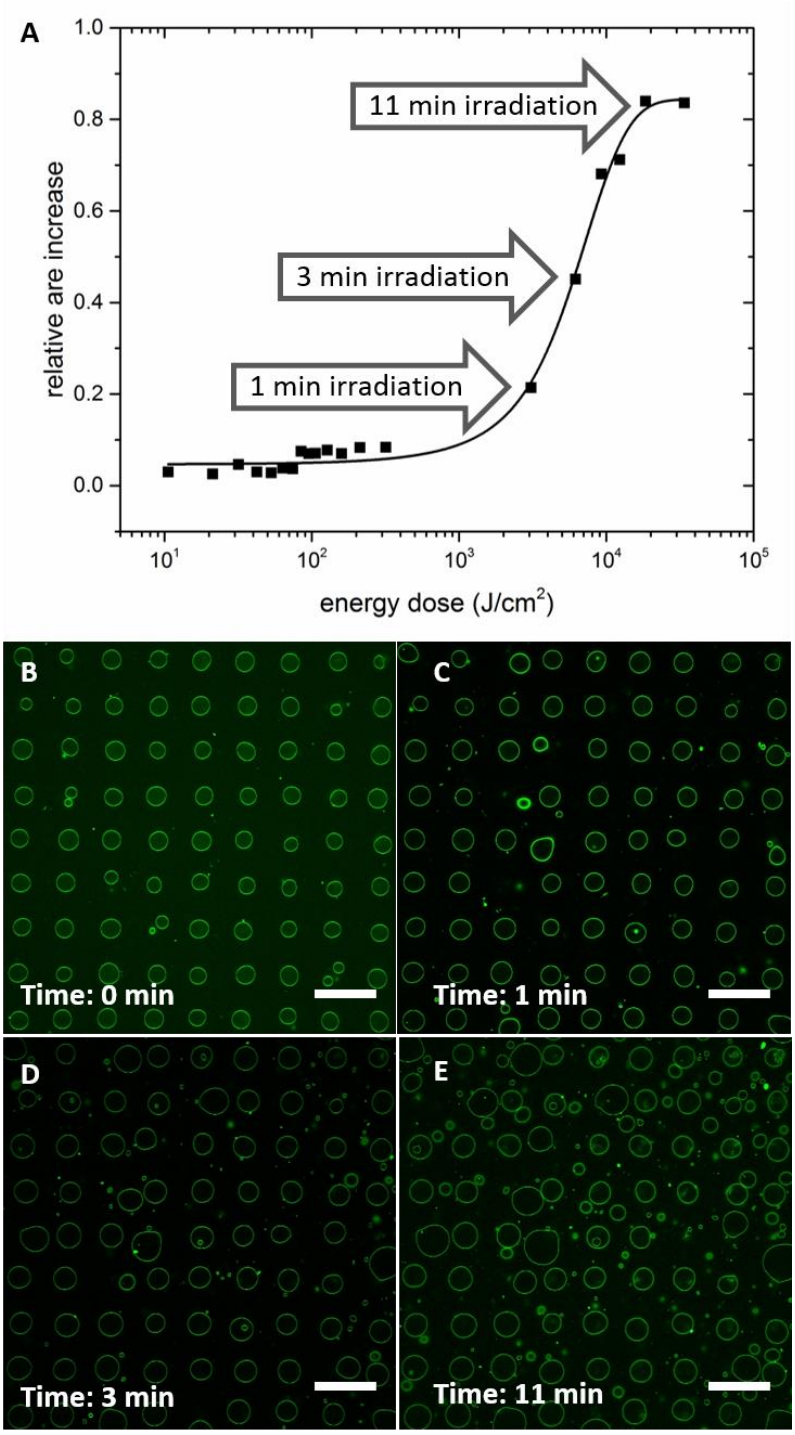

Figure 27: Results of the photo-oxidation experiments on GUAVs with the photo-oxidizer molecule erythrosine. (A) Area Increase of the GUAVs equator at different irradiation energy doses. (B-E) Confocal laser scanning images of the equator of GUAVs at different irradiation times: (B) Before irradiation the GUAVs are uniform and completely round shaped. (C) After 1 min irradiation of the photo-oxidizer erythrosine (corresponds to an energy dose of 3.1 kJ/cm^2) the GUAVs are larger, deform and move from their positions. (D) After 3 min (9.3 kJ/cm^2) the GUAVs are even larger and more of them deform and move from their position. (E) After 11 min (33.9 kJ/cm^2) the GUAVs reach their final size and most of them have moved from their initial position.

3.4 Summary and Outlook

Research on biological cells, our smallest living building units, is important to understand life in general, but also to understand and treat diseases. For a better research on cells and cell membranes, model systems are useful tools. Very promising cell model systems are giant unilamellar vesicles (GUVs). They can be prepared from different procedures. All of them have their advantages and disadvantages. The presented method for GUV formation is polymer hydrogel based and overcame the disadvantages of the known gel-based methods. This GUV formation was based on a functionalized PNIPAAm terpolymer hydrogel film. A benzophenone unit inside the polymer chain allowed to cross-link the polymer and anchored it to a glass substrate by UV irradiation. Hence, the polymer gel stayed at its position and did not dissolve. Hence, no free polymer was found in the GUVs after their formation. The formation of GUVs was possible on the surface of the polymer film by spreading phospholipids on the film and growing them with a buffer solution (simulating physiological conditions). Furthermore, the GUV growing process worked without the addition of organic solvents. Only the addition of the lipids beforehand was done from a lipid-chloroform solution, because of the solubility of the used phospholipids. The greatest development of this method was the GUV size control. GUVs were grown in a size-defined manner, by forming them from a micro-patterned PNIPAAm terpolymer hydrogel. The GUV diameter corresponded to the pattern diameter. In this procedure, hundreds of uniform vesicles were prepared within a few minutes. Additionally, this method resulted in GUVs, which were anchored to the polymer gel, enabling studies on hundreds of vesicle simultaneously, without the necessity to immobilize them as it is needed for other GUV formation methods.

The PNIPAAm gel-assisted method for GUV preparation is very promising and overcomes several disadvantages that other methods have, but it is still in the fledgling stages. In the future work, it could be interesting to test the

method with a large variety of phospholipids and phospholipid mixtures as well as amphiphilic polymers to generate polymersomes. For studies on the cell membrane model it might be interesting to encapsulate particles, such as drug molecules into the GUVs and study their behavior to pass the membrane. The same could be interesting for polymersomes as drug delivery vehicles. Another future work could be the detachment of the GUVs. Even though the advantage of anchored vesicles is part of this method, it would be good to have the possibility to detach the GUVs. This might be achieved by temperature changes. PNIPAAm is a thermo-responsive polymer with an LCST around 30-35 °C. Above this temperature, the polymer collapses and this can result in GUV detachment.

The PNIPAAm terpolymer hydrogel-assisted method enables the formation of size-defined giant unilamellar vesicles within a few minutes. On a micro-patterned polymer, hundreds of anchored cell membrane models were generated.

4 Monitoring Polymer Nanoparticle Formation using a Fluorescent Molecular Rotor

Nanoparticles are objects with a size between 1 nm and a few 100 nm and they are of high interest in many disciplines.[2,3] Because of their small size, nanoparticles show different properties compared to their bulk materials.[4] The particles can be synthesized either biologically or chemically.[4] One of the extensively studied groups of nanoparticles are the polymer nanoparticles.[2] Many studies were performed, focusing on the preparation of a diversity of different polymer particles and a lot of effort was put on their applications.[2,3,118] The preparation and characterization of polymer nanoparticles is of large interest in the fields of chemistry, material science and biomedicine, e.g. in tumor therapy.[8,119] The polymer nanoparticles can be synthesized from micelles or emulsion droplet templates or they can be prepared from pre-synthesized polymers from emulsified solutions of the polymer (e.g. by SEED - solvent evaporation from emulsion droplets).[119,120]

Polymer nanoparticles are small and show a fast diffusion. Hence, it is very difficult to get information on how the formation process is taking place. In the SEED procedure, the drying process of the nanodroplets is not fully understood yet. This project investigated the drying process of polystyrene nanoparticles prepared by solvent evaporation. Herein, polystyrene was a model system to test and develop the method. In this project, fluorescence correlation spectroscopy and fluorescence lifetime measurements were used to monitor both size and concentration changes in the nanodroplets with the help of a fluorescent molecular rotor molecule.

4.1 Chemical Concepts and Methods

This chapter introduces the chemical background about nanoparticles, especially polystyrene and the preparation methods of nanoparticles with a focus on the formation via solvent evaporation from emulsion droplets. The physical concepts of fluorescence, fluorescent molecules and the analytical methods are explained in section 2.

4.1.1 Polystyrene Nanoparticles

Polystyrene (PS) is one of the most extensively studied polymers. This aromatic polymer is a commodity plastic and has been widely used in research reports because it is relatively chemically inert. It can be synthesized from its monomer styrene by many different polymerization types. Often free radical polymerization (Figure 28) is used.[121] In this method, styrene can function as electron acceptor or electron donor and the polymerization does not necessarily need to be started with an initiator. Styrene can form the initiating radicals itself.[121–123] The chain growth process mainly terminates with a recombination step.[121] The resulting polymer is a linear hydrocarbon chain with phenyl side groups, which is soluble in aromatic and halogenated hydrocarbons, esters, ketones and aliphatic ethers, but not in aliphatic hydrocarbons and alcohols.[121] Amorphous atactic PS homopolymers are durable and transparent and commonly used as molded or expanded foams. Other applications of PS can be found in the food industry, because PS is hardly biodegradable. Furthermore, the usage of PS in medical products and laboratory equipment is of interest, because it is very cheap and biocompatible.[124] The special properties of PS results in a very wide range of applications and make PS to one of the most quantitatively important chemicals. It is produced in industrial process since the 1920s.[121]

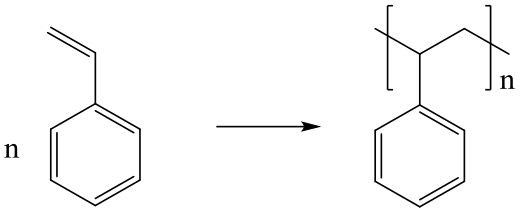

Figure 28: Synthesis of polystyrene (PS) from its monomer styrene (vinyl benzene).

Considering PS nanoparticles, the properties and applications differ from the bulk material. The surface area is very high compared to their volume, affecting the mechanical, electrical and optical properties as well as the chemical reactivity. PS nanoparticles are used in self-assembling nanostructures or as biosensors.[125,126] One of the most promising application field for nanoparticles and -carriers is drug delivery. Biocompatible nanoparticles are needed. Often, drug molecules are poorly soluble in biological media, due to their hydrophobicity. This can be solved by encapsulating these drugs into protective nanocarriers, generating a hydrophilic surface and enabling drug delivery.

4.1.2 Nanoparticle Formation Techniques

Nanoparticles as well as their preparation techniques are manifold. The material of the particle can vary from proteins or polysaccharides to synthetic polymers, on which this work is focused. The choice of nanoparticle formation method depends on numerous factors that define the desired properties for particular applications. Size, size distribution, solubility and stability, surface characteristics as well as biocompatibility and biodegradability are factors to take into account when choosing the nanoparticle preparation technique.[2,3,127]

In general, there are two main methods for the formation of polymer nanoparticles (Figure 29): direct polymerization of monomers and dispersion of preformed polymers. Other possibilities are ionic gelation or coacervation of hydrophilic polymers or particle replication in non-wetting templates, giving an absolute control of particle size and shape.[2,3]

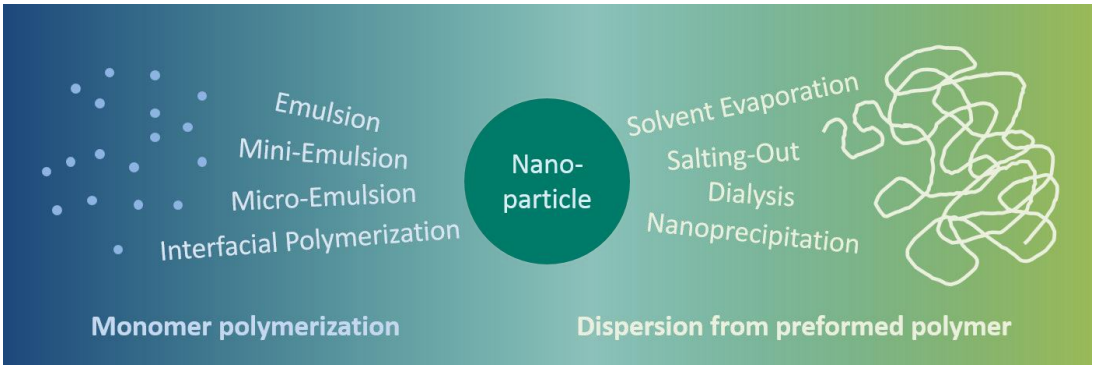

Figure 29: Summary of the two main polymer nanoparticle formation processes: monomer polymerization and dispersion from preformed polymer.

During the nanoparticle formation by monomer polymerization in direct systems, such as oil-in-water, monomers are polymerized in aqueous solution to form nanoparticles.[2,3] This can be performed in different methods. The emulsion polymerization is the most commonly used technique in this field. The nanoparticle formation can be done on the conventional way with water, a monomer with low solubility in water, water-soluble initiator and surfactant, but it is also possible to perform a surfactant-free emulsion polymerization. Different to emulsion polymerization, in miniemulsion polymerization a low molecular mass compound is used as a co-stabilizer together with the other ingredients, such as water, monomer, surfactant and initiator. Furthermore, high shear forces, e.g. ultrasound, are necessary for the miniemulsion. Micro-emulsion polymerization or interfacial polymerization are other techniques to form polymer nanoparticles.[127]

The dispersion of preformed polymers is the second main technique for nanoparticle formation. Here, nanoparticles can be obtained from a salting-out process, which avoids surfactants and chlorinated solvents, from nanoprecipitation, also called solvent displacement method, or from dialysis. But most commonly, nanoparticles are prepared by solvent evaporation. It is the first and most widely used method for the preparation of nanoparticles from a preformed polymer. In principle, a polymer dissolved in the organic solvent forms the oil-phase, and the aqueous solution with the stabilizer forms the aqueous phase. Two main preparation strategies are possible: single- or double-emulsion. Oil-in-water (o/w) is an example for the single-

emulsion preparation, whereas (water-in-oil)-in-water (w/o)/w is an example for the double-emulsion preparation.[127]

4.1.3 Solvent Evaporation from Emulsion Droplets

One possible way to prepare polymer nanporaticles is decribed in detail with the solvent evaporation from emulsion droplets (SEED) process. Herein, a presynthesized polymer is dissolved in a good organic solvent and then emulsified in water with the help of a stabilizer or surfactant. High-speed homogenization or ultrasound are necessary to obtain the emulsion. In the next step the organic solvent is evaporated through the continious aqueous phase and so a polymeric emulsion is formed. Therefore, contineous magentic stirring or reduced pressure are needed. The solvent evaporation leads to the formation of surfactant stabilized polymer nanoparticles dispersed in the aqueous phase (Figure 30).[119,120,127]

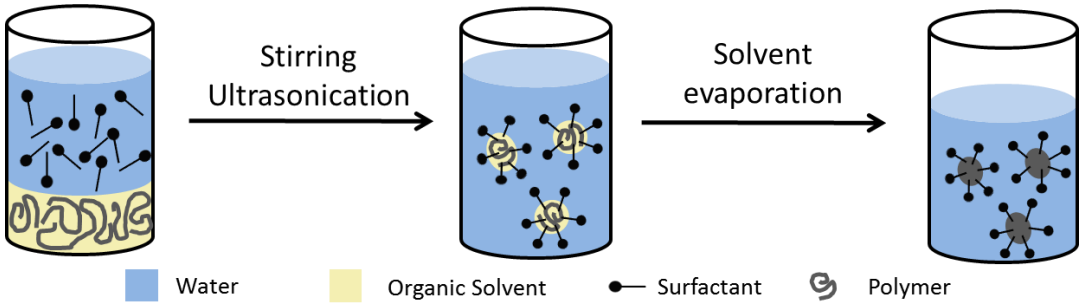

Figure 30: Solvent evaporation from emulsion droplets (SEED) process. A pre-synthesized polymer is dissolved in a good organic solvent and emulsified with an aqueous surfactant solution, giving stabilized polymer/organic solvent-droplets. Solvent evaporation leads to polymer nanoparticles. Adapted from [119,120].

The SEED process has the great advantage that it is free from impurities in the final product, e.g. monomers, catalyst or even toxic residuals.[120] Additionally, the process is easy and very fast. The particle size can be influenced by the process parameters, such as type and concentration of the stabilizer, polymer concentration or speed of homogenization or ultrasonication.[3]

4.2 Experiments und Materials

In this section, the chemicals and materials as well as the analytical setups that were used for this work are summarized. Furthermore, the experiments with all important parameters are described in detail.

4.2.1 Materials

Chloroform (≥ 99 %) was purchased from Acros Organics and anhydrous toluene (100 %) from VWR Chemicals. The solvents were used as received. Sodium dodecyl sulfate (SDS, 99 %) was purchased from AlfaAesar and diluted in ultrapure water (Milli-Q water, 18.2 MΩ·cm) to a concentration of 1 g/L. The fluorescent dye Atto425 was purchased from ATTO-TEC GmbH (Siegen, Germany) and diluted in ultrapure water (Milli-Q, 18.2 MΩ·cm). Polystyrene (M_w = 75 kg/mol, PDI = 1.03) was provided by J. Thiel (MPI-P). The molecular rotor LBX37 was provided in a $5 \cdot 10^{-4}$ M solution in toluene from the group of Roberto Simonutti (Department of Materials Science, University of Milano-Bicocca, Italy).

4.2.2 Time-Correlated Single Photon Counting (TCSPC)

Time-correlated single photon counting (TCSPC) data were recorded on a confocal setup. A PicoQuant diode laser (405 nm) was coupled into a Zeiss LSM 880 microscope (Carl Zeiss, Jena, Germany) using a MBS405 dichroic mirror (Carl Zeiss, Jena, Germany). The laser beam was focused through a Zeiss C-Apochromat 40×/1.2 W water immersion objective into the sample solutions. Emitted fluorescence light was collected with the same objective, passed through a pinhole and a band pass filter EM525/50 (Chroma Technology, Vermont, USA), detected by a PDM SPAD (Micro Photon Devices, Bolzano, Italy) and processed using a TimeHarp 260. An eight-well

polystyrene, chambered cover glass (Laboratory-Tek, Nalge Nunc International) was used as a sample cell for aqueous samples and an Attofluor® cell chamber (Invitrogen, Paisley, UK) was used for organic solutions and dry samples. If not mentioned in particular, the focus of the beam was positioned 30 µm inside the solution or emulsion, above the glass surface. Analysis of the TCSPC data was performed using the PicoQuant SymPhoTime 64 software. The instrument response function (IRF) was reconstructed with the PicoQuant SymPhoTime 64 software by directly evaluating the onset of the decay.

4.2.3 TCSPC Measurements of the Molecular Rotor in Toluene

A 500 nM solution of LBX37 in toluene was prepared. The sample was measured in an Attofluor® cell chamber at room temperature (T = 22 °C). The setup specifications are described in section 4.2.2. The sample was measured for 120 s and the resulting decay curve was fitted with a single exponential reconvolution fit (see equation 1). The experiment was repeated five times.

4.2.4 TCSPC Measurements of Atto425 in Water

A 50 nM solution of Atto425 in water was prepared. The sample was measured in a NUNC chamber at room temperature (T = 22 °C). The setup specifications are described in section 4.2.2. The sample was measured for 120 s and the resulting decay curve was fitted with a single exponential reconvolution fit (see equation 1). The experiment was repeated five times.

4.2.5 TCSPC Measurements in Polystyrene Solutions

Polystyrene (PS, 75 kg/mol) was dissolved in toluene. The PS fractions were ranging from 10 % PS in toluene up to 90 % PS in toluene. To each solution

the molecular rotor LBX37 was added in a concentration of $5 \cdot 10^{-6}$ M. Polystyrene solutions below 60 % were prepared by dissolving PS in the appropriate amount of toluene. The solutions were stirred for 24 h to obtain homogeneous solutions. For samples with PS concentrations above 60 %, the viscosity was too high to dissolve the polymer appropriately in the comparably low amount of toluene. The high viscosity also precludes stirring. To overcome this problem, samples with a high PS concentration were prepared from a sample with initial 50 % PS. This sample was dried at ambient atmosphere and room temperature. The resulting PS concentration was calculated from the weight of the initial sample and the dried sample. Since the weight loss only appeared from evaporated toluene, the concentration could be determined. With this preparation method, it was possible to obtain samples with PS concentrations up to 90 %. To measure the rotor molecule in pure polystyrene, a polymer film was prepared from the 50 % PS solution by drying it for 72 h at 50 °C under vacuum. Samples were measured in Attofluor® cell chambers at 22 °C as describes in section 4.2.2. The measurement time was 180 s and the obtained decay curves were fitted with a biexponential reconvolution fit (equation 2) for the PS toluene mixtures and a monoexponential reconvolution fit for pure PS (equation 1).

4.2.6 Polystyrene Nanoparticle Formation via SEED in Toluene

50 mg PS (M_w = 75 kg/mol) were dissolved in 1.44 mL toluene. The solvent contained the molecular rotor LBX37 in a concentration of $1 \cdot 10^{-6}$ M. 10 mL of an aqueous solution of SDS (1 g/L) were added to the organic solution. A macroemulsion was obtained by stirring for 1 h at 1250 rpm at room temperature. The macroemulsion was sonicated using a Branson W450-D sonifier with ½-inch tip in a pulsed regime (30 s sonication, 10 s pause) for 2 min at 70 % amplitude under ice cooling. The obtained emulsion was either directly measured or stirred at 40 °C at 500 rpm to evaporate the organic solvent. For the kinetic measurements from the large volume, after specific time intervals 100 µL of the emulsion were diluted 5x in water and measured. In case of the droplet measurement, 150 µL of the diluted emulsion were

used for the measurement. The samples were measured in a NUNC chamber at room temperature (T = 22 °C). The setup specifications are described in section 4.2.2. The samples were measured for 120 s and the resulting decay curves were fitted with a biexponential reconvolution fit (see equation 2).

4.2.7 Dried Polystyrene Nanoparticles

Polystyrene nanoparticles were prepared as explained in section 4.2.6. To study the fluorescence lifetime of the molecular rotor in dry PS nanoparticles, the dispersions from the final SEED step were dried from small dispersion droplets on round microscope cover slides. The drops were dried for 30 min under vacuum at 50 °C and then a next portion of droplet was added to the dry thin layer. The process was repeated five times to obtain a layer of PS nanoparticles. The beam was focused into the nanoparticle layer and TCSPC measurements were performed as describes above. The decay curves were fitted with a single exponential reconvolution fit (equation 1). Four samples were prepared and measured.

4.2.8 SEED Process Without Polymer for Studying SDS Influence

1.44 mL toluene, containg the molecular rotor LBX37 in a concentration of $1 \cdot 10^{-6}$ M were added to 10 mL of an aqueous solution of SDS (1 g/L). A macroemulsion was obtained by stirring for 1 h at 1250 rpm at room temperature. The macroemulsion was sonicated using a Branson W450-D sonifier with ½-inch tip in a pulsed regime (30 s sonication, 10 s pause) for 2 min at 70 % amplitude under ice cooling. The obtained emulsion was stirred at 40 °C at 500 rpm to evaporate the organic solvent. The sample was measured in a NUNC chamber at room temperature (T = 22 °C). The setup specifications are described in section 4.2.2. The sample was measured for 120 s and the resulting decay curve was fitted with a single exponential reconvolution fit (see equation 1).

4.2.9 Polystyrene Nanoparticle Formation via SEED in Chloroform

50 mg PS (M_w = 75 kg/mol) were dissolved in 0.84 mL chloroform. The solvent contained the molecular rotor LBX37 in a concentration of $1 \cdot 10^{-6}$ M. 10 mL of an aqueous solution of SDS (1 g/L) were added to the organic solution. A macroemulsion was obtained by stirring for 1 h at 1250 rpm at room temperature. The macroemulsion was sonicated using a Branson W450-D sonifier with ½-inch tip in a pulsed regime (30 s sonication, 10 s pause) for 2 min at 70 % amplitude under ice cooling. The obtained emulsion was either directly measured or stirred at 40 °C at 500 rpm to evaporate the organic solvent. For the kinetic measurements from the large volume, after specific time intervals 100 µL of the emulsion were diluted 5x in water and measured. In case of the droplet measurement, 150 µL of the diluted emulsion were used for the measurement. The samples were measured in a NUNC chamber at room temperature (T = 22 °C). The setup specifications are described in section 4.2.2. The samples were measured for 120 s and the resulting decay curves were fitted with a biexponential reconvolution fit (see equation 2).

4.2.10 Fluorescence Correlation Spectroscopy (FCS)

Fluorescence correlation spectroscopy data were recorded with the same setup as describes for TCSPC measurements. The recorded photon data were correlated to FCS autocorrelation curves, giving the diffusion times of the nanoparticles, according to equation 6. The observation volume was calibrated using Atto425 as reference dye. FCS Data were analyzed using the software ZEN. The hydrodynamic radii were calculated from the measured diffusion coefficients using the Stokes-Einstein relation (equation 10).

4.3 Results and Discussion

This chapter focuses on the formation of polystyrene nanoparticles. A lot of work was done regarding the synthesis and preparation of nanoparticles and their applications, especially as drug delivery systems. Understanding the process and its physico-chemical properties is another important aspect to study. The formation of polystyrene nanoparticles from solvent evaporation from emulsion droplets (SEED) was monitored by using a fluorescence molecular rotor. With the help of the rotor, it was possible to monitor the size and concentration change of the nanodroplets by fluorescence correlation spectroscopy and time-correlated single photon counting experiments.

4.3.1 Fluorescence Lifetime of Molecular Rotor LBX37 in Toluene

A fluorescent molecular rotor was used to study the formation of polystyrene nanoparticles. This rotor is called LBX37 and is composed of a naphthalene part, acting as the electron-acceptor, and a dibenzoazepine part, which is the electron-donor (Figure 2C and Figure 31). Its fluorescence lifetime depends on the microenvironment, mostly defined by the viscosity (see section 2.2). To understand the behavior of the rotor, the fluorescence lifetime was measured in pure toluene. Toluene was chosen, because it is a good solvent for the molecular rotor and it is suitable for the following nanoparticle formation experiments. The fluorescence lifetime was determined using time-correlated single photon counting (TCSPC) experiments. The decay curve of this experiment is pictured in Figure 31. From the experimental decay a single exponential fit gave a fluorescence lifetime of 0.6 ns.

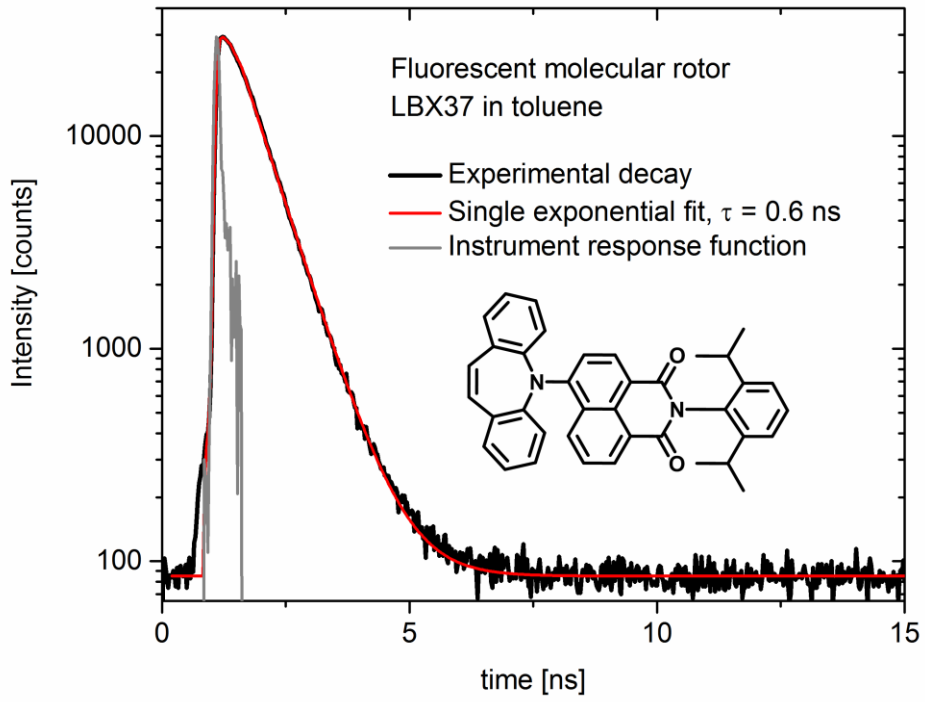

Figure 31: Experimental decay curve (black) of the fluorescent molecular rotor LBX37 in toluene, together with the single exponential fit (red) and the instrument response function (IRF, grey). The fluorescence lifetime was found to be 0.6 ns. The chemical structure of the molecular rotor LBX37 is depicted in the figure.

The fluorescence lifetime of LBX37 in toluene was quite small compared to conventional fluorescent dyes, such as Atto425. The reason was the special property of the molecular rotor, as discussed in section 2.2. The intramolecular rotation of the molecule is high in a low-viscosity environment, such as pure toluene, resulting in a short fluorescence lifetime. To assure, that the method and setup worked correctly, an additional experiment with a fluorescent dye with known fluorescence lifetime was measured. Atto425 is a commercially available fluorescent dye with a fluorescence lifetime of $\tau = 3.6$ ns.[128] The decay curve of the Atto425 measurement is shown in Figure 32. The fluorescence lifetime was found to be 3.6 ns, which corresponds to the literature value. This measurement reassured the method for the fluorescence lifetime determination.

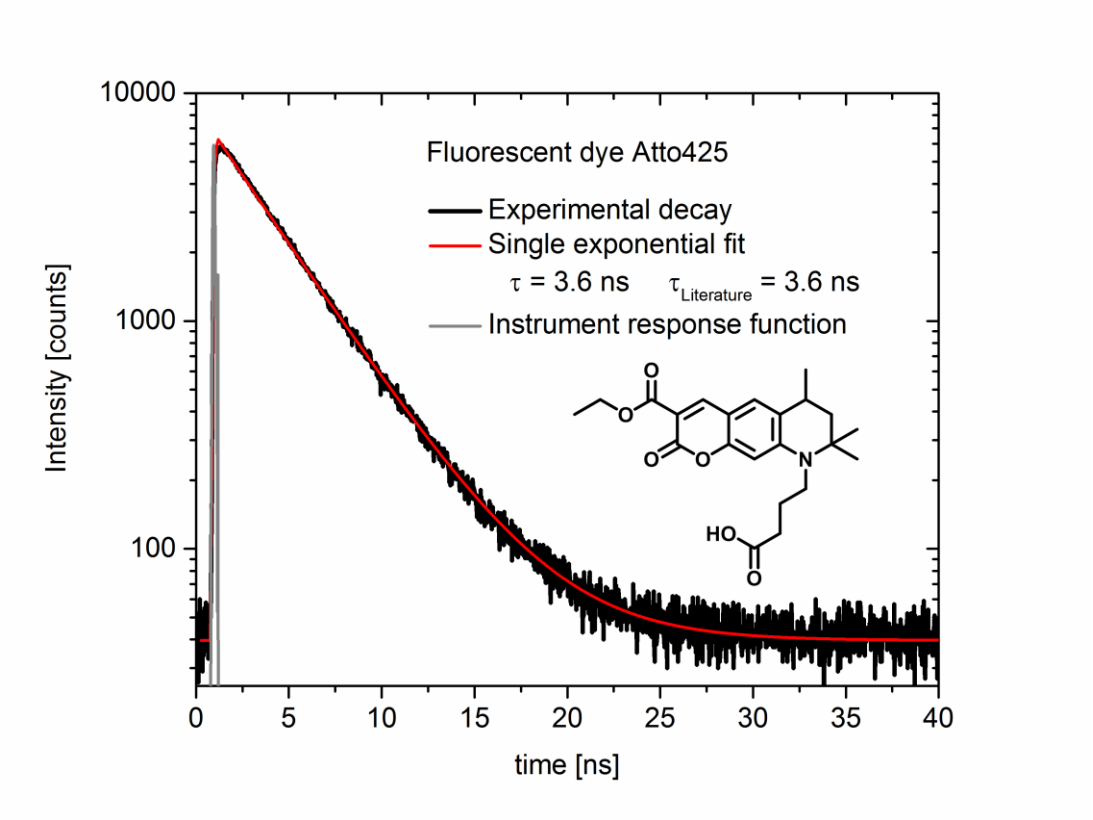

Figure 32: Experimental decay curve (black) of the fluorescent dye Atto425 in water, together with the single exponential fit (red) and the instrument response function (IRF, grey). The fluorescence lifetime was found to be 3.6 ns, as it is described in the literature. The chemical structure of the dye Atto425 is depicted in the figure.

4.3.2 Master Curve for Polystyrene Toluene Mixtures

The aim of this work was to monitors the formation process of polystyrene (PS) nanoparticles from the solvent evaporation from emulsion droplets (SEED) process. During this process, toluene evaporated from surfactant stabilized toluene-polystyrene droplets, forming polystyrene nanoparticles. The concentration of PS inside the droplets was investigated during the drying process.

Before performing the SEED experiments, a master curve was created by measuring the fluorescence lifetime of the molecular rotor present in polystyrene toluene solutions of different concentrations.

Therefore, solutions of different PS concentrations in toluene containing the molecular rotor were prepared. Additionally, a sample with the rotor molecule in pure PS was prepared. To study the behavior of the molecular rotor, the fluorescence lifetimes of the samples were measured. The decay curves are shown in Figure 33. The decay curves shifted to longer times with increasing amount of PS in toluene. These results were in agreement with the theoretical concept, as explained in section 2.2. The fluorescence lifetime of a molecular rotor was longer, the higher the viscosity of the microenvironment was. In case of 10 % up to 40 % PS in toluene, the viscosity was comparably low and the shift in the decay curves was small. A clear shift was observed between 50 % and 80 % PS in toluene. PS amounts, that were larger than 80 % showed small shifts until the lifetime of LBX37 in pure polystyrene was reached.

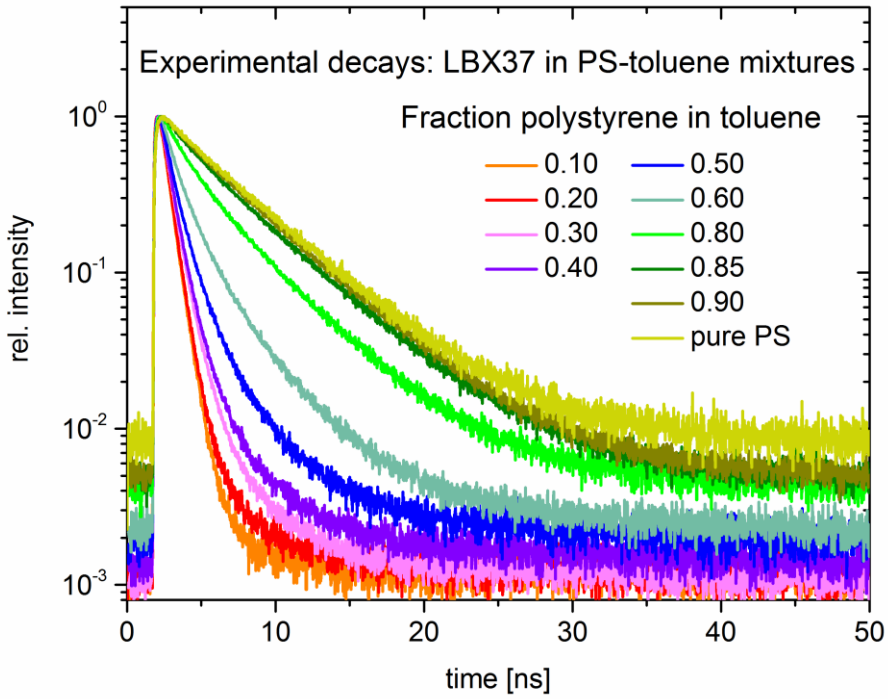

Figure 33: Experimental decay curves of the molecular rotor LBX37 in different PS concentration in toluene, ranging from 10 % polystyrene up to 90 % polystyrene in toluene and additionally the experimental decay in pure polystyrene, showing longer decay times with increasing PS fraction (increasing viscosity).

The decays of the PS toluene mixtures were fitted with a biexponential fit function, resulting in two fluorescence lifetimes, as shown in Figure 34. The short lifetime increased from 0.6 ns in pure toluene and up to a fraction of 20 % PS to 3 ns when the PS fraction reached 90 %. The long lifetime started around 3 ns in very diluted PS solutions and increased to 5.1 ns in pure polystyrene.

The reason for two (or more) different fluorescence lifetimes was the presence of two different microenvironments the molecular rotor was surrounded by. Rotor molecules that were closer to the toluene molecules may show faster fluorescence lifetimes than rotor molecules that interacted more with the polystyrene chains. Hence, two different lifetimes appeared in the decay. The short fluorescence lifetimes in the samples with less than 50 % PS were in the same range as the fluorescence lifetime of the molecular rotor in pure toluene.

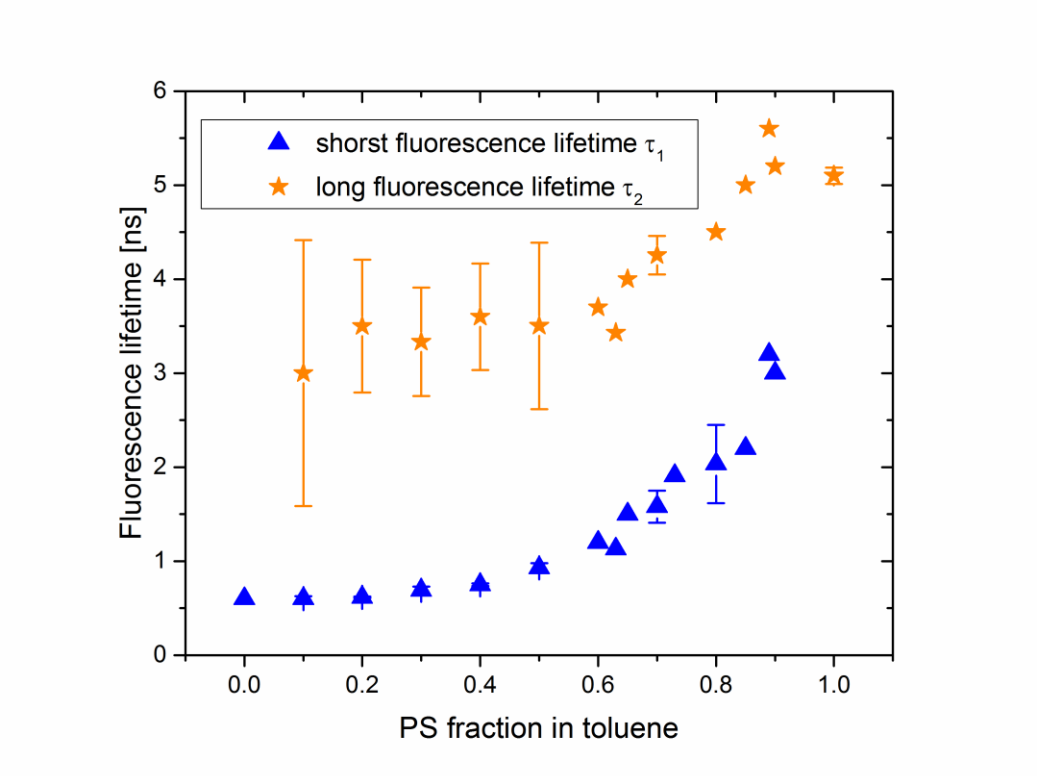

Figure 34: Fluorescence lifetimes of the molecular rotor LBX37 in PS toluene solutions of various concentrations. Blue stars show the short fluorescence lifetime τ_1 and orange stars resemble the long fluorescence lifetime τ_2.

The accuracy of the small lifetime τ_1 was much better in the low PS fraction range, whereas the accuracy for the larger lifetime τ_2 was low, as the error bars in Figure 34 indicate. This occurs from the fractions of the two lifetimes, which are defined as their amplitudes, as they will be called in the rest of the thesis. The corresponding amplitudes for the PS-toluene samples are presented in Figure 35.

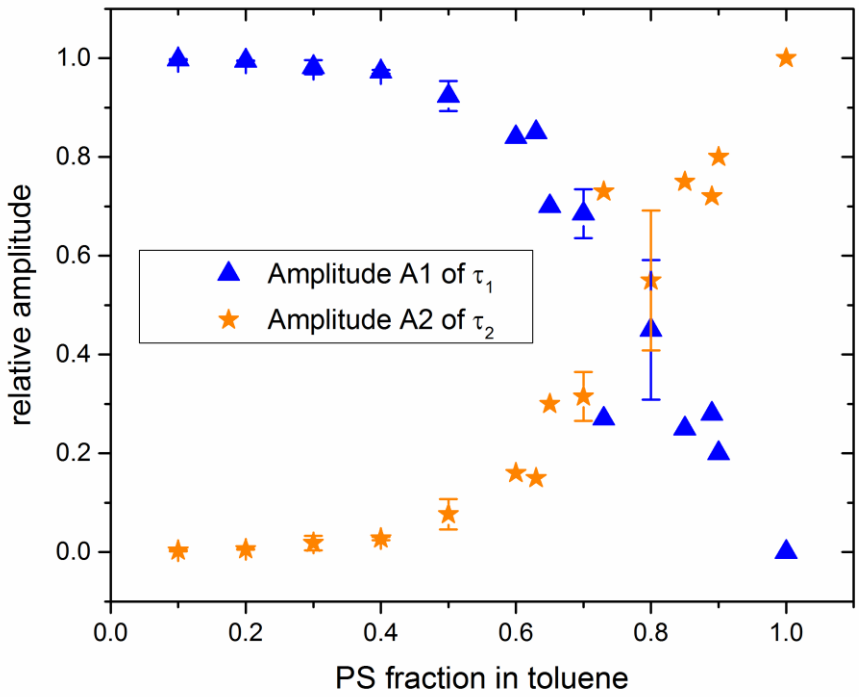

Figure 35: Amplitudes of the fluorescence lifetimes of the molecular rotor LBX37 in PS toluene solutions of various concentrations. Blue triangles show the amplitude A1 of the short fluorescence lifetime τ_1 and orange stars resemble the amplitude A2 of the long fluorescence lifetime τ_2.

In the regime of 10 % to 30 % PS in the solution, the short fluorescence lifetime is dominant and the long lifetime is almost negligible. That was the reason for the low accuracy of the value for the long lifetime in the low PS fraction range. Between 40 % and 70 % PS concentration the short lifetimes was still dominant, but the amplitude and the influence of the long lifetime increased. At concentrations about 80 % PS in toluene the amplitudes of both lifetimes were equal and the long lifetime dominated in regimes higher than 80 % PS concentration.

To define one fluorescence lifetime value for each measurement or each decay curve, the weighted average fluorescence lifetime τ_{wa} can be used (see equation 4). This lifetime takes the different single lifetimes τ_i as well as their amplitudes A_i into account. The weighted average fluorescence lifetime is a helpful value to simplify very complex systems and to be able to compare data more easily, as it was shown in the literature, e.g. for the polymerization of PMMA.[129]

The dataset of the fitted curves can be found in Table 3 in the appendix. The weighted average fluorescence lifetimes of the above shown samples' decay curves were plotted against the PS fraction in toluene to obtain a master curve (Figure 36).

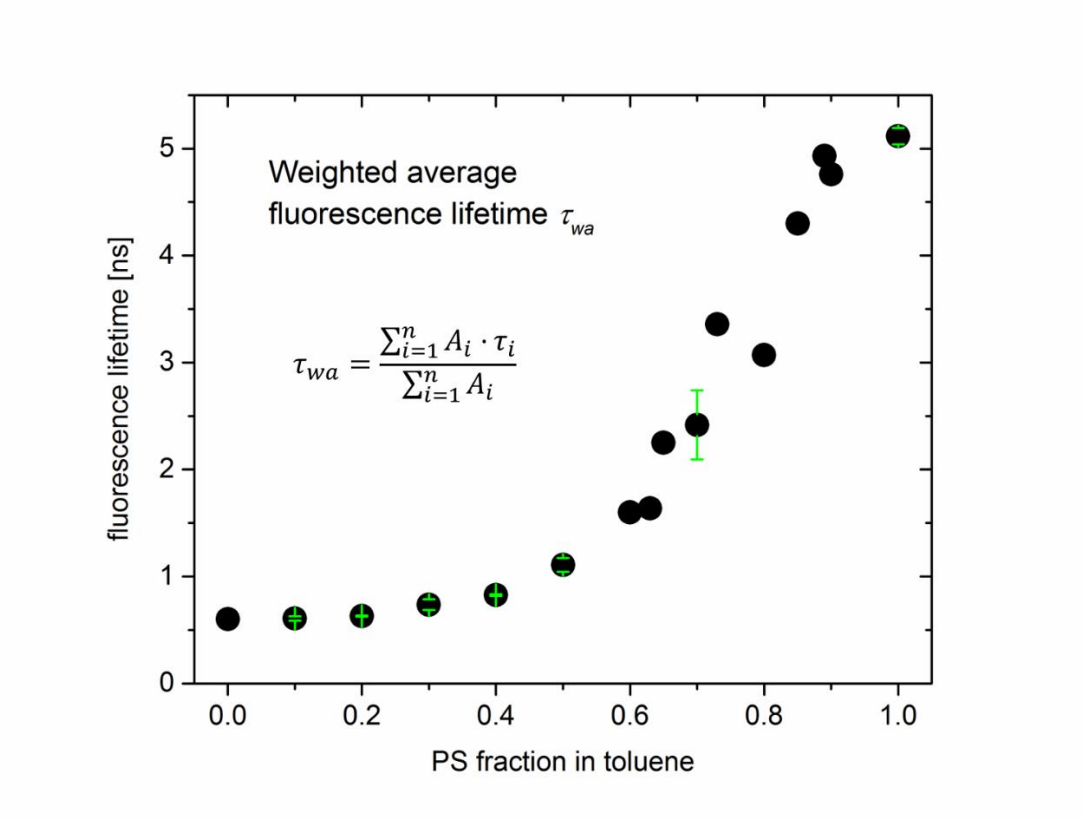

Figure 36: Master curve. Weighted average fluorescence lifetimes of the molecular rotor LBX37 in solutions of polystyrene in toluene in various concentrations.

The fluorescence lifetime of LBX37 in pure toluene was 0.6 ns, which did not change significantly when 10 – 20 % polystyrene were present. Until a PS fraction of 0.4 was reached, the lifetime was still below 1 ns. A stronger

change was observed from 50 % PS with a lifetime of 1.1 ns to 70 % PS and 2.5 ns up to 90 % PS with a lifetime of 4.8 ns. In pure polystyrene the fluorescence lifetime was found to be 5.1 ns.

The weighted average fluorescence lifetimes in the master curve clearly confirm the trend that the fluorescence lifetime increased with increasing amount of polystyrene in the solution, due to higher viscosity in the molecular rotors microenvironment. The fluorescence lifetimes from the master curve were used in the following to determine the PS concentration in the nanodroplets of the SEED process.

4.3.3 Monitoring the Polystyrene Nanoparticle Formation via SEED

The aim of this project was to monitor the formation of polystyrene nanoparticles, which were formed in a solvent evaporation process (SEED). The formation process and especially the drying process of the nanodroplets is not fully understood, yet. From sections 4.3.1 and 4.3.2 the basic parameters as well as the range of fluorescence lifetimes were known. Therefore, polystyrene with the molecular rotor LBX37 was dissolved in toluene. To the organic solution an aqueous surfactant (SDS) solution was added and emulsified, in order to obtain surfactant-stabilized toluene-droplets that contained the polymer and the rotor molecule. The process of interest was the evaporation of toluene from these nanodroplets, forming PS nanoparticles. Herein, the solvent evaporation process itself was studied. Therefore, the fluorescence lifetimes were determined at several time intervals during the evaporation process to obtain kinetic information. Additionally to the fluorescence lifetime, which was obtained from TCSPC experiments, the hydrodynamic radius of the toluene-PS-rotor-droplets was determined by fluorescence correlation spectroscopy (FCS). During the evaporation process, the droplet was expected to shrink due to the loss of the solvent. In the case that no coalescence was happening in the process, as described in the literature, the droplet had a larger size in the beginning

compared to the end of the process.[119] The final hydrodynamic radius was the one from the PS nanoparticles.

Sample V1 was prepared as described (4.2.6) and directly used for the TCSPC as well as for the FCS experiments. Hourly a 100 µL probe was taken from the sample to be measured. The decay curves (Figure 37) show a clear shift to higher fluorescence lifetimes with increasing toluene evaporation time. In the first two hour, the decay curves were similar. After 3 h a clear shift to longer decay time was observable. After 4 h the system reached its final stage, because no more shift of the decays was observed in the following 3 h.

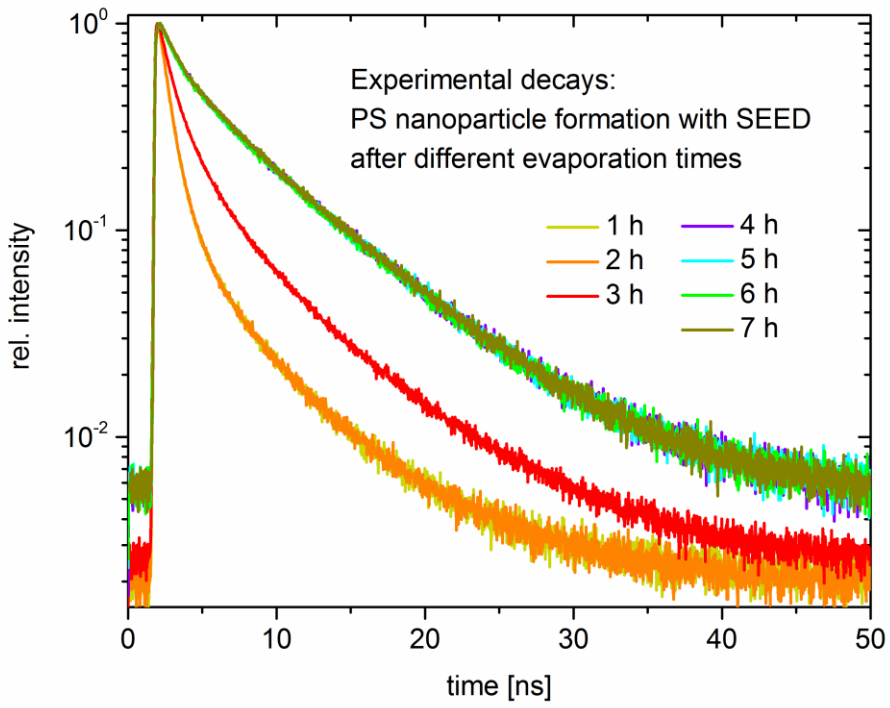

Figure 37: Experimental decay curves of sample V1 (formation of polystyrene nanoparticle from solvent evaporation from emulsion droplets). In 1-h-time intervals a probe was measured via time-correlated single photon counting, giving the plotted decay curves. In the first 2 h the decays did not change, whereas the process was finished after 4 h.

The decay curves signalized that the behavior of the molecular rotor changed between two and four hours of the toluene evaporation process. Before and afterwards the signal was constant. That means that there was a delay of the

evaporation start. One hypothesis for the behavior is the following: If the water that surrounded the nanodroplets was saturated with the maximum miscible fraction of toluene, no more toluene could move from the nanodroplets towards the water phase. First, the toluene in water needed to evaporate at the liquid air interface and then the droplets were able to loose toluene. To reach this state a certain time was needed to start the process. As long as the nanodroplet was not changing, the molecular rotor stayed in the same microenvironment and no change in the decays or fluorescence lifetimes was observed. Furthermore, the evaporation process was carried out at 40 °C, but directly after sonication the emulsion was at room temperature and needed some time to heat up to 40 °C. This may also shift this starting point for the toluene evaporation.

The dataset of the fitted curves can be found in Table 4 in the appendix. The weighted average fluorescence lifetimes, calculated from the decay curves, were plotted in Figure 38 against the evaporation time. In the first two hours the lifetime was around 1 ns, whereas the final lifetime was found to be 4.5 – 5 ns.

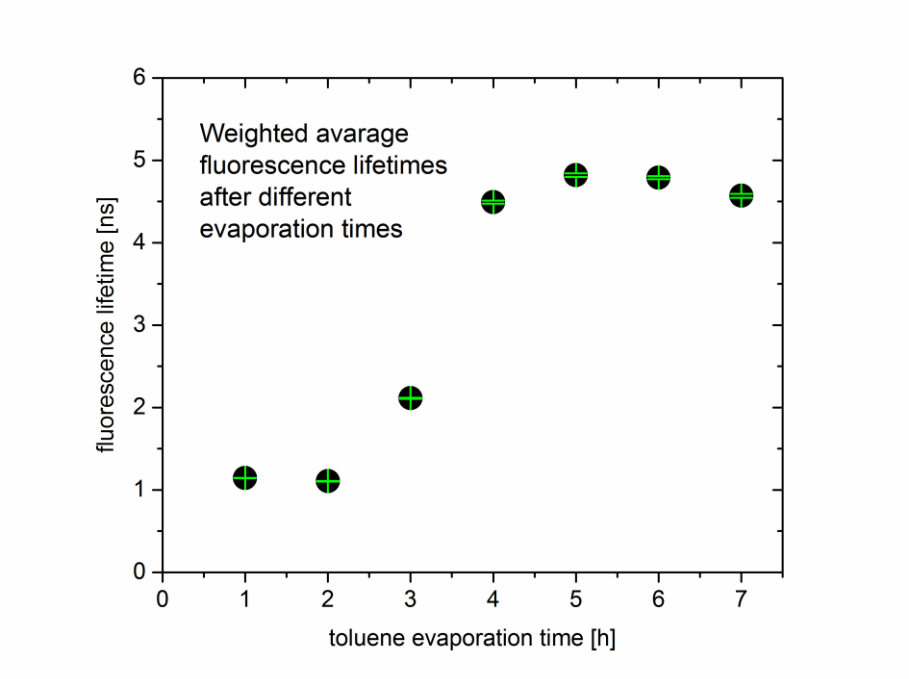

Figure 38: Weighted average fluorescence lifetimes at different evaporation times from TCSPC measurements of sample V1.

Comparisons of these fluorescence lifetimes to the master curve showed that the evaporation process started with a polystyrene concentration of around 45 – 50 %. From the preparation process, the initial PS fraction was 5 %. Hence, there was a significant loss of toluene between the preparation and the evaporation step. Most likely, toluene evaporated during the sonication process. During this step, the glass bottle with the sample was open and even with ice cooling, the sample heated up during the sonication. Within the 2.5 min sonication a large amount of toluene evaporated, so PS toluene nanodroplets with roughly 50 % PS were present at the beginning of the actual evaporation process.

From the weighted average fluorescence lifetimes and the master curve, the PS concentration of the nanodroplets was determined. Black squares in Figure 39 show the PS concentration plotted against the evaporation time. As already discussed the evaporation process starts with 50 % PS. Regarding the data calculated from the master curve, the fluorescence lifetime for the final state (after 4 h and more), only reaches 90 % PS, but not 100 %, as it was expected for the final PS nanoparticles. One reason might be, that even after 7 h evaporation time, toluene did not evaporate completely and that the last 10 % toluene evaporate very slowly or not at all.

Two more experiments (V2 and V3) were performed in the same way as described here, giving comparable results, which are shown in the appendix. One difference was the delay time of the evaporation start. In both cases the delay was more than 4.5 h and the evaporation process was finished after 24 h.

One great advantage of the applied method of fluorescence spectroscopy is, that the diffusion coefficient of the nanodroplets can be determined simultaneously to the TCSPC measurements via fluorescence correlation spectroscopy (FCS). The hydrodynamic radius and therefore the droplet size can thus be determined via FCS. Assuming that the size, measured in the final state of the process, was the actual nanoparticle size, without toluene, the PS concentration inside the nanodroplet was recalculated from the

hydrodynamic radius. The data were plotted as red circles in Figure 39. The final nanoparticle size was a hydrodynamic radius of R_H = 45 nm.

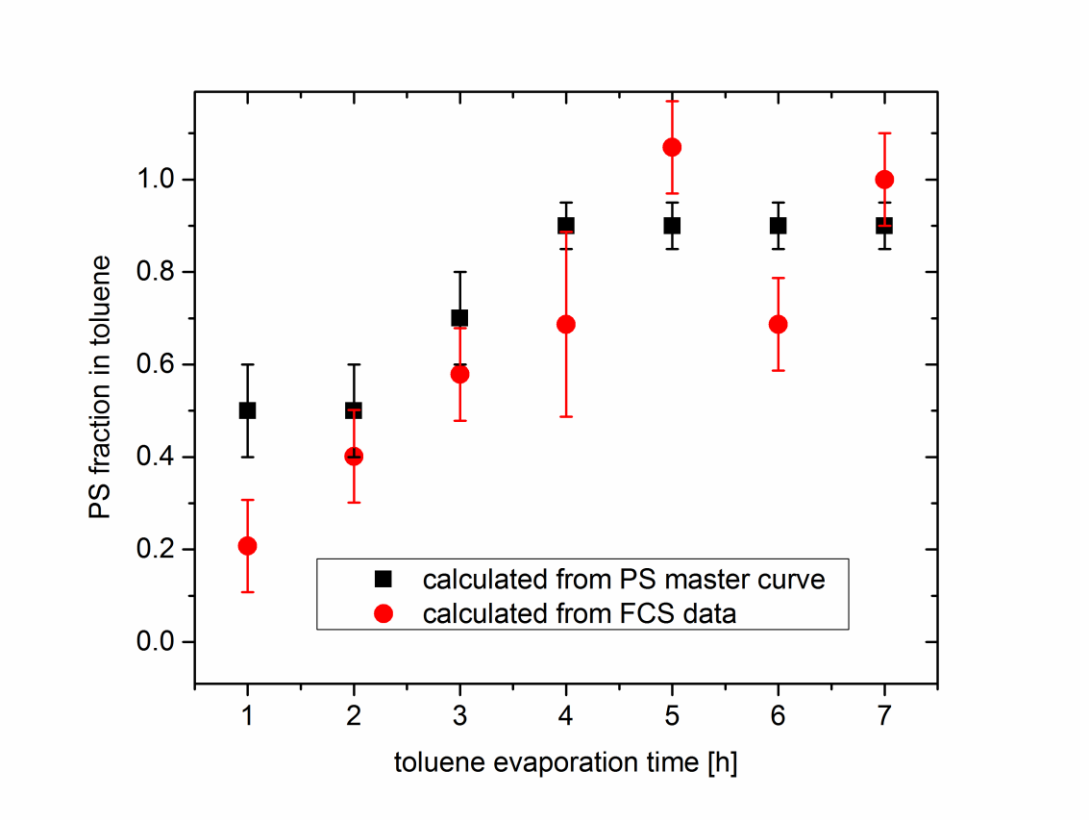

Figure 39: Fraction of polystyrene in the nanodroplet of the solvent evaporation process at different evaporation times, calculated from the PS master curve (black squares) and calculated from the droplets' hydrodynamic radii, as determined by fluorescence correlation spectroscopy (FCS, red circles) for sample V1.

Figure 39 shows that the PS fraction in the SEED nanodroplet could be determined from TCSPC and FCS measurements simultaneously. Both datasets showed the increase of PS fraction with increasing toluene evaporation. This method enables to monitor the nanoparticle formation from the emulsion droplets.

4.3.4 Monitoring the Nanoparticle Formation in a Droplet

Additionally to the above discussed experiment, the evaporation process was also monitored from a small sample volume, in the size of a 150 µL droplet

(D1). The advantage was on the one hand that the evaporation process was faster, due to the better surface to volume ratio. On the other hand, exactly the same sample droplet could be monitored during the whole process and was not disturbed mechanically. In the previous experiment, for each measurement always a new probe was takes from the reaction volume, but here the probe stayed the same.

A sample (D1) was prepared similar to the discussed sample, but a 150 µL droplet was used for the measurements. In the beginning of the process, every 5 min, later every 10 – 20 min a measurement was performed. The decay curves are shown in Figure 40. The curves show the increase of the decays during the process. The complete evaporation process took about 45 min, whereas the strongest changes were observed in the first 15 min.

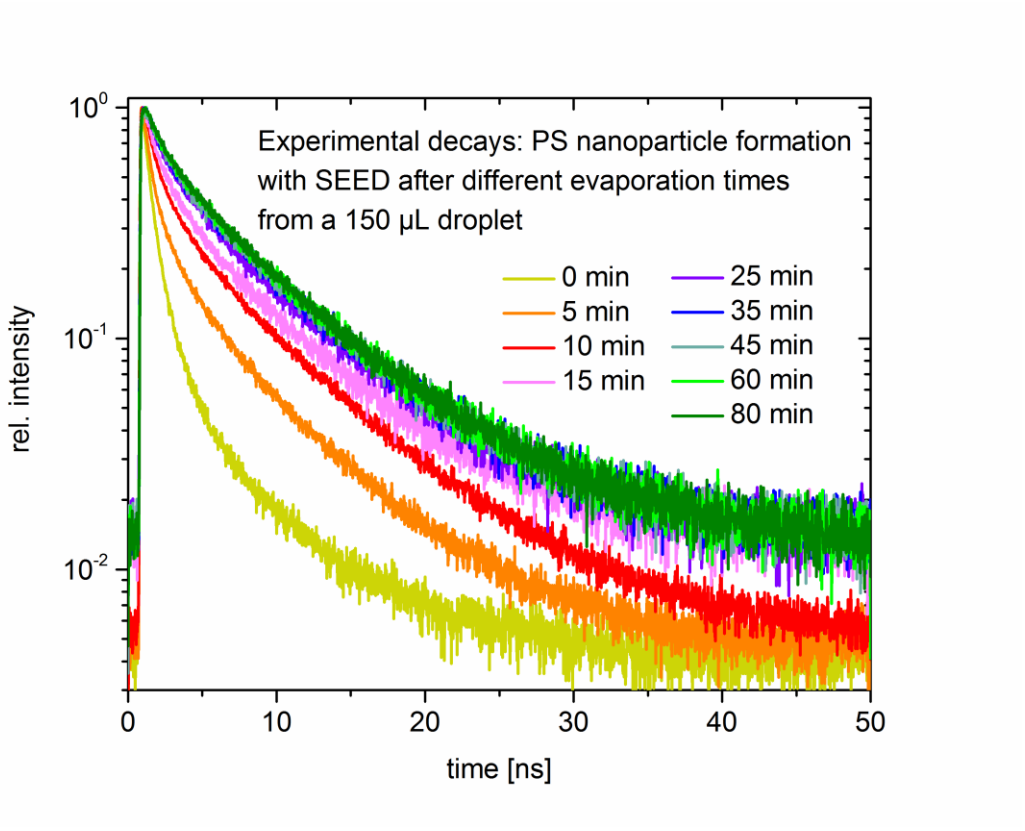

Figure 40: Experimental decay curves of sample D1 (formation of polystyrene nanoparticle from solvent evaporation from emulsion droplets), a 150 µL droplet. Every 5 – 20 min a probe was measured via time-correlated single photon counting, giving the plotted decay curves. The process was finished after 45 min.

From the decay curves the weighted average fluorescence lifetime were calculated and plotted against the evaporation time. Figure 42 shows that the obtained data were similar to the data from sample V1. The initial lifetime was around 1 ns and increased to 5 ns in the final state of the evaporation process. In a second experiment (D2) the findings were comparable to D1 and are shown in the appendix (Figure 52).

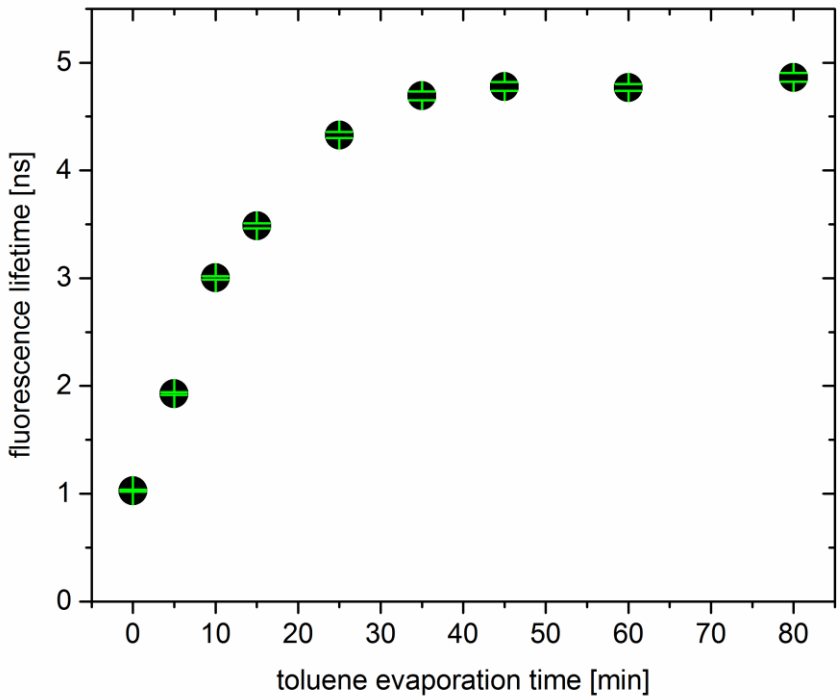

Figure 41: Weighted average fluorescence lifetimes at different toluene evaporation times from TCSPC measurements of sample D1.

To obtain information about the nanodroplets, the data points were compared to the master curve and the PS fraction in the nanodroplet was plotted against the toluene evaporation time. Again, the data showed that the initial PS concentration in the droplet was around 50 %, as discussed for sample V1. The increase of PS fraction during the evaporation process was clearly observable. The final state of the process was again comparable to a polystyrene fraction of 90 %. In this sample as well as in sample V1 the

fluorescence lifetime of the molecular rotor in pure polystyrene was not reached.

Maybe it is just a question of the error of the measurements and calculations or it might be possible that the complex SEED system influenced the fluorescence lifetime. In case of the master curve, only the rotor dye, PS and toluene were present. In the SEED samples, water and the surfactant SDS were also present. It might be possible that their presence influenced the rotors fluorescence lifetime. Sections 4.3.5, 4.3.6 and 4.3.7 focus on this problem in more details.

Additional to the PS concentrations determined from the master curve the obtained dataset were used for FCS autocorrelation to calculate the PS concentration from the nanodroplet sizes.

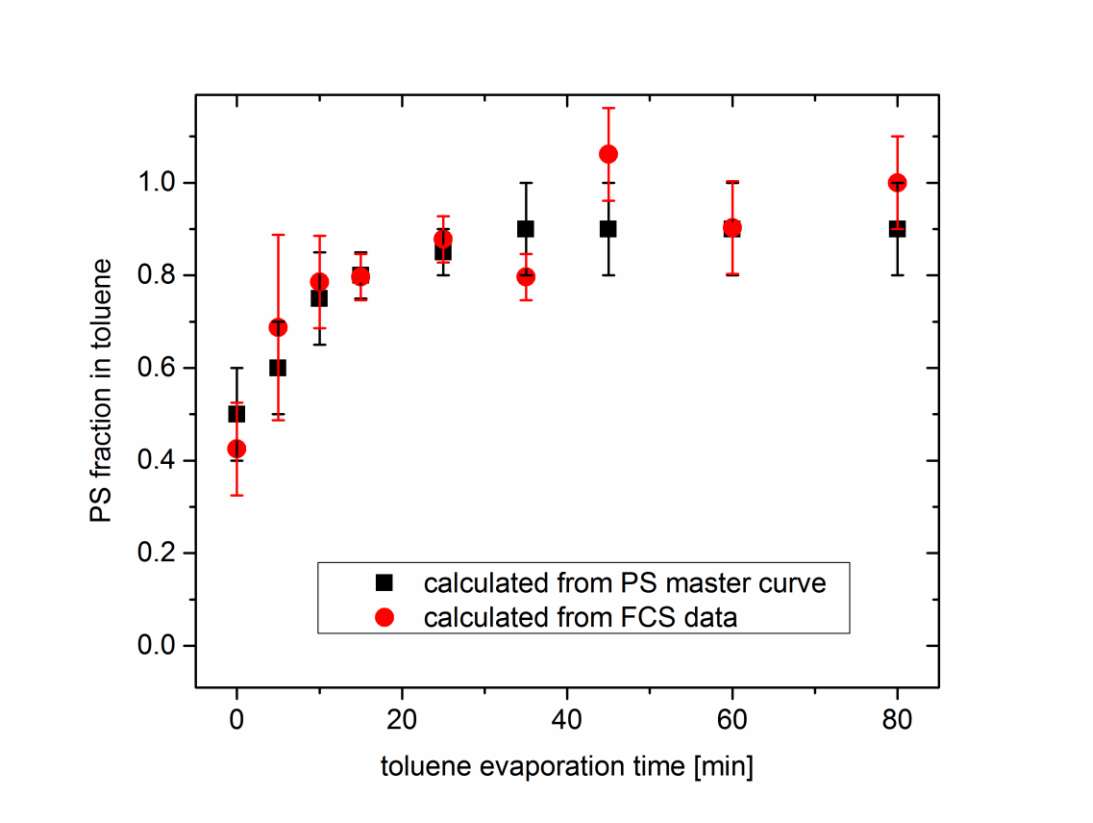

Figure 42: Fraction of polystyrene in the nanodroplet of the solvent evaporation process at different evaporation times, calculated from the PS master curve (black squares) and calculated from the droplets' hydrodynamic radii, as determined by fluorescence correlation spectroscopy (FCS, red circles) for sample D1.

The PS concentrations calculated from the master curve were in good agreement with the PS concentrations calculated from the FCS data. The final size of the nanoparticle was R_H = 20 nm.

The presence of the molecular rotor LBX37 in the SEED process allowed monitoring the shrinkage of the nanodroplets during the solvent evaporation and therefore the formation of the nanoparticles. The actual evaporation process started with a much lower solvent concentration as initially present in the preparation process, which was most likely caused by the sonication step. But the question why the final state of the process did not give a fluorescence lifetime that is similar to the lifetime measured in pure PS was still not clear.

4.3.5 Polystyrene Nanoparticles in Dry Environment

To exclude that the behavior of the fluorescent molecular rotor is different in bulk PS compared to PS nanoparticles, the prepared nanoparticle dispersions were dried and a thin film of solvent free PS nanoparticles was measured. The obtained decay curve is depicted in Figure 43. The measured data resulted in a fluorescence lifetime of τ = 5.4 ns. This value corresponded to 100 % PS in the master curve.

Hence, it was clear, that the fluorescence lifetime of PS nanoparticles prepared from solvent evaporation from emulsion droplets was not lower than in bulk polystyrene. The experiment was repeated with four different batches of polystyrene nanoparticles prepared from the SEED process. All samples gave the same results.

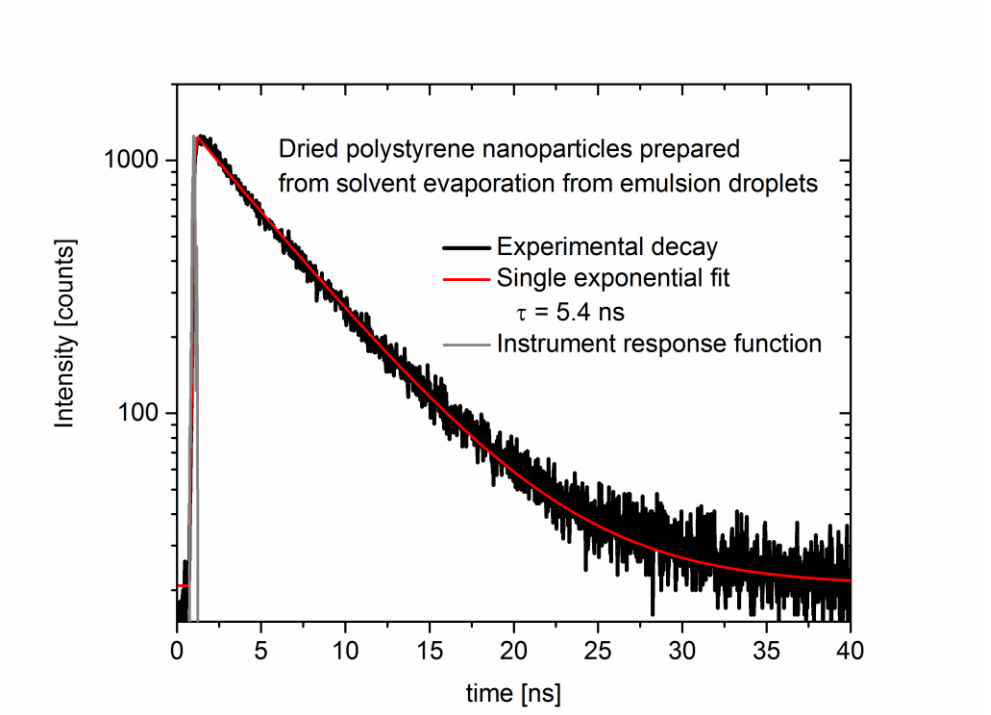

Figure 43: Experimental decay curve (black) of the fluorescent molecular rotor LBX37 in PS nanoparticles prepared from SEED. The instrument response function (IRF) is shown in grey. The decay was fitted with a single exponential fit function (red), giving a fluorescence lifetime of τ = 5.4 ns. The lifetime is comparable to 100 PS in the master curve.

The nanoparticle formation by solvent evaporation can be monitored via time-correlated single photon counting and fluorescence correlation spectroscopy. The concentration change inside the nanodroplet as well as the droplet shrinkage can be monitored. The experiment can either be performed from a larger reaction volume or from a small droplet. Both experiments show the same process behavior, but at different timescales.

4.3.6 Long Term Study of the Drying Process

Kinetic studies of the nanoparticle formation via solvent evaporation from emulsion droplets showed a fluorescence lifetime of less than 5 ns. This value was observed for studies from a large reaction volume as well as for monitoring the process from a small reaction droplet. In comparison to the master curve, the obtained fluorescence lifetime corresponded to a

polystyrene concentration of 90 %. But in the final state of the evaporation process a PS nanoparticle and therefore 100 % PS were expected. From the previous study of dried PS nanoparticle it was clear that the final SEED state was different from the dry particles. So the question occurred whether the SEED particles are really in their final state. The experiments showed that the evaporation process was very slow in the last phase. To be sure that no more toluene evaporateed after more than 24 h, one sample was measured again after three months. The measurements gave exactly the same fluorescence lifetimes values and amplitudes as obtained for the same sample after 24 h of evaporation. Hence, the evaporation process was completed in less than 24 h and no change was monitored after a longer time interval.

So, the assumed short evaporation was not the reason for the final lifetime in the SEED process that represented a PS concentration of 90 %.

4.3.7 Influence of SDS

As already mentioned it is possible that the presence of the surfactant SDS played a role in the experiments. SDS was needed to stabilize the emulsion and later the PS particle dispersion. The SDS molecules were present everywhere in the aqueous solution. Mainly they were separating the PS toluene emulsion droplets from the aqueous solution, but SDS could have also been present in form of micelles. It could be possible that these micelles encapsulated rotor molecules without polystyrene being present in the micelles.

To investigate the hypothesis of the SDS influence, an experiment was performed, in which a sample was prepared in the same way as it was done for the SEED kinetic experiments, but without any polystyrene.

The aim was to monitor the behavior of the molecular rotor in SDS solutions. After the evaporation of toluene (same procedure as done before), a decay curve as shown in Figure 44 was obtained. The fluorescence lifetime was

found to be 4 ns. Considering that this experiment showed only one species, it is most likely that these were rotor molecules in SDS micelles. These micelles could have been present in the actual SEED process for the formation of PS nanoparticles. If that is the case, the amount of micelles might be comparably small, but can still have an influence on the weighted average fluorescence lifetime.

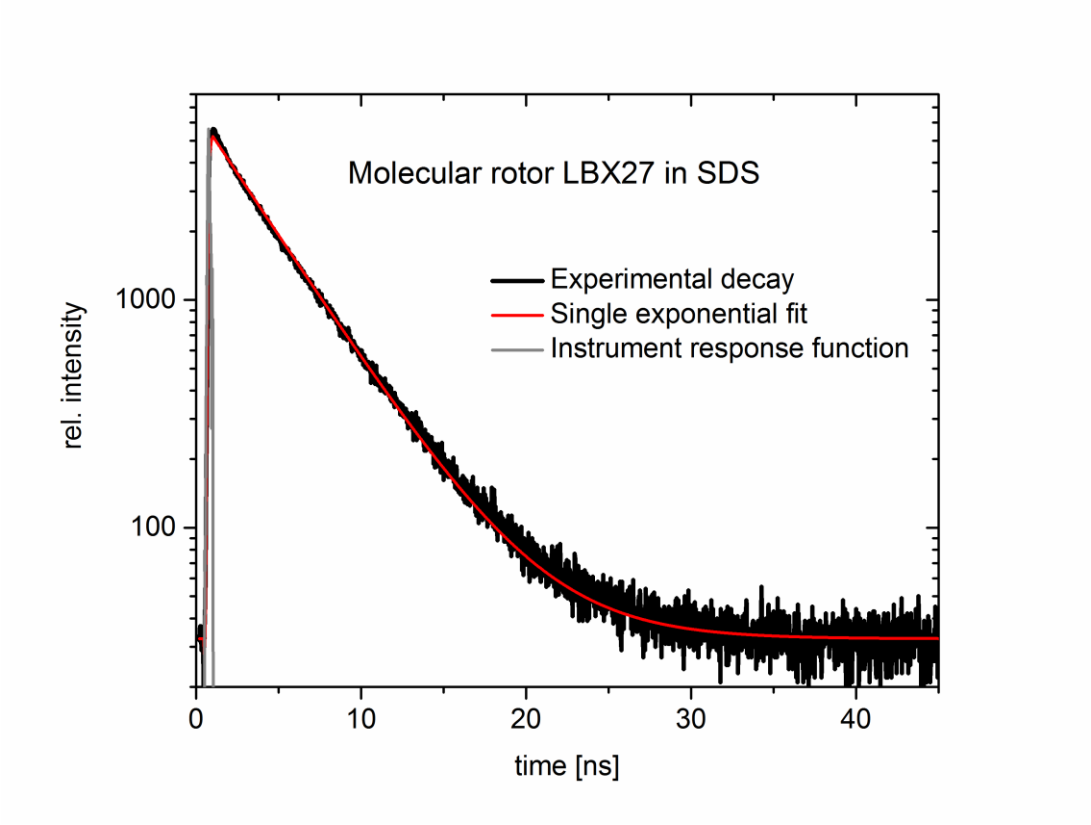

Figure 44: Experimental decay curve of the molecular rotor LBX37 in an SDS solution. The sample was prepared as described for the polymer nanoparticle formation via SEED, but without polymer to obtain data for the behavior of the rotor in SDS.

This study can explain that the average fluorescence lifetime of the final state particles was lower than expected, because SDS influenced the lifetime and changed it to lower values.

In conclusion, the formation of polystyrene nanoparticles via solvent evaporation from emulsion droplets was successfully monitored. The presence of the fluorescent molecular rotor LBX37 enabled determining the PS concentration as well as the size of the nanodroplet via TCSPC and FCS

measurements. Both analysis techniques can be performed simultaneously, giving comparable results. This method can be applied for samples from large reactions volumes as well as for small volumes, such as single droplets. Since the system is very complex, herein only the weighted average fluorescence lifetimes were taken into account. But as the results show, the influence of SDS, water or other factors can play a role. Therefore, the fluorescence lifetimes need to be analyzed in more details to obtain even more information about the drying process of the nanodroplet and the formation of the nanoparticles. This analysis is very complex, but more than interesting as a follow up project. Some initial studies are presented in the following.

4.3.8 A Closer Look Inside the Nanodroplets

In the previous experiments only the weighted average fluorescence lifetimes of the samples were discussed. But, if the decay could not be fitted with a single exponential fitting function, two or more fluorescence lifetimes were present. These lifetimes as well as their fractions might give a closer look inside the microenvironment and the nanoparticle formation process.

As an example, the short and long fluorescence lifetimes and amplitudes of sample D1 are shown in Figure 45 and Figure 46. The values for the short lifetimes increased from 0.6 ns to 2 ns with increasing toluene evaporation time. These values were also found in the master curve for PS concentrations up to 70 %. The long fluorescence lifetime increased from 4.3 ns up to 7.4 ns, values that could not be found in the master curve. The weighted average fluorescence lifetimes were suitable for comparisons to the master curve, but the short and long lifetimes were not. Maybe the drying process influenced the particle formation quite a lot.

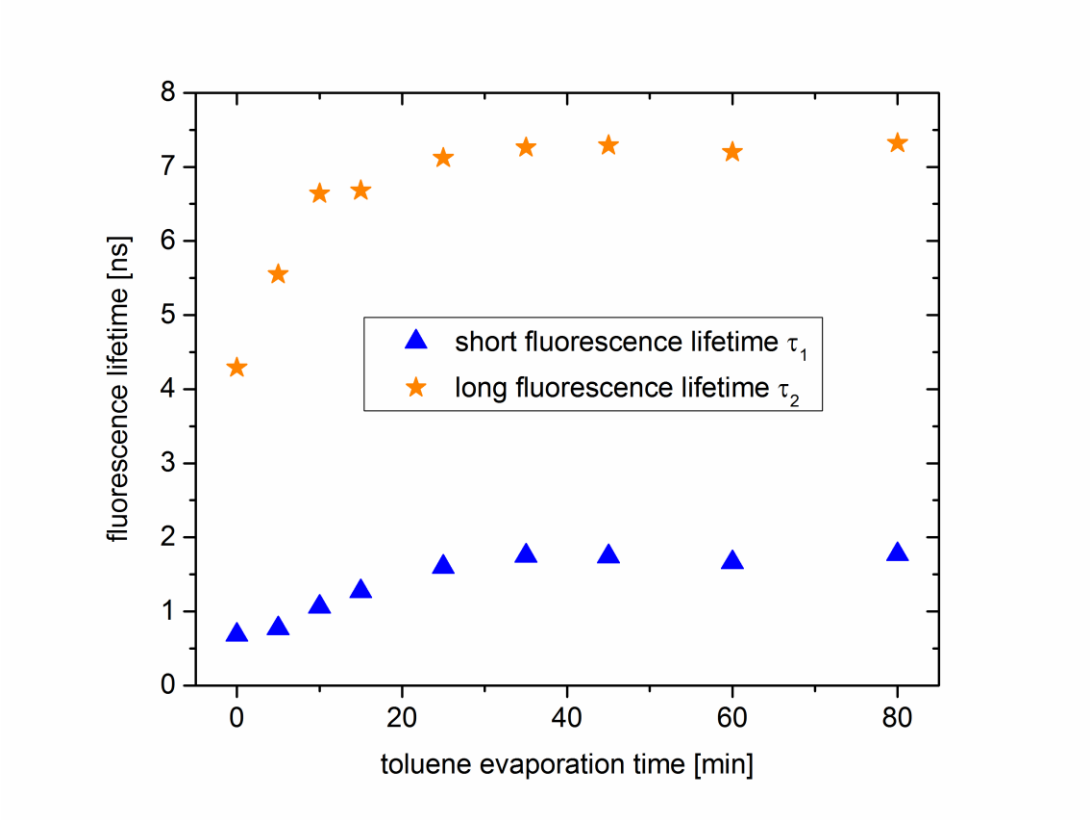

Figure 45: Fluorescence lifetimes of sample D1. Blue triangles show the short fluorescence lifetime τ_1 and orange stars resemble the long fluorescence lifetime τ_2.

To get a better insight, a closer look to the amplitudes of both lifetimes can be helpful. Figure 46 shows that the amplitudes of the short lifetime were dominant in the first minutes of toluene evaporation, but the amplitudes for the long lifetime increased and dominated the process in the final state. Nevertheless, both lifetimes were present in the final state of the particle formation. One hypothesis is that the particles were not homogeneous particles, but they may have been dried in a capsule like shape. Maybe there was an outer layer, or skin, that consisted of dry polystyrene, whereas inside there was still a fraction of toluene present. Both microenvironments would give different fluorescence lifetimes. Two different domains might also occur for the molecular rotor from the interaction with PS and SDS molecules and only with PS molecules.

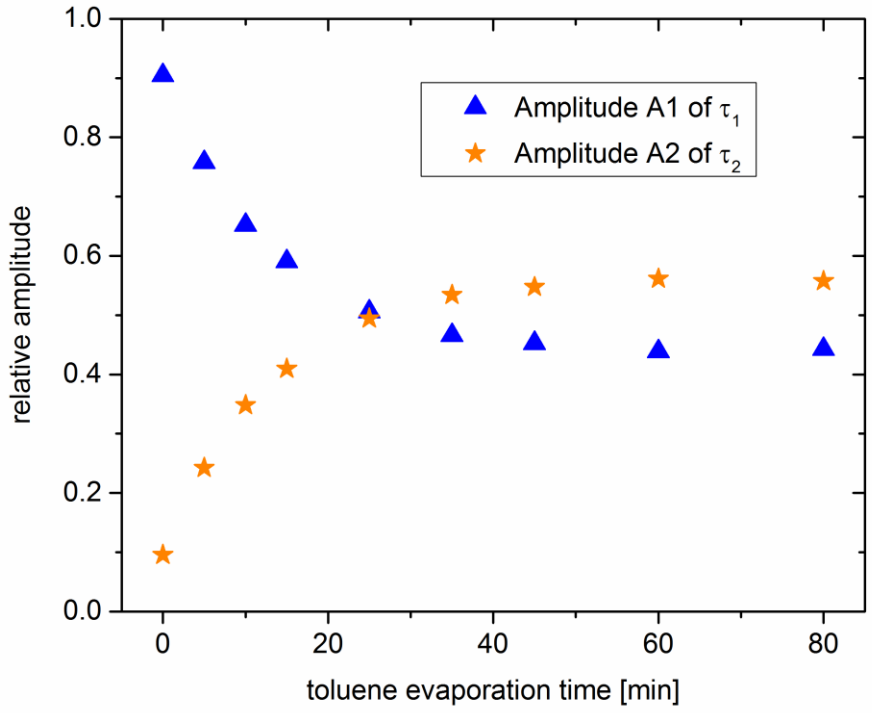

Figure 46: Amplitudes of the fluorescence lifetimes of sample D1. Blue triangles show the amplitude A1 of the short fluorescence lifetime τ_1 and orange stars resemble the amplitude A2 of the long fluorescence lifetime τ_2.

4.3.9 Polystyrene Nanoparticles from SEED with Chloroform

Another interesting factor for investigating the nanodroplet drying behavior is the solvent. Toluene as solvent for the nanoparticle formation was used for several reasons, but mainly because it did not evaporate too fast at room temperature, that measurements were possible in the time scale of the evaporation process. But, to gain more information about the influence of the solvent, the particle formation via SEED was also performed with chloroform as solvent. Both ways, from a large reaction volume (CV1) and from a single droplet (CD1) were tested. As an example the decay curves, fluorescence lifetimes and amplitudes of the droplet sample CD1 are presented and discussed in the following. Figure 47 presents the decay curves for sample CD1 that shifted to longer times during the chloroform

evaporation. The behavior was similar to the samples made from toluene. The data for the experiment from a large reaction volume CV1 are shown in the appendix.

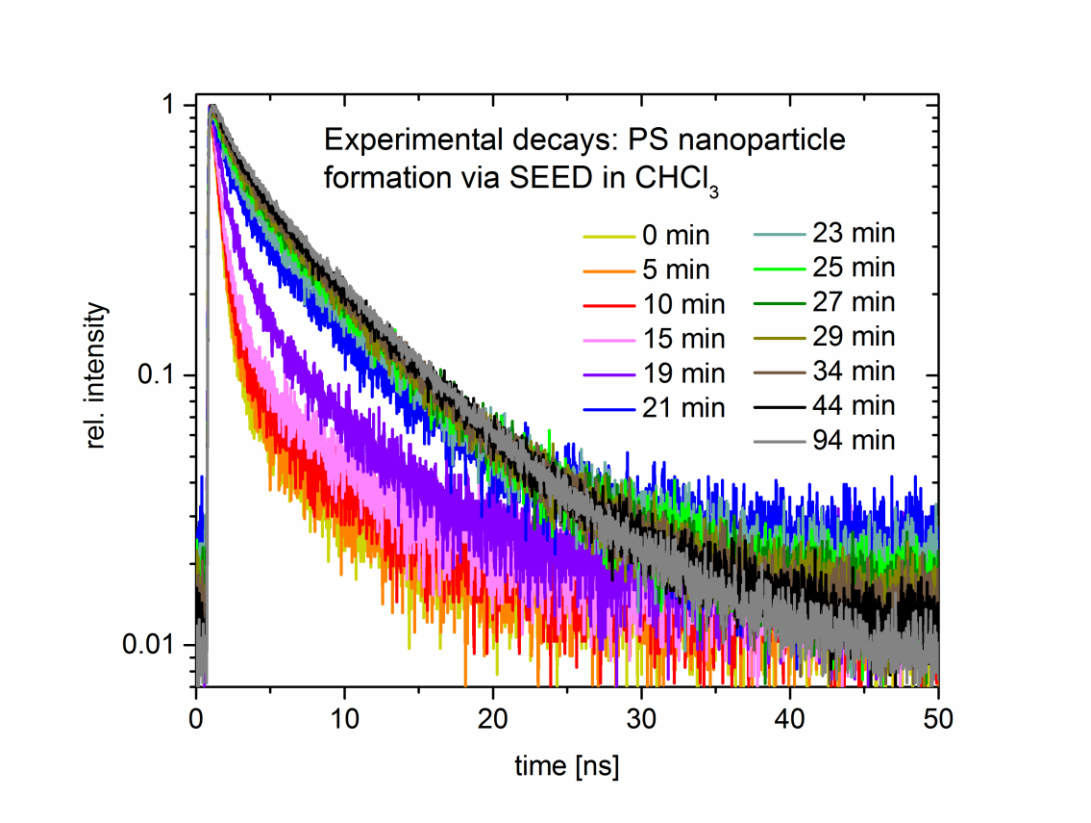

Figure 47: Experimental decay curves of sample CD1 (formation of polystyrene nanoparticle from solvent evaporation from emulsion droplets with chloroform as solvent), a 150 µL droplet. In appropriate time intervals a probe was measured via time-correlated single photon counting, giving the plotted decay curves. The process was finished after 44 min.

A closer look to the fluorescence lifetimes was made in Figure 48. The short, long and weighted average fluorescence lifetimes were plotted against the chloroform evaporation time. All three datasets showed a similar behavior. In the first minutes of the evaporation process, the changes were small, but within 15 min a strong change appeared. In this time range, the main process has happened. After 44 min the complete process was in the final state. If the lifetime values from Figure 48 were compared to the values obtained from toluene samples, the datasets were similar and the nanoparticle formation looked the same.

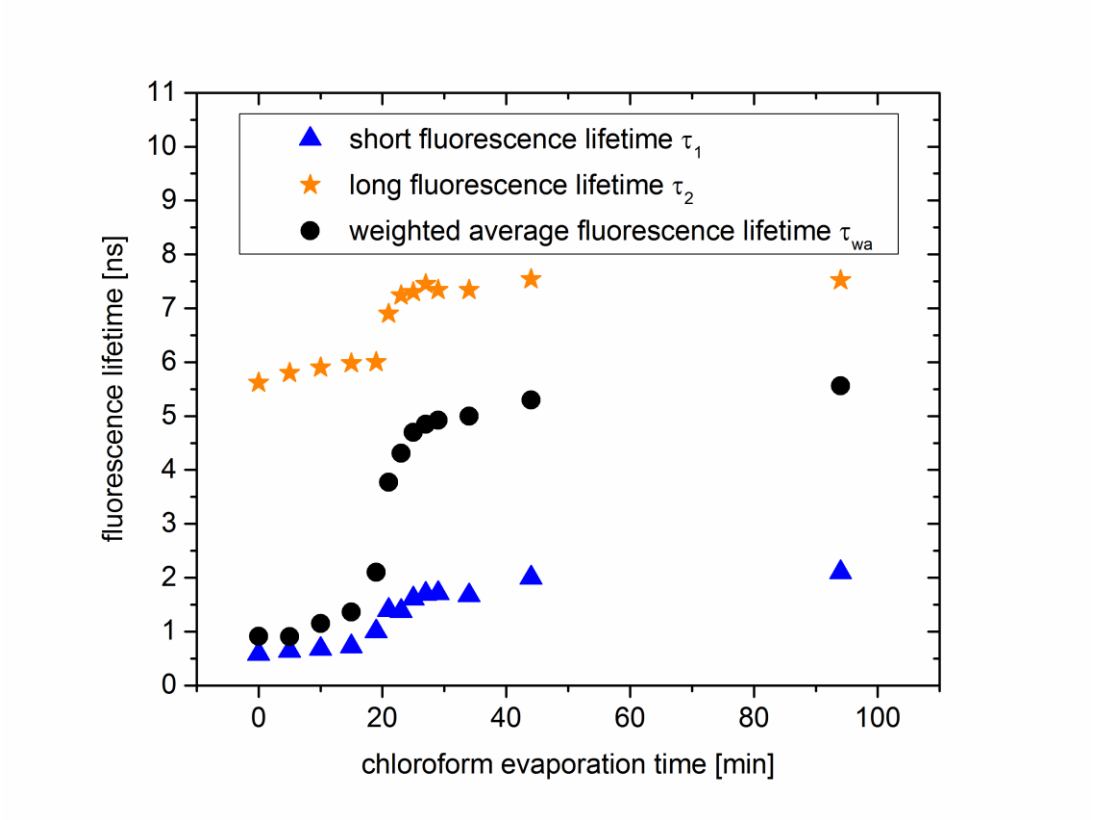

Figure 48: Fluorescence lifetimes of sample CD1. Blue triangles show the short fluorescence lifetime τ_1, orange stars resemble the long fluorescence lifetime τ_2 and black circles resemble the weighted average fluorescence lifetime τ_{wa}.

Looking at the amplitudes in Figure 49, the fast evaporation and the lifetime change was observed, too. The short lifetime had a high amplitude in the first minutes, but the fraction of the long lifetime increased drastically within 15 min, that showed the strong jump of the lifetimes. Herein, as well as in the toluene samples, the final state of the nanoparticle formation showed a long lifetime to short lifetime ratio of 6:4.

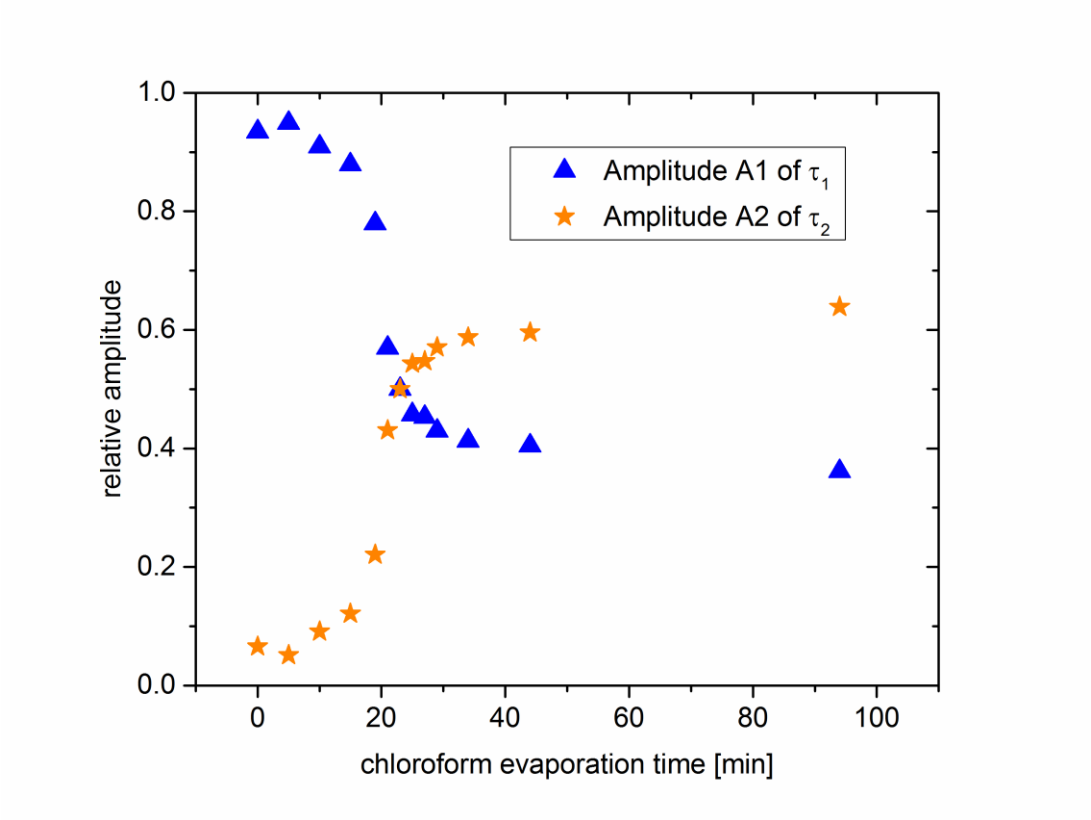

Figure 49: Amplitudes of the fluorescence lifetimes of sample CD1. Blue triangles show the amplitude A1 of the short fluorescence lifetime τ_1 and orange stars resemble the amplitude A2 of the long fluorescence lifetime τ_2.

In conclusion, the nanoparticle formation via solvent evaporation from emulsion droplets can be monitored in the presence of different solvents, such as toluene and chloroform and the obtained data show a similar behavior of the fluorescence lifetimes and amplitudes of the molecular rotor.

4.4 Summary and Outlook

This project presents a different perspective in the field of polymer nanoparticles, besides the preparation methods themselves or the possible applications of the particles. Herein, the formation process of nanoparticles was studied, to gain more information about the technique, in order to use this process for the formation of nanoparticle drug delivery systems.

In this work, the nanoparticle formation of the SEED (solvent evaporation from emulsion droplets) process was studied. With this method, nanoparticles for drug delivery issues could be prepared. A deeper understanding of the formation process, would enable easier formation of new drug delivery systems. Polystyrene (PS) nanoparticles were prepared by the evaporation of toluene from an emulsified system. This evaporation process was monitored by adding a fluorescent molecular rotor to the procedure. This rotor showed a fluorescence lifetime, which depends on the microenvironment and mainly on the viscosity. Hence, the determination of the lifetime, led to information about each stage in the process of nanoparticle formation.

Experiments regarding the fluorescence lifetime of the rotor molecule in different environments from pure toluene, various PS-toluene solutions and pure PS, clearly showed the viscosity-dependent behavior. In a low viscosity environment, as in toluene, the lifetime was 0.6 ns and increased with increasing fraction of PS in the solutions until a fluorescence lifetime of 5.1 ns was reached in a pure PS film. The weighted average fluorescence lifetimes of these samples formed the master curve for later determination of the PS concentration.

To understand the particle formation during the evaporation process, the weighted average fluorescence lifetimes were determined via TCSPC measurements and with the help of the master curve the PS concentration

in the nanodroplets was calculated. Hence, the method enabled the determination of the stage of the particle formation process.

Additionally to the lifetime measurements, fluorescence correlation spectroscopy (FCS) was used to investigate the size of the toluene-PS droplets during the evaporation process. The hydrodynamic radius of the droplet was calculated from the diffusion coefficients. FCS data showed a decreasing droplet size from the beginning of the evaporation process until the final particles size was reached. Furthermore, FCS data were used to determine the PS concentrations in the nanodroplets, which were in good agreement to the concentrations calculated from TCSPC experiments and the master curve.

The presence of two fluorescence lifetimes in the particle formation process has shown that the nanoparticles may form in an inhomogeneous way. It is possible that a core-shell-like drying process was present in the SEED nanoparticle formation procedure. Further investigations are necessary to understand the process in more details.

Fluorescence molecular rotors are helpful molecules to monitor the nanoparticle formation via SEED and give the possibility to understand the evaporation process. Even though, this work gives just a first glance on what is possible, further studies could be beneficial to understand the process even more. An interesting aspect would be to investigate in much more details, if the particles dry in a homogeneous way or if they end up more heterogeneous, e.g. forming capsules. Therefore, the precise determination of the fluorescence lifetimes from multi-exponential decays needs to be improved further. Another interesting study could be to monitor the same particle formation, but with another rotor molecule and compare the results.

Besides the SEED process for nanoparticle formation, there are many more other ways. The investigation of these methods, such as miniemulsion polymerization, would be beneficial to understand the ways to prepare nanoparticles for drug delivery in a defined process.

4.5 Appendix – Additional Datasets

Additional data are presented in the figures and tables of this section.

Table 3: Fluorescence lifetimes, amplitudes and weighted average fluorescence lifetime data of the master curve (molecular rotor in different concentrations of polystyrene PS in toluene).

Fraction PS in toluene	Fluorescence lifetime 1 τ_1 in ns	Fluorescence lifetime 2 τ_2 in ns	Amplitude of τ_1 A1	Amplitude of τ_2 A2	Weighted average fluorescence lifetime τ_{wa} in ns
0	0.60	-	-	-	0.60
0.1	0.60	3.0	0.997	0.003	0.61
0.2	0.62	3.5	0.995	0.006	0.63
0.3	0.69	3.3	0.982	0.018	0.74
0.4	0.75	3.6	0.973	0.028	0.83
0.5	0.93	3.5	0.923	0.077	1.11
0.6	1.20	3.7	0.84	0.16	1.60
0.63	1.13	3.4	0.85	0.15	1.64
0.65	1.50	4.0	0.70	0.30	2.25
0.7	1.58	4.3	0.68	0.32	2.42
0.73	1.91	4.9	0.27	0.73	3.36
0.8	2.03	4.5	0.45	0.55	3.07
0.85	2.20	5.0	0.25	0.75	4.30
0.89	3.20	5.6	0.28	0.72	4.93
0.9	3.00	5.2	0.20	0.80	4.76
1	-	5.1	-	-	5.1

Table 4: Fluorescence lifetimes, amplitudes and weighted average fluorescence lifetime data sample V1 (SEED of PS toluene nanodroplets – large reaction volume).

Toluene evapo-ration time t in h	Fluorescence lifetime 1 τ_1 in ns	Fluorescence lifetime 2 τ_2 in ns	Amplitude of τ_1 A1	Amplitude of τ_2 A2	Weighted average fluorescence lifetime τ_{wa} in ns
1	0.797	5.10	0.92	0.08	1.16
2	0.801	5.20	0.92	0.08	1.16
3	1.22	6.04	0.80	0.20	2.19
4	1.55	6.91	0.45	0.55	4.52
5	1.52	6.92	0.45	0.55	4.50
6	1.53	6.92	0.46	0.54	4.47
7	1.58	6.93	0.44	0.56	4.57

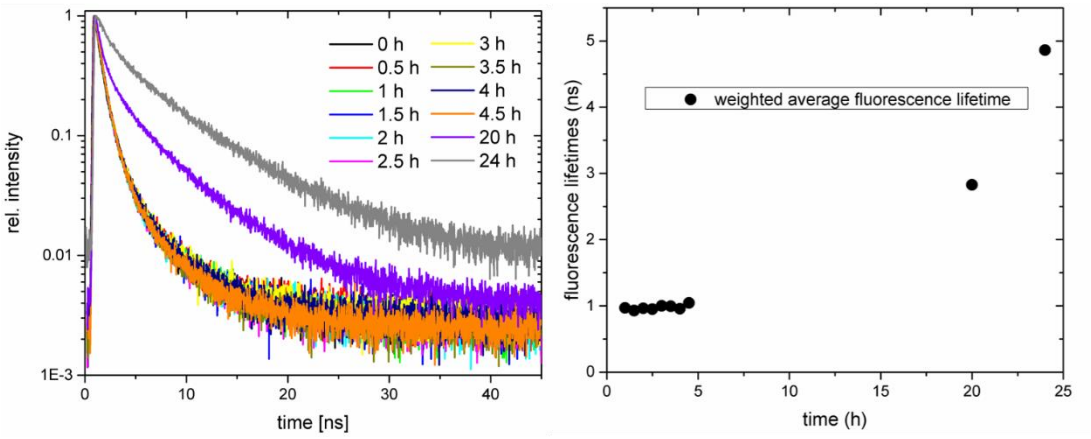

Figure 50: Sample V2 – SEED of polystyrene toluene nanodroplets. Left: Experimental decay curves measured via TCSPC at different time intervals of the evaporation process. Right: Weighted average fluorescence lifetimes, obtained from the experimental decays.

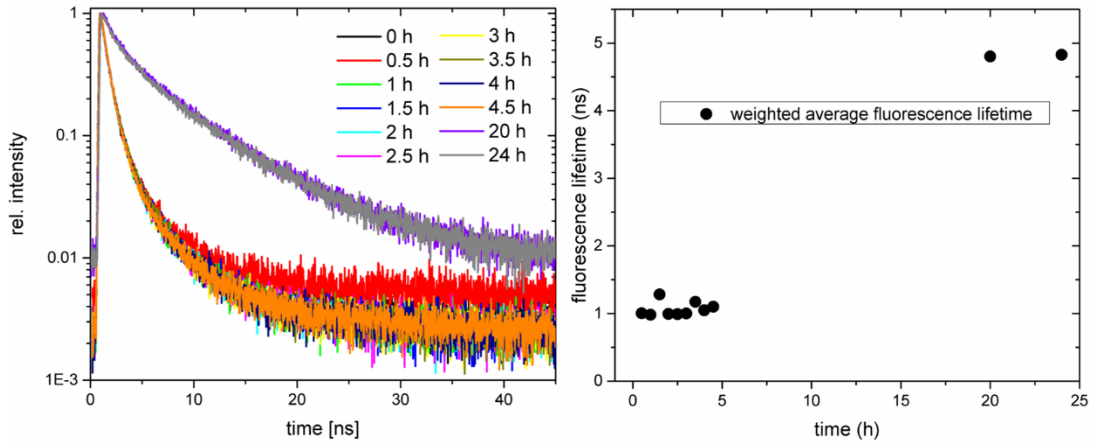

Figure 51: Sample V3 – SEED of polystyrene toluene nanodroplets. Left: Experimental decay curves measured via TCSPC at different time intervals of the evaporation process. Right: Weighted average fluorescence lifetimes, obtained from the experimental decays.

Table 5: Fluorescence lifetimes, amplitudes and weighted average fluorescence lifetime data sample D1 (SEED of PS toluene nanodroplets from a 150 µL droplet).

Toluene evapo-ration time t in min	Fluorescence lifetime 1 τ_1 in ns	Fluorescence lifetime 2 τ_2 in ns	Amplitude of τ_1 A1	Amplitude of τ_2 A2	Weighted average fluorescence lifetime τ_{wa} in ns
0	0.68	4.29	0.904	0.096	1.03
5	0.77	5.55	0.758	0.242	1.93
10	1.06	6.64	0.652	0.348	3.00
15	1.27	6.68	0.591	0.409	3.49
25	1.60	7.12	0.506	0.494	4.33
35	1.75	7.26	0.466	0.534	4.69
45	1.74	7.29	0.452	0.548	4.78
60	1.66	7.2	0.439	0.561	4.77
80	1.77	7.32	0.443	0.557	4.86

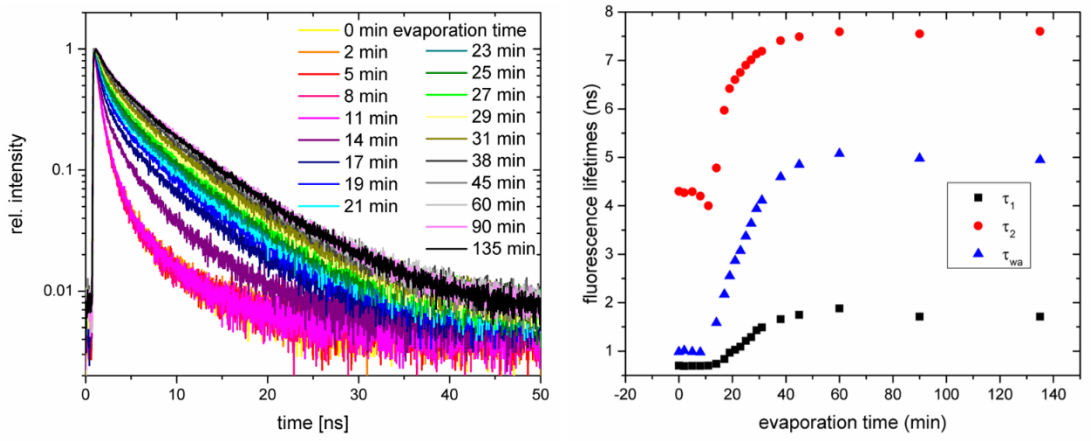

Figure 52: Sample D2 – SEED of polystyrene toluene nanodroplets in a 50 µL droplet. Left: experimental decay curves measured via TCSPC at different time intervals of the evaporation process. Right: Fluorescence lifetimes, obtained from the experimental decays.

Table 6: Fluorescence lifetimes, amplitudes and weighted average fluorescence lifetime data sample CD1 (SEED of PS chloroform nanodroplets from a 150 µL droplet).

$CHCl_3$ evapo-ration time t in min	Fluorescence lifetime 1 τ_1 in ns	Fluorescence lifetime 2 τ_2 in ns	Amplitude of τ_1 A1	Amplitude of τ_2 A2	Weighted average fluorescence lifetime τ_{wa} in ns
0	0.585	5.62	0.934	0.066	0.91
5	0.640	5.80	0.949	0.051	0.90
10	0.677	5.90	0.909	0.091	1.15
15	0.724	5.98	0.879	0.121	1.36
19	1.00	6.00	0.779	0.221	2.10
21	1.40	6.90	0.569	0.431	3.77
23	1.38	7.24	0.499	0.501	4.31
25	1.61	7.30	0.457	0.543	4.70
27	1.70	7.45	0.453	0.547	4.85
29	1.71	7.34	0.429	0.571	4.92
34	1.67	7.34	0.413	0.587	5.00
44	2.0	7.54	0.404	0.596	5.30
94	2.1	7.52	0.361	0.639	5.56

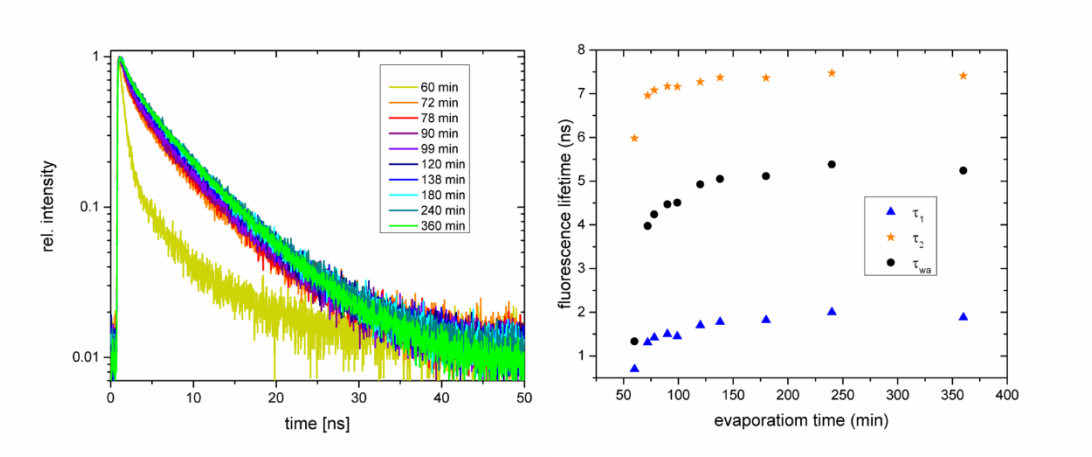

Figure 53: Sample CV1 – SEED of polystyrene chloroform nanodroplets from a large reaction volume. Left: Experimental decay curves measured via TCSPC at different time intervals of the evaporation process. Right: Fluorescence lifetimes, obtained from the experimental decays.

5 Concluding Remarks

In this thesis, two different methods which were dealing with drug delivery systems were presented. The first method represents a newly developed technique to prepare uniform and size-defined cell membrane models, whereas the second method facilitates to monitor and understand the preparation of nanoparticles. The main commonality of both methods besides the application for drug delivery systems is the usage of fluorescent molecules and fluorescence based methods.

A new method for the preparation of biological cell models was developed in the first part of this work. The huge variety of different kinds of cell membrane models that were already in use for many years was improved by this new technique, which enables to form giant unilamellar vesicles as cell models in a size-defined way. Three different diameters were presented in this work, all of them in size dimensions of biological cells. The vesicle formation was realized using a polymer hydrogel template that was micro-patterned via photolithography. The very defined composition of the polymer hydrogel, its cross-linking and swelling behavior were investigated and resulted in an ideal template for growing hundreds of vesicles on one template. The research on biological cells won't stop in the near future, because cells are our smallest living building units and researchers want to understand their properties and functions, especially in the field of drug delivery systems. New systems can overcome old and new diseases. Hopefully, this method will help to understand the functions of biological cells and cell membranes a bit more.

As just said, the field of drug delivery systems is huge and promising to fight against certain diseases. The second part of this work focused on the formation of nanoparticles which can be used as drug carriers. Polystyrene as a cheap and well known polymer is often used in this regard, because it

is biocompatible. The precise formation of the nanoparticles is essential for the formation of very defined drug delivery systems. To understand the formation of polystyrene nanoparticles, their preparation via solvent evaporation from emulsion droplets was monitored. Even though, the here presented method is still in the beginning of its development, it can be very helpful to understand and tune the formation process depending on the desired properties of the nanoparticles.

The whole work is based on polymer systems. Polymers are versatile and have their use and applications in various disciplines and research fields. Herein, two completely different polymer systems were studied. The first system was based on a terpolymer, whose monomer units were statistically distributed. It contained a special unit, which was activated by UV light and cross-linked the polymer chains to a covalently bound network. Additionally this network was able to absorb water, because it served as hydrogel. A completely different polymer system – polymer nanoparticles – were studied in the second project. Polymer nanoparticles are interesting systems, because their properties differ from their bulk systems, due to their very small sizes. And besides the two polymer systems that were investigated in this thesis, many other types of polymer systems exist and are worth to study. The manifoldness of polymers, their combinations, functionalities and properties will provide the fundaments of polymer research for many more decades.

6 FCS Analysis of Polymer-Based Systems - Cooperative Projects

Fluorescence correlation spectroscopy (FCS) is a unique tool, that is used in many scientific disciplines. In this chapter, the manifold usage of FCS in different collaborative projects, is shown. In cooperation with the collaborative research center (CRC) 1066 – "Nanodimensional polymer therapeutics for tumor therapy" – and as the work of the Q2 project (Querschnittsprojekt – cross section project) – "Optical methods to study endocytosis, intracellular trafficking and cargo release" – FCS was used to determine the diffusion time and coefficient as well as the hydrodynamic radius of different (mainly polymeric) species. Specific functionalizations, conjugations and coatings were characterized and confirmed. Investigating the formations of aggregates and determining the labeling efficiency are more experiments, which can be performed using FCS.

A cooperative project with M. Schinnerer (JGU Mainz, manuscript in preparation) focuses on a polymer brush based system for tumor immune therapy. With FCS the size of the molecules was determined and the absence of aggregates and free fluorescent dyes in the system was ensured. Furthermore, the number of dyes per brush and the number of conjugated antibodies per polymer brush was calculated from the fluorescence brightness of the freely diffusing dye or antibody and the polymer brush.

Fluorescence cross-correlation spectroscopy (FCCS) was used in some of the collaborative projects. The main difference to FCS is the usage of two differently colored fluorescent molecules, instead of one. Both dyes have an individual beam path, but an overlapping confocal volume. If both dye-molecules are diffusing together, both intensity fluctuations correlate, leading to a cross-correlation curve.

6.1 Fluorescence Correlation Spectroscopy (FCS) Characterizes Antibody-Polyplex-Conjugates for Cell Targeting

The chemical attachment of DEC205 antibodies to polyplexes was investigated in this work. The DEC205 antibody is specific for targeting dendritic immune cells (DCs) and thus interesting for cancer immune therapy. Azide-containing block copolymers P(Lys)-*b*-P(HPMA) were used for the complexation of plasmid-DNA (pDNA). The conjugation of the block copolymer and the antibody was performed using strain-promoted alkyne-azide cycloaddition (SPAAC). Dibenzocyclooctyne (DBCO) moieties were incorporated site-specific to the DEC205 antibody. The chemical accessibility of DBCO molecules within the antibody and the accessibility of azide-functionalities on the surface of the polyplex were characterized by fluorescence correlation spectroscopy.

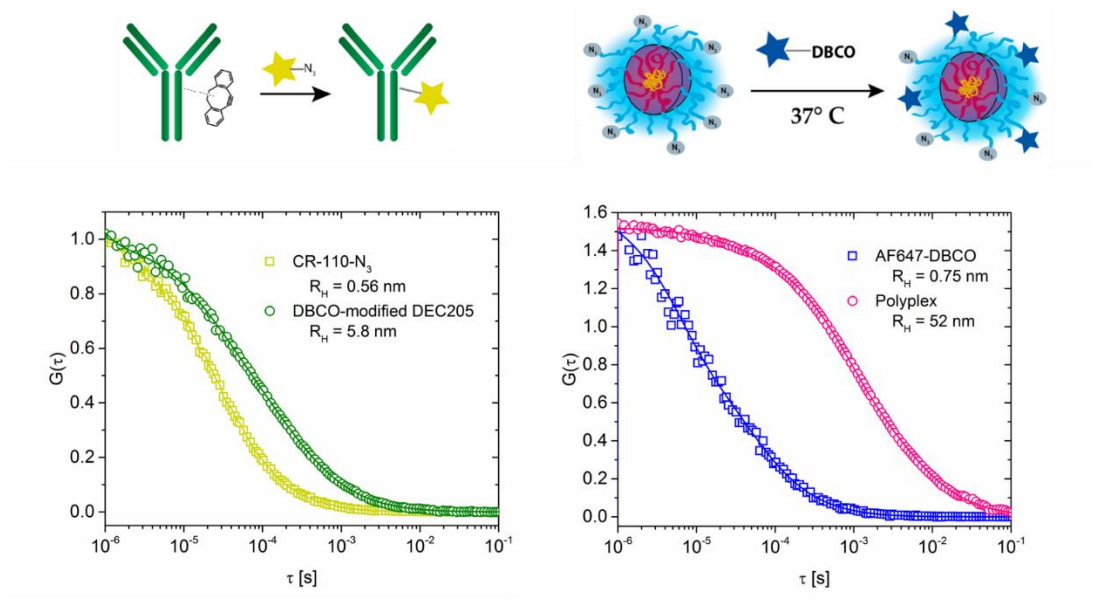

Figure 54: Left: Experimental FCS autocorrelation curves for the azide-dye (CR-110-N3) and the DBCO-modified DEC205 antibody. The shift of the correlation curve indicated slower diffusion and confirmed that the azide-dye was covalently attached to the antibody. Right: Experimental autocorrelation curves of the DBCO-dye (AF647-DBCO) and the azide-functionalized polyplex. The shift towards longer diffusion times confirmed the addition of DBCO-dye to the azide-functionalized polyplex.

The experimental autocorrelation curves are shown in Figure 54: On the left, the DBCO functionalization of the DEC205 antibody was confirmed by the successful SPAAC of an azide-containing fluorescent dye. Furthermore, the conjugation of a DBCO-dye to the azide-functionalized polyplex is shown on the right side of Figure 54. The measurements show the general accessibility of the azide functionalities on the polyplex' surface. The reaction of DBCO-functionalized DEC205 antibody with the azide functionalized polyplex was also studied via FCS. The measurements showed the successful SPAAC reaction, but a huge amount of non-conjugated antibody remained.

FCS was an ideal method to characterize SPAAC reactions of macromolecules with small amounts of reactive groups by determining the size increase of the fluorescent species resulting from the performed conjugation reaction. This work presents the concept of the functionalization of nanoparticles with antibodies with site-specific DBCO-modifications.

This work was published in *Polymers* (2018, 10, 141), entitled "Site-Specific DBCO Modification of DEC205 Antibody for Polymer Conjugation" as joint project of the CRC1066 together with S. Beck, H.-J. Räder, R. Holm, M. Schinnerer, M. Barz, K. Koynov and R. Zentel.

6.2 Fluorescence Correlation Spectroscopy Confirms Successful Coating of Dendritic Mesoporous Silica Nanoparticles (DMSN) with a pH-Responsive Block Copolymer for Drug Delivery

This project focused on a new drug delivery system for the tumor necrosis factor-alpha (TNF-α), a highly toxic drug used in cancer therapy. Herein, dendritic mesoporous silica nanoparticles (DMSN) were coated with a pH-responsive block copolymer gate system. The system combined charged hyperbranched polyethylenimine (PEI) and nonionic hydrophilic polyethylenglycol (PEG) to encapsulate and deliver TNF-α into cancer and dendritic cells. FCS was used to confirm that the nanoparticles were coated with the pH-responsive block copolymer.

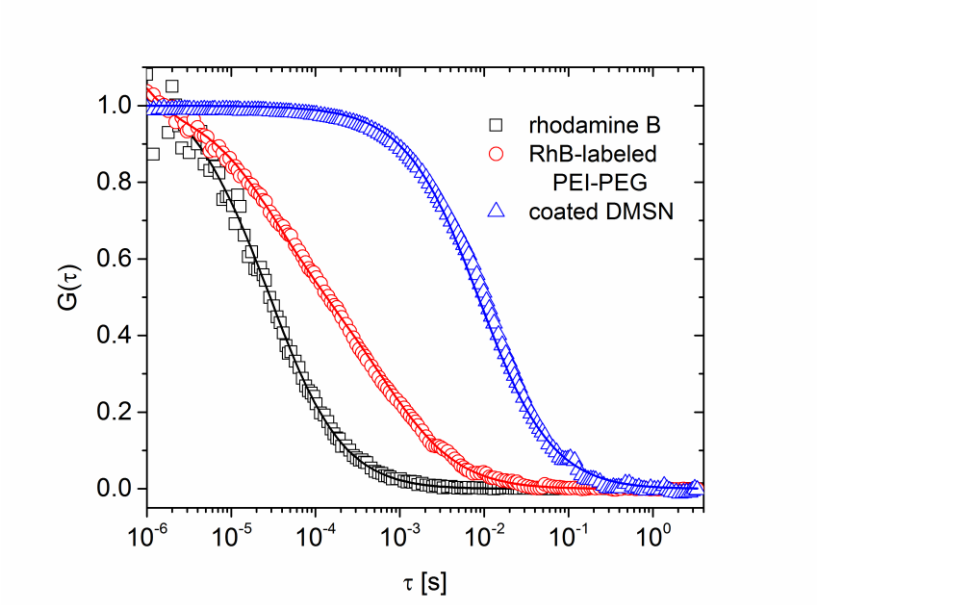

Figure 55: FCS autocorrelation curve of the free rhodamine B (black squares), RhB-labeled PEI-PEG (red circles), and the coated DMSN (blue triangles). The shift of the curves towards slower diffusion times and the resulting hydrodynamic radius R_h of 115 nm for the coated DMSN demonstrates successful functionalization with the gatekeeper.

Figure 55 shows the autocorrelation curves of freely diffusing rhodamine B (RhB, black squares), rhodamine B labeled block copolymer PEI-PEG (red

circles) and the PEI-PEG coated DMSN (blue triangles). The shift towards longer diffusion times indicated a significant change in the size of the diffusing species. The shift of the autocorrelation curve for DMSN towards longer diffusion times confirmed the successful coating with the polymer. DMSN encapsulation with pH-sensitive PEI-PEG is a promising approach drug delivery in cancer therapy.

This work was published in *Advanced Healthcare Materials* (2017, 1700012), entitled ”Dendritic Mesoporous Silica Nanoparticles for pH-Stimuli-Responsive Drug Delivery of TNF-Alpha” as joint project of the CRC1066 together with A. Kienzle, S. Kurch, J. Schlöder, C. Berges, R. Ose, J. Schupp, A. Tuettenberg, H. Weiss, S. Winzen, M. Schinnerer, K. Koynov, M. Mezger, N. K. Haass, W. Tremel and H. Jonuleit.

In a second cooperative project (manuscript in preparation), the dendritic mesoporous silica nanoparticles (DMSNs) were coated with ferrocene-carboxyaldehyde and fluorescence cross-correlation spectroscopy was used to confirm the in situ coordination of a cyclodextrine sugar cap to the ferrocene moiety on the DMSNs. The aim was to seal a small molecule for drug delivery into the DMSN with the help of the sugar cap.

6.3 Fluorescence Cross-Correlation Spectroscopy (FCCS) Verifies the Functionalization of Dual Labeled Block Copolymers

This project introduced a new synthetic approach for trifunctional block copolymers that enable site-specific conversion of the reactive entities in one step. Herein, polysarcosine-*block*-poly(*S*-alkylsulfonyl)-*L*-cysteine (PSar-*b*-PCys(SO_2Et)) block copolymers self-assembled into core-shell nanostructures. The hydrophilic moiety was labeled with a DBCO-CR110 dye and the hydrophobic part with a Cy5-NHS dye to confirm the simultaneous functionalization of the reactive groups. The dual labeled core-cross-linked particles were analyze by fluorescence cross-correlation spectroscopy (FCCS). The advantage of FCCS is that both fluorescent dyes are exited simultaneously with two different lasers. Their diffusion is recorded as in conventional FCS experiments and the autocorrelation curves of both dyes are cross-correlated to confirm the joint diffusion of the dyes, when they are attached to the same molecule.

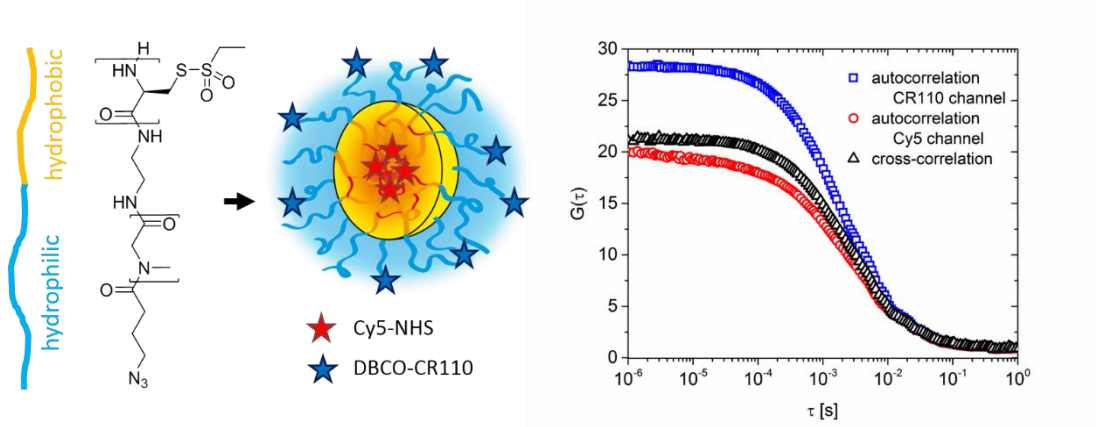

Figure 56: Left: Polysarcosine-*block*-poly(S-alkylsulfonyl)-L-cysteine block copolymer was self-assembled to a micelle with Cy5-NHS dyes in the core and DBCO-CR110 dyes in the corona. Right: FCCS auto- and cross-correlation curves of the dual labeled particles show strong cross-correlation, confirming dual labeling.

The FCCS experiment confirmed the simultaneous functionalization of the core and the corona of the polymer micelle. The amplitude of the cross-

correlation curve (black triangles) is comparable to the amplitudes of the autocorrelation curves, implying that both dyes were attached to the core-cross-linked micelle. The PSar-*b*-PCys(SO_2Et) block copolymers showed independently addressable and spatially separated functional groups, enabling simultaneous functionalization of the core and the shell. In a single step, active targets and fluorophores for detection can be introduced in the block copolymer micelles.

This work was published in *ACS Macro Letters* (2017, 6, 1140−1145), entitled ”Combining Orthogonal Reactive Groups in Block Copolymers for Functional Nanoparticle Synthesis in a Single Step” as joint project of the CRC1066 together with O. Schäfer, K. Klinker, L. Braun, D. Huesmann, K. Koynov and M. Barz.

6.4 Fluorescence Correlation Spectroscopy Demonstrates the Covalent Linkage of Functional Groups to Polymersomes

In this project, multifunctional polymersomes with controlled properties were prepared. The importance of studies on the cellular level has been discussed already in the first project of the thesis. Herein, polymeric vesicles, also called polymersomes and able to mimic cellular functions, were investigated. The polymersomes are artificial cells made from poly(butadiene)-*block*-poly(ethylene oxide) (PB-*b*-PEO). Via film hydration or a microfluidic approach PB-*b*-PEO was self-assembled into polymersomes. These vesicles exhibit a multifunctional surface, which allowed the integration of various molecules into this synthetic membrane. Fluorescence correlation spectroscopy was needed to demonstrate the covalent linkage of the different functionalities to the terminal groups of the polymer. The acrylate functionality was confirmed using a bodipy-amine dye and the alkyne functionality was confirmed with the help of a chromeo-azide dye. Both dyes can only bind to the polymer, when the equivalent functionality is present in the polymer, verifying the covalent linkage to the polymer (see Figure 57).

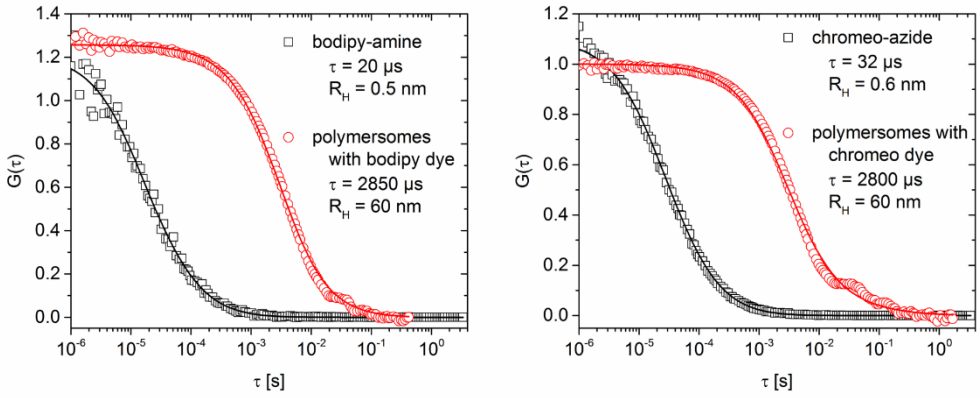

Figure 57: Experimental FCS autocorrelation curves of functionalized polymersomes with (left) bodipy-amine dye to confirm the presence of acrylate functionalities in the polyersome and (right) chromeo-azide dye to confirm the alkyne functionality.

For both dye labeled polymersomes the autocorrelation curves, generated from FCS experiments, were delayed compared to the freely diffusing dyes, confirming the attachment of the dyes to the larger species which diffuses much slower. Fitting with a single component model function showed that only one species was present and that the dye molecules were completely attached to the polymer (no free dye was present in the polymer and polymersomes). From the experiments the diffusion times and the hydrodynamic radii were obtained.

This work was published in *Soft Matter* (2017, 14, 6, 894-900), entitled ”A modular approach for multifunctional polymersomes with controlled adhesive properties” as joint project together with J. Petit, L. Thomi, M. Makowski, I. Negwer, K. Koynov, S. Herminghaus, F. Wurm, O.Bäumchen and K. Landfester.

6.5 Fluorescence Correlation Spectroscopy Determines the Critical Micelle Concentration

Fluorescence correlation spectroscopy can be used in many different research fields. Herein, FCS helps to investigate the dewetting dynamics of surfactant solutions. To understand the correlation between the dewetting dynamics and the surfactant properties, low and high molecular weight surfactants were compared. As high molecular weight surfactant a PEO-PPO-PEO triblock copolymer, also called Pluronic F-127, was used for this work.

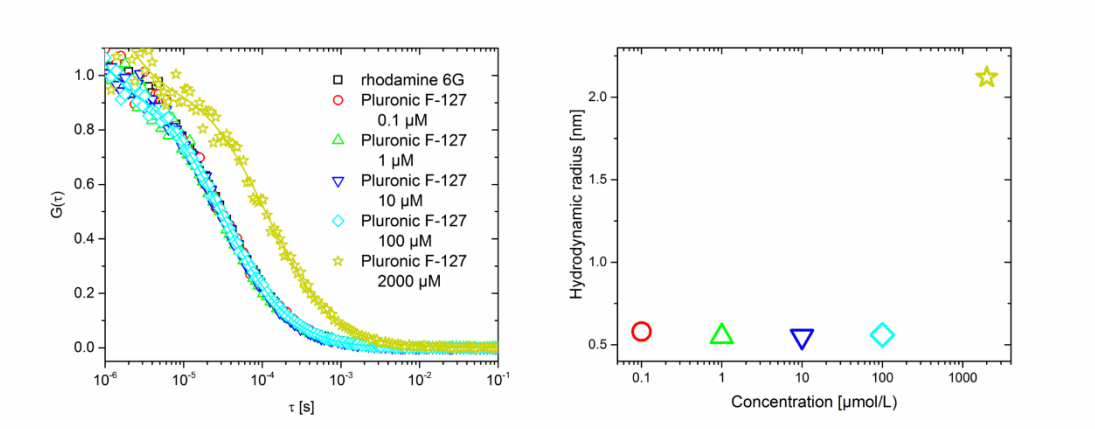

Figure 58: Left: Experimental FCS autocorrelation curves for rhodamine 6G in Pluronic F-127 sultions of different concentrations. Right: Hydrodynamic radii of rhodamine 6G at different surfactant concentrations. The hydrodynamic radius is the same as in water for surfactant concentrations up to 100 µM. The radius is larger at concentrations above CMC, because the dye molecules are encapsulated in surfactant micelles, which are larger and diffuse slower.

With FCS, the surfactant concentration was determined, at which the surfactant forms aggregates. Therefore, the weakly hydrophobic fluorescent dye rhodamine 6G was added to the Pluronic F-127 solution. The hydrodynamic radius of the dye was measured at different surfactant concentrations. The experimental autocorrelation curves and the hydrodynamic radii are shown in Figure 58. At low surfactant concentrations (0.1 – 100 µM) the hydrodynamic radius is identical to the one from rhodamine 6G (R_H = 0.55 nm). Above the critical micelle concentration, resembled with the 2 mM sample, the fluorescent dye became incorporated

into the surfactant micelle and the hydrodynamic radius increased to the size of a Pluronic F-127 micelle.

FCS was used to determine the behavior of the surfactant Pluronic F-127 below and above the critical micelle concentration to understand the dewetting dynamics of the surfactant.

This work was published in *Colloids and Surfaces A: Physicochemical and Engineering Aspects* (2017, 30–37), entitled ”Forced dewetting dynamics of high molecular weight surfactant solutions” as joint project together with D. Truszkowska, F. Henrich, K. Koynov, H. J. Räder, H.-J. Butt and G. K. Auernhammer.

6.6 Fluorescence Correlation Spectroscopy Studies of Molecular Tracer Diffusion

The diffusion dynamics of molecular tracers in polymer networks was studied by fluorescence correlation spectroscopy. To understand the polymer tracer interactions, the tracer diffusion was measured at different molecular weights, various polymer architectures and different polymer concentrations for three polymers: polydimethylsiloxane (PDMS), polystyrene (PS) and polybutadiene (PB). The diffusion slowdown of the tracer is expressed as $D(c)/D_0$ (D_0 is the diffusion coefficient of the tracer) and plotted against the concentration, see Figure 59. The experiments gave polymer-specific master curves, which are independent of the molecular weight and independent of the polymer architectures.

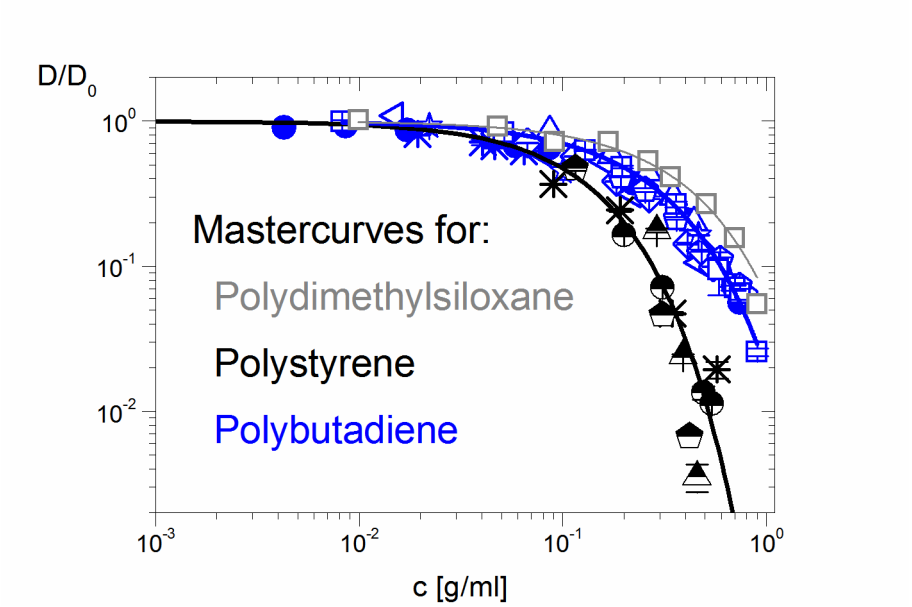

Figure 59: Normalized diffusion slowdown $D(c)/D_0$ vs concentration of a molecular tracer. Linear PS at different molecular weights has black symbols. Black pentagons present PS combs. Linear PB is shown at two different molecular weights (PB 170 kg/mol: blue stars and PB 52 kg/mol: blue pentagons) and star PB at different molecular weights (PB 30 kg/mol: double-crossed blue symbols, PB 500 g/mol: blue triangles, PB 80 kg/mol: blue circles, PB 4.4 kg/mol: blue squares). The diffusion slowdown data for the tracer in linear PDMS (M_w = 60 kg/mol) are depicted by the grey squares. The solid black, blue and grey lines through the data represent the corresponding master curves.

Understanding the tracer diffusion in polymer systems helps to improve applications, such as drug delivery, chromatography or hydrogel-based sensors, in which tracers are needed.

This work was published in *Macromolecules* (2015, 48, 8907−8912), entitled ”Molecular Tracer Diffusion in Nondilute Polymer Solutions: Universal Master Curve and Glass Transition Effects” as joint project together with A. Vagias, M. Doroshenko, K. Koynov, H.-J. Butt, M. Gauthier, G. Fytas and D. Vlassopoulos.

7 Bibliography

[1] Y. Zhang, H. F. Chan, K. W. Leong, *Adv. Drug Deliv. Rev.* **2013**, *65*, 104–120.

[2] C. S. P. Nikam A.P., Mukesh P., R., *Int. J. Res. Dev.Pharm. L. Sci.* **2014**, *3*, 1121–1127.

[3] V. Mohanraj, Y. Chen, M. & Chen, *Trop. J. Pharm. Res. Trop J Pharm Res* **2006**, *5*, 561–573.

[4] S. Hasan, *Res. J. Recent Sci.* **2015**, *4*, 1–3.

[5] O. Salata, *J. Nanobiotechnology* **2004**, *2*, 3.

[6] R. Singh, J. W. Lillard, *Exp. Mol. Pathol.* **2009**, *86*, 215–223.

[7] A. H. Faraji, P. Wipf, *Bioorganic Med. Chem.* **2009**, *17*, 2950–2962.

[8] L. Nuhn, L. Braun, I. Overhoff, A. Kelsch, D. Schaeffel, K. Koynov, R. Zentel, *Macromol. Rapid Commun.* **2014**, *35*, 2057–2064.

[9] L. Nuhn, M. Hirsch, B. Krieg, K. Koynov, K. Fischer, M. Schmidt, M. Helm, R. Zentel, *ACS Nano* **2012**, *6*, 2198–2214.

[10] B. Mishra, B. B. Patel, S. Tiwari, *Nanomedicine Nanotechnology, Biol. Med.* **2010**, *6*, 9–24.

[11] K. Tappertzhofen, M. Bednarczyk, K. Koynov, M. Bros, S. Grabbe, R. Zentel, *Macromol. Biosci.* **2014**, *14*, 1444–1457.

[12] I. Tabujew, C. Freidel, B. Krieg, M. Helm, K. Koynov, K. Müllen, K. Peneva, *Macromol. Rapid Commun.* **2014**, *35*, 1191–1197.

[13] T. Fritz, M. Voigt, M. Worm, I. Negwer, S. S. Müller, K. Kettenbach, T. L. Ross, F. Roesch, K. Koynov, H. Frey, et al., *Chem. - A Eur. J.* **2016**, *22*, 11578–11582.

[14] M. A. Hood, U. Paiphansiri, D. Schaeffel, K. Koynov, M. Kappl, K. Landfester, R. Muñoz-Espí, *Chem. Mater.* **2015**, *27*, 4311–4318.

[15] J. R. Lakowicz, *Principles of Fluorescence Spectroscopy*, Springer, New York, **2006**.

[16] W. Becker, *Advanced Time-Correlated Single Photon Counting Techniques*, Springer, Berlin, Heidelberg, New York, **2005**.

[17] Thermo Fisher Scientific, "Alexa Fluor Dyes—Across the Spectrum," can be found under: https://www.thermofisher.com/de/de/home/brands/molecular-probes/key-molecular-probes-products/alexa-fluor/alexa-fluor-dyes-across-the-spectrum.html, **2018**.

[18] W. L. Goh, M. Y. Lee, T. L. Joseph, S. T. Quah, C. J. Brown, C. Verma, S. Brenner, F. J. Ghadessy, Y. N. Teo, *J. Am. Chem. Soc.* **2014**, *136*, 6159–6162.

[19] M. A. Haidekker, E. A. Theodorakis, *J. Biol. Eng.* **2010**, *4*, 11.

[20] M. A. Haidekker, M. Nipper, A. Mustafic, D. Lichlyter, M. Dakanali, E. A. Theodorakis, *Advanced Fluorescence Reporters in Chemistry and Biology I: Fundamental and Molecular Design*, Springer, Berlin Heidelberg, **2010**.

[21] M. A. Haidekker, T. P. Brady, D. Lichlyter, E. A. Theodorakis, *Bioorg. Chem.* **2005**, *33*, 415–425.

[22] F. Zhou, J. Shao, Y. Yang, J. Zhao, H. Guo, X. Li, S. Ji, Z. Zhang, *European J. Org. Chem.* **2011**, 4773–4787.

[23] N. Amdursky, Y. Erez, D. Huppert, *Acc. Chem. Res.* **2012**, *45*, 1548–1557.

[24] T. Atsbeha, A. M. Mohammed, M. Redi-Abshiro, *J. Fluoresc.* **2010**, *20*, 1241–1248.

[25] M. A. Haidekker, T. Ling, M. Anglo, H. Y. Stevens, J. A. Frangos, E. A. Theodorakis, *Chem. Biol.* **2001**, *8*, 123–131.

[26] R. Ramadass, J. Bereiter-Hahn, *J. Phys. Chem. B* **2007**, *111*, 7681–7690.

[27] G. Vaccaro, A. Bianchi, M. Mauri, S. Bonetti, F. Meinardi, A. Sanguineti, R. Simonutti, L. Beverina, *Chem. Commun.* **2013**, *49*, 8474–8476.

[28] S. Sawada, T. Iio, Y. Hayashi, S. Takahashi, *Anal. Biochem.* **1992**, *204*, 110–117.

[29] M. Wahl, *PicoQuant Tech. Note* **2014**, 1–14.

[30] PicoQuant GmbH, *8th European Short Course in "Time-Resolved Microscopy and Correlation Spectroscopy,"* Berlin, **2016**.

[31] S. W. Paddock, *Biotechniques* **1999**, *27*, 992–1004.

[32] M. Minsky, *Scanning* **1988**, *10*, 128–138.

[33] R. H. Webb, *Reports Prog. Phys.* **1999**, *59*, 427–471.

[34] M. D. DB. Murphy, in *Fundam. Light Microsc. Electron. Imaging*, **2012**, pp. 265–305.

[35] O. Krichevsky, G. Bonnet, *Rep. Prog. Phys* **2002**, *65*, 251–297.

[36] P. Schwille, J. Bieschke, F. Oehlenschläger, *Biophys. Chem.* **1997**, *66*, 211–228.

[37] R. Rigler, E. S. Elson, *Fluorescence Correlation Spectroscopy: Theory and Applications*, Springer, Berlin Heidelberg New Vork, **2011**.

[38] D. Magde, E. L. Elson, W. W. Webb, *Phys. Rev. Lett.* **1972**, *29*, 705–708.

[39] D. Magde, E. L. Elson, W. W. Webb, *Biopolymers* **1974**, *13*, 29–61.

[40] E. L. Elson, *Biophys. J.* **2011**, *101*, 2855–2870.

[41] E. L. Elson, D. Magde, *Biopolymers* **1974**, *13*, 1–27.

[42] P. Schwille, *Cell Biochem. Biophys.* **2001**, *34*, 383–408.

[43] P. Schwille, E. Haustein, *Fluorescence Correlation Spectroscopy An Introduction to Its Concepts and Applications*, **2009**.

[44] A. J. García-Sáez, P. Schwille, *Methods* **2008**, *46*, 116–122.

[45] S. Chiantia, J. Ries, P. Schwille, *Biochim. Biophys. Acta - Biomembr.* **2009**, *1788*, 225–233.

[46] K. Koynov, H.-J. Butt, *Curr. Opin. Colloid Interface Sci.* **2012**, *17*, 377–387.

[47] E. Bianconi, A. Piovesan, F. Facchin, A. Beraudi, R. Casadei, F. Frabetti, L. Vitale, M. C. Pelleri, S. Tassani, F. Piva, et al., *Ann. Hum. Biol.* **2013**, *40*, 463–71.

[48] B. Alberts, A. Johnson, J. Lewis, M. Raff, K. Roberts, P. Walter, in *Mol. Biol. Cell*, Garland Science, New York, **2002**.

[49] P. Yeagle, *The Membranes of Cells*, Elsevier, **1993**.

[50] Y.-H. M. Chan, S. G. Boxer, *Curr. Opin. Chem. Biol.* **2007**, *11*, 581–587.

[51] A. D. Bangham, M. M. Standish, J. C. Watkins, *J. Mol. Biol.* **1965**, *13*, 238–252.

[52] S. F. Fenz, K. Sengupta, *Integr. Biol.* **2012**, *4*, 982–995.

[53] J. H. Fendler, *Membrane Mimetic Chemistry*, Wiley, New York, **1982**.

[54] H. T. Tien, S. Carbone, E. A. Dawidowicz, *Nature* **1966**, *212*, 718–719.

[55] M. Winterhalter, *Curr. Opin. Colloid Interface Sci.* **2000**, *5*, 250–255.

[56] L. K. Tamm, H. M. McConnell, *Biophys. J.* **1985**, *47*, 105–113.

[57] P. Walde, K. Cosentino, H. Engel, P. Stano, *ChemBioChem* **2010**, *11*, 848–865.

[58] O. Wesołowska, K. Michalak, J. Maniewska, A. B. Hendrich, *Acta Biochim. Pol.* **2009**, *56*, 33–39.

[59] A. Weinberger, F.-C. C. Tsai, G. H. H. Koenderink, T. F. F. Schmidt, R. Itri, W. Meier, T. Schmatko, A. Schroder, C. Marques, A. Schröder, et al., *Biophys. J.* **2013**, *105*, 154–164.

[60] A. Jesorka, M. Markstro, O. Orwar, *Langmuir* **2005**, *21*, 1230–1237.

[61] K. Karamdad, R. V. Law, J. M. Seddon, N. J. Brooks, O. Ces, *Lab Chip* **2015**, *15*, 557–562.

[62] E. B. Working, A. C. Andrews, *Chem. Rev.* **1941**, *29*, 245–256.

[63] J. Berg, J. Tymoczko, L. Stryer, in *Biochemistry*, W H Freeman, New York, **2002**.

[64] B. R. Lentz, *Prog. Lipid Res.* **2003**, *42*, 423–438.

[65] M. Mishkind, *Trends Cell Biol.* **2000**, *10*, 368.

[66] M. J. Hope, M. B. Bally, G. Webb, P. R. Cullis, *BBA - Biomembr.* **1985**, *812*, 55–65.

[67] B. Pépin-Donat, C. Campillo, F. Quemeneur, M. Rinaudo, C. Marques, A. Schröder, G. Maret, *Int. J. Nano Dimens.* **2011**, *2*, 17–23.

[68] R. B. Lira, R. Dimova, K. a Riske, *Biophys. J.* **2014**, *107*, 1609–1619.

[69] S. I. M. Nomura, K. Tsumoto, T. Hamada, K. Akiyoshi, Y. Nakatani, K. Yoshikawa, *ChemBioChem* **2003**, *4*, 1172–1175.

[70] K. Ishikawa, K. Sato, Y. Shima, I. Urabe, T. Yomo, *FEBS Lett.* **2004**, *576*, 387–390.

[71] F. M. Menger, M. I. Angelova, *Acc. Chem. Res.* **1998**, *31*, 789.

[72] J. P. Reeves, R. M. Dowben, *J. Cell. Physiol.* **1969**, *73*, 49–60.

[73] M. I. Angelova, D. S. Dimitrov, *Faraday Discuss. Chem. SO* **1986**, *81*, 303–311.

[74] R. Dimova, S. Aranda, N. Bezlyepkina, V. Nikolov, K. A. Riske, R. Lipowsky, *J. Phys. Condens. Matter* **2006**, *18*, 1151–1176.

[75] T. Pott, H. Bouvrais, P. Méléard, *Chem. Phys. Lipids* **2008**, *154*, 115–119.

[76] T. Shimanouchi, H. Umakoshi, R. Kuboi, *Langmuir* **2009**, *25*, 4835–4840.

[77] F. Tao, P. Yang, *Sci. Rep.* **2015**, *5*, DOI 10.1038/srep09839.

[78] Y. P. Patil, S. Jadhav, *Chem. Phys. Lipids* **2014**, *177*, 8–18.

[79] D. Massenburg, B. R. Lentz, *Biochemistry* **1993**, *32*, 9172–9180.

[80] A. L. Bailey, P. R. Cullis, *Biochemistry* **1997**, *36*, 1628–1634.

[81] C. K. Haluska, K. A. Riske, V. Marchi-Artzner, J.-M. Lehn, R. Lipowsky, R. Dimova, *Proc. Natl. Acad. Sci. U. S. A.* **2006**, *103*, 15841–6.

[82] N. Oku, R. C. Macdonald, *BBA - Biomembr.* **1983**, *734*, 54–61.

[83] K. S. Horger, D. J. Estes, R. Capone, M. Mayer, *J. Am. Chem. Soc.* **2009**, *131*, 1810–1819.

[84] T. Tanaka, *Polymer (Guildf).* **1979**, *20*, 1404–1412.

[85] A. Suzuki, T. Tanaka, *Nature* **1990**, *346*, 345–347.

[86] M. Heskins, J. E. Guillet, *J. Macromol. Sci. Part A - Chem.* **1968**, *2*, 1441–1455.

[87] H. G. Schild, *Prog. Polym. Sci.* **1992**, *17*, 163–249.

[88] R. Pelton, *J. Colloid Interface Sci.* **2010**, *348*, 673–674.

[89] G. Panambur, N. Davis, *Aldrich Mater. Sci.* **2016**, 22–25.

[90] E. H. Specht, H. Valley, A. Neuman, N. Hills, H. T. Neher, *Preparation of Acrylamides*, **1954**.

[91] H.-G. Elias, *Macromolecules - Industrial Polymers and Synthesis*, **2007**.

[92] J. M. Hoffman, P. S. Stayton, A. S. Hoffman, J. J. Lai, *Bioconjug. Chem.* **2015**, *26*, 29–38.

[93] M. Cetintas, J. de Grooth, A. H. Hofman, H. M. van der Kooij, K. Loos, W. M. de Vos, M. Kamperman, *Polym. Chem.* **2017**, *8*, 2235–2243.

[94] H. Wei, X.-Z. Zhang, W.-Q. Chen, S.-X. Cheng, R.-X. Zhuo, *J. Biomed. Mater. Res. Part A* **2006**, 980–989.

[95] P. W. Beines, I. Klosterkamp, B. Menges, U. Jonas, W. Knoll, *Langmuir* **2007**, *23*, 2231–2238.

[96] A. Vagias, P. Košovan, C. Holm, H. Butt, K. Koynov, G. Fytas, *Prog. Colloid Polym. Sci.* **2013**, *140*, 53–62.

[97] G. Dormán, G. D. Prestwich, *Biochemistry* **1994**, *33*, 5661–5673.

[98] O. Prucker, C. a. Naumann, J. Rühe, W. Knoll, C. W. Frank, *J. Am. Chem. Soc.* **1999**, *121*, 8766–8770.

[99] N. A. Peppas, A. R. Khare, *Adv. Drug Deliv. Rev.* **1993**, *11*, 1–35.

[100] V. Carias, J. Wang, R. Toomey, *Langmuir* **2014**, 4105–4110.

[101] E. Caló, V. V. Khutoryanskiy, *Eur. Polym. J.* **2015**, *65*, 252–267.

[102] K. Zubik, P. Singhsa, Y. Wang, H. Manuspiya, R. Narain, *Polymers (Basel).* **2017**, *9*, 1–17.

[103] S. J. Buwalda, K. W. M. Boere, P. J. Dijkstra, J. Feijen, T. Vermonden, W. E. Hennink, *J. Control. Release* **2014**, *190*, 254–273.

[104] M. Giannelli, P. W. Beines, R. F. Roskamp, K. Koynov, G. Fytas, W. Knoll, *J. Phys. Chem. C* **2007**, *111*, 13205–13211.

[105] J. Fickert, M. Makowski, M. Kappl, K. Landfester, D. Crespy, *Macromolecules* **2012**, *45*, 6324–6332.

[106] R. Raccis, R. Roskamp, I. Hopp, B. Menges, K. Koynov, U. Jonas, W. Knoll, H.-J. J. Butt, G. Fytas, *Soft Matter* **2011**, *7*, 7042–7053.

[107] R. Macháň, M. Hof, *Biochim. Biophys. Acta* **2010**, *1798*, 1377–1391.

[108] W. S. Trimble, S. Grinstein, *J. Cell Biol.* **2015**, *208*, 259–271.

[109] S. J. Singer, G. L. Nicolson, *Science* **1972**, *175*, 720–731.

[110] G. Lindblom, in *Encycl. Biophys.* (Ed.: G.C.K. Roberts), Springer, Berlin, Heidelberg, **2013**.

[111] J. Kriegsmann, I. Gregor, I. Von Der Hocht, J. Klare, M. Engelhard, J. Enderlein, J. Fitter, *ChemBioChem* **2009**, *10*, 1823–1829.

[112] F. A. Thomas, I. Visco, Z. Petrášek, F. Heinemann, P. Schwille, *Data Br.* **2015**, *5*, 537–541.

[113] E. L. Crockett, *J. Comp. Physiol. B Biochem. Syst. Environ. Physiol.* **2008**, *178*, 795–809.

[114] B. N. Ames, M. K. Shigenaga, T. M. Hagen, *Proc. Natl. Acad. Sci. U. S. A.* **1993**, *90*, 7915–7922.

[115] P. H. B. Aoki, L. F. C. Morato, F. J. Pavinatto, T. M. Nobre, C. J. L. Constantino, O. N. Oliveira, *Langmuir* **2016**, *32*, 3766–3773.

[116] S. P. Stratton, D. C. Liebler, *Biochemistry* **1997**, *36*, 12911–12920.

[117] W. Caetano, P. S. Haddad, R. Itri, D. Severino, V. C. Vieira, M. S. Baptista, A. P. Schröder, C. M. Marques, *Langmuir* **2007**, *23*, 1307–1314.

[118] R. Sauer, A. Turshatov, S. Baluschev, K. Landfester, *Macromolecules* **2012**, *45*, 3787–3796.

[119] D. Schaeffel, R. H. Staff, H. J. Butt, K. Landfester, D. Crespy, K. Koynov, *Nano Lett.* **2012**, *12*, 6012–6017.

[120] R. H. Staff, D. Schaeffel, A. Turshatov, D. Donadio, H.-J. Butt, K. Landfester, K. Koynov, D. Crespy, *Small* **2013**, *9*, 3514–3522.

[121] J. Maul, B. G. Frushour, J. R. Kontoff, H. Eichenauer, K.-H. Ott, C. Schade, *Ullmann's Encycl. Ind. Chem.* **2012**, *29*, 475–521.

[122] A. W. Hui, A. E. Hamielec, *J. Appl. Polym. Sci.* **1972**, *16*, 749–769.

[123] K. S. Khuong, W. H. Jones, W. A. Pryor, K. N. Houk, *J. Am. Chem. Soc.* **2005**, *127*, 1265–1277.

[124] C. Loos, T. Syrovets, A. Musyanovych, V. Mailänder, K. Landfester, G. U. Nienhaus, T. Simmet, *Beilstein J. Nanotechnol* **2014**, *5*, 2403–2412.

[125] A. K. Boal, F. Ilhan, J. E. Derouchey, T. Thurn-Albrecht, T. P. Russell, V. M. Rotello, *Nature* **2000**, *404*, 746–748.

[126] O. D. Velev, E. W. Kaler, *Langmuir* **1999**, *15*, 3693–3698.

[127] J. P. Rao, K. E. Geckeler, *Prog. Polym. Sci.* **2011**, *36*, 887–913.

[128] ATTO-TEC GmbH, "Atto 425," can be found under https://www.atto-tec.com/attotecshop/product_info.php?language=en&info=p4_atto-425.html&, **2018**.

[129] J. M. Nölle, C. Jüngst, A. Zumbusch, D. Wöll, *Polym. Chem.* **2014**, *5*, 2700.

8 Abbreviations

AC	Autocorrelation
AIBN	Azobisisobutyronitrile
APD	Avalanche photodiode
CLSM	Confocal laser scanning microscopy
CMC	Critical micelle concentration
CR110	Carboxyrhodamine 110, fluorescent dye
CRC	Collaborative research center
Cy5-NHS	Cyanine-*5*-monosuccinimidyl ester, fluorescent dye
DBCO	Dibenzocyclooctyne
DC	Dendritic immune cell
DCM	Dichloromethane
DEC205	Specific antibody
DMSN	Dendritic mesoporous silica nanoparticle
DNA	Deoxyribonucleic acid
DOPC	1,2-dioleoyl-*sn*-glycero-3-phosphocholine
DOPE	1,2-dioleoyl-*sn*-glycero-3-phosphoethanolamine
DOPS	1,2-dioleoyl-*sn*-glycero-3-phosphoserine
FCCS	Fluorescence cross-correlation spectroscopy
FCS	Fluorescence correlation spectroscopy
FLIM	Fluorescence lifetime imaging microscopy
FRET	Förtst resonance energy transfer
GUAV	Giant unilamellar anchored vesicle

GUV	Giant unilamellar vesicle
IRF	Instrument response function
JGU	Johannes Gutenberg University (Mainz)
LBX37	Fluorescent molecular rotor: 6-(5*H*-dibenzo[*b*,*f*]azepin-5-yl)-2-(2,6-diisopropylphenyl)-1*H*-benzo[*de*]isoquinoline-1,3(2*H*)-dione
LCST	Lower critical solution temperature
LED	Light-emitting diode
LUV	Large unilamellar vesicle
MAA	Methacrylic acid
MABP	4-Methacryloyloxybenzophenone
MEP	Miniemulsion polymerization
MPI-P	Max Planck-Institute for Polymer Research
NIPAAm	*N*-isopropylacrylamide
NMR	Nuclear magnetic resonance (spectroscopy)
PB	Polybutadiene
PBS	Phosphate buffered saline
PDI	Polydispersity index
PDMS	Polydimethylsiloxane
pDNA	Plasmid deoxyribonucleic acid
PEG	Polyethyleneglycol
PEI	Polyethyleneimide
PEO	Polyethyleneoxid
PET	Polyethylenetherephtalate
P(Lys)-*b*-P(HPMA)	Polylysine-*block*-poly(*N*-(2-hydroxypropyl) methacrylamide
PMT	Photomultiplier tube
PNIPAAm	Poly(*N*-isopropylacrylamide)

PS	Polystyrene
PSar-*b*-PCys(SO_2Et)	Polysarcosine-*block*-poly(*S*-alkylsulfonyl)-*L*-cysteine
PVA	Polyvinyl alcohol
RhB	Rhodamine B
SDS	Sodium dodecyl sulfate
SEED	Solvent evaporation from emulsion droplets
SPAAC	Strain-promoted alkyne-azide cycloaddition
SUV	Small unilamellar vesicle or sonicated unilamellar vesicle
TCSPC	Time-correlated single photon counting
TEA	Triethylamine
TICT	Twisted intramolecular charge transfer
TNF-α	Tumor necrosis factor alpha
UV	Ultraviolet
V59	Initiator: 2,2'-Azobis(2-methylbutyronitrile)

9 Symbols

A_i	Amplitude of the i-th fluorescence lifetime, e.g. A_1, A_2
c	Concentration
D	Diffusion coefficient
$F(t)$	Fluorescence intensity at a time t
$G(\tau^*)$	Normalized fluctuation autocorrelation function
$h\upsilon$	Energy
h_d	Thickness of the dry polymer film
h_{df}	Thickness of the dry patterned polymer film
h_{dh}	Thickness of the hole of the dry patterned polymer film
h_s	Thickness of the swollen polymer film
η	Viscosity of the solution
I	Intensity (Number of photons)
I_0	Intensity at time 0
I_t	Intensity at time t
φ	Polymer volume fraction, $\varphi = 1/R_s$.
k	Boltzmann constant, k = $1.38 \cdot 10^{-23}$ J/K
λ	Wavelength
M_n	Number average molecular weight
M_w	Weight avareage molceular weight
N	Number of particle in the confocal observation volume
r_0	Radial dimension of the observation volume
R_H	Hydrodynamic radius
R_s	Swelling ratio, $R_s = h_s/h_d$

S	Structural parameter of the observation volume, $S = z_0 / r_0$
S_0	Electronic ground state
S_1	First singlet electronic state
S_2	Second singlet electronic state
t	Time
T	Temperature
T_1	First triplet electronic state
τ_i	i-th fluorescence lifetime, e.g. τ_1, τ_2
τ_D	Diffusion time
τ_{wa}	Weighted average fluorescence lifetime
τ^*	Delay time
v	Energy dose
V_{obs}	Observation volume
z_0	Axial dimension of the observation volume

Danksagung

[nicht in der Online-Version enthalten]

Wissenschaftliche Beiträge

Artikel	„PNIPAAm Gel-assisted Formation of Monodisperse Giant Unilamellar Anchored Vesicles” **J. Schultze**, A. Vagias, E. Prantl, V. Breising, A. Best, H.-J. Butt, C. Marques, K. Koynov In Bearbeitung zur Einreichung bei *Nature Communications.*
Artikel	„Site-Specific DBCO Modification of DEC205 Antibody for Polymer Conjugation” S. Beck, **J. Schultze**, H.-J. Räder, R. Holm, M. Schinnerer, M. Barz, K. Koynov, R. Zentel *Polymers*, 2018, 10, 141.
Artikel	„A modular approach for multifunctional polymersomes with controlled adhesive properties” J. Petit, L. Thomi, **J. Schultze**, M. Makowski, I. Negwer, K. Koynov, S. Herminghaus, F. Wurm, O. Bäumchen, K. Landfester *Soft Matter* 2017, 14, 6, 894-900.
Poster	„Fluorescence correlation spectroscopy studies of nanocarrier-based drug delivery systems” **J. Schultze**, I. Negwer, H.-J. Butt, M. Helm, K. Koynov Fluorescence Correlation Spectroscopy Workshop, Garching, Oktober 2017.
Artikel	„Combining Orthogonal Reactive Groups in Block Copolymers for Functional Nanoparticle Synthesis in a Single Step” O. Schäfer, K. Klinker, L. Braun, D. Huesmann, **J. Schultze**, K. Koynov, M. Barz *ACS Macro Lett.* 2017, 6, 1140−1145.
Artikel	„Dendritic Mesoporous Silica Nanoparticles for pH-Stimuli-Responsive Drug Delivery of TNF-Alpha” A. Kienzle, S. Kurch, J. Schlöder, C. Berges, R. Ose, J. Schupp, A. Tuettenberg, H. Weiss, **J. Schultze**, S. Winzen, M. Schinnerer, K. Koynov, M. Mezger, N. K. Haass, W. Tremel, H. Jonuleit *Adv. Healthcare Mater.* 2017, 1700012.

Artikel	„Forced dewetting dynamics of high molecular weight surfactant solutions” D. Truszkowska, F. Henrich, **J. Schultze**, K. Koynov, H.J. Räder, H.-J. Butt, G.K. Auernhammer *Colloids and Surfaces A: Physicochem. Eng. Aspects* 2017, 30–37.
Vortrag	„Structured PNIPAAm hydrogels as smart templates for the preparation of monodisperse giant unilamellar vesicles” **J. Schultze**, H.-J. Butt, K. Koynov, C. Marques, A. Vagias Bratislava International Conference on Macromolecules, Bratislava, Slowakei, September 2016. Auszeichnung für den besten Konferenzvortrag
Poster	„Preparation of monodisperse giant unilamellar vesicles via gel-assisted formation” **J. Schultze**, A. Vagias, C. Marques, K. Koynov, H.-J. Butt 18. JCF-Frühjahrssymposium, Kiel, März 2016.
Artikel	„Molecular Tracer Diffusion in Nondilute Polymer Solutions: Universal Master Curve and Glass Transition Effects” A. Vagias, **J. Schultze**, M. Doroshenko, K. Koynov, H.-J. Butt, M. Gauthier, G. Fytas, D. Vlassopoulos *Macromolecules* 2015, 48, 8907−8912.

Curriculum Vitae

[nicht in der Online-Version enthalten]